



8-2000

## **Modification, identification and control of chaotic bubbling with electrostatic potential**

Sachin Udaya Sarnobat

Follow this and additional works at: [https://trace.tennessee.edu/utk\\_gradthes](https://trace.tennessee.edu/utk_gradthes)

---

### **Recommended Citation**

Sarnobat, Sachin Udaya, "Modification, identification and control of chaotic bubbling with electrostatic potential. " Master's Thesis, University of Tennessee, 2000.  
[https://trace.tennessee.edu/utk\\_gradthes/9484](https://trace.tennessee.edu/utk_gradthes/9484)

This Thesis is brought to you for free and open access by the Graduate School at TRACE: Tennessee Research and Creative Exchange. It has been accepted for inclusion in Masters Theses by an authorized administrator of TRACE: Tennessee Research and Creative Exchange. For more information, please contact [trace@utk.edu](mailto:trace@utk.edu).

To the Graduate Council:

I am submitting herewith a thesis written by Sachin Udaya Sarnobat entitled "Modification, identification and control of chaotic bubbling with electrostatic potential." I have examined the final electronic copy of this thesis for form and content and recommend that it be accepted in partial fulfillment of the requirements for the degree of Master of Science, with a major in Chemical Engineering.

Duane D. Bruns, Major Professor

We have read this thesis and recommend its acceptance:

David W. DePaoh, Ke Nguyen, Stuart Daw, Wesley J. Hines

Accepted for the Council:


Carolyn R. Hodges

Vice Provost and Dean of the Graduate School

(Original signatures are on file with official student records.)


To the Graduate Council

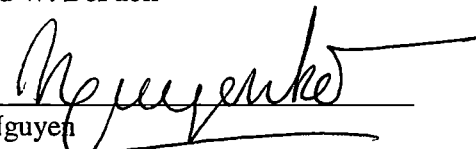
I am submitting herewith a dissertation written by Sachin Udaya Sarnobat entitled, "Modification, Identification And Control Of Chaotic Bubbles Using Electrostatic Potential " I have examined the final copy of this dissertation for form and content and recommend that it be accepted in partial fulfillment of the requirements for the degree of Master of Science, with a major in Chemical Engineering.

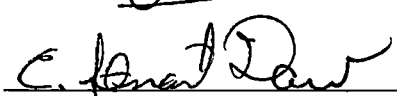
  
Duane D Bruns, Chairperson

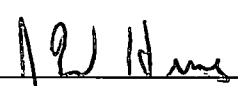
We have read this dissertation

And recommend its acceptance

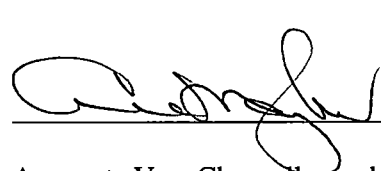
  
David W. DePaoli

  
Ke Nguyen

  
Stuart Daw

  
Wesley J. Hines

Accepted for the Council

  
Associate Vice Chancellor and  
Dean of the Graduate School

***Modification, Identification And Control Of  
Chaotic Bubbling With Electrostatic Potential***

A Thesis  
Presented for the  
Master of Science  
Degree  
The University of Tennessee, Knoxville

Sachin Udaya Sarnobat

August, 2000



Copyright © Sachin Udaya Sarnobat, 2000

All rights reserved

## ***Dedication***

This thesis is dedicated to my grandfather,

Ramchandra R Kulkarni

(आबा)

and grandmother,

Leela A Deshpande

(आई)

who have taught me to look beyond what the world sees

## ***Acknowledgements***

This thesis has been more a culmination of interdisciplinary research and collaboration between colleagues, than a simple foray into unknown territory. I am grateful to my advisor Prof Duane D. Bruns (University of Tennessee, Chemical Engineering), co-advisor Dr. David W. DePaoli (Oak Ridge National Laboratory), Dr. Wesley J. Hines (University of Tennessee, Nuclear Engineering), Prof. Ke Nguyen (University of Tennessee, Mechanical Engineering), Dr. Stuart Daw (Oak Ridge National Laboratory), Dr. Belle Upadhyaya (University of Tennessee, Nuclear Engineering) among many others who helped kindle ideas and bifurcate to new research directions.

Among my colleagues I would like to acknowledge and thank the solid support of Charles Finney, Mike Brotherton, Andrew Blankenship, Dean Edwards, Sandeep Rajput and Boyce O. Griffith.

I also would like to express my appreciation for the faculty and staff of the Department of Chemical Engineering. They have supported me both on professional and friendship levels. I would like to thank Division of Chemical Sciences, Office of Basic Energy Sciences, U.S. Department of Energy, for their generous funding under contract DE-AC05-00OR22725 with UT-Battelle, LLC.

Lastly I would like to thank my family for giving me a chance to be myself.

## ***Abstract***

The effect of an applied electric potential on the dynamics of bubble formation from a single nozzle was studied experimentally. Bubbling of dry nitrogen into glycerol through a nozzle having an electrified tip was examined by pressure measurements upstream of the nozzle. As the applied electric potential is increased from zero, the bubble size is reduced and the bubbling frequency is increased. It has been found that, at constant flow rate, bubble-formation dynamics exhibit the classic signs of a period-doubling bifurcation to chaos with increasing applied potential. The behavior is similar to that for increasing flow rate of the well-studied dripping faucet and of bubble formation in liquids. A three-dimensional bifurcation map was determined as a function of gas flow rate and electrostatic potential. The data indicate that although bifurcation route is similar for applied voltage and flow, the effect on bubbling for applied voltage is significantly smaller than that for flow as measured by dimensionless variables. Electrostatic potential was successfully harnessed as the manipulated variable to track a set-point of a constant average bubbling frequency with disturbances due to flow-rate. It was found that an increase/decrease in electrostatic potential can be used to compensate a 50% change in the flow rate. A control scheme suggested by Ott, Grebogi and Yorke was implemented to tame the chaos of bubbles with partial success. Software tools namely the Bubble Toolbox for Chaotic Analysis and the Automation Workbench for LabView were developed in conjunction with this experiment.

# Contents

<b>1.</b>	<b>Chapter 1: Introduction.....</b>	<b>1</b>
<b>2.</b>	<b>Chapter 2: Background.....</b>	<b>4</b>
2 1	Electrostatic potential as an additional bifurcation variable	4
2 2	Chaos & feedback control	8
2 2 1	Concepts of chaos	9
2 2 2	OGY control	13
2 3	Summary	20
<b>3.</b>	<b>Chapter 3: Methods</b>	<b>22</b>
3 1	Experimental	22
3 1 1	Introduction	22
3 1 2	Set-up Details	23
3 1 2 1	The glass column	23
3 1 2 2	Gas flow and metering system	25

3 1 2 3	Liquid selection	27
3 1 2 4	Data acquisition system	28
3 1 2 5	Nozzle construction	28
3 1 3	Procedure	30
3 2	Data analysis	31
3 2 1	Power spectra	31
3 2 2	Bifurcation and route to chaos	32
3 2 3	Time return maps	32
3 2 4	Phase space reconstruction	33
3 2 5	Multivariate statistical techniques	33
3 2 6	Neural network model for regime identification	35
<b>4.</b>	<b>Chapter 4: Observations and analysis.....</b>	<b>37</b>
4 1	Formation of a single bubble	37
4 2	Regimes of bubbling	40
4 2 1	Period-1 bubbling	42
4 2 2	Period-2 bubbling	45
4 2 3	Period-4 bubbling	49
4 2 4	Chaotic bubbling	52
4 3	Effect of electrostatic potential on bubbling	54

4 3 1	Pressure traces	54
4 3 2	Periods of formation . .	56
4 3 3	Time return maps	59
4 3 4	Phase space analysis	65
4 3 5	Power spectrum distribution	65
4 3 6	Bifurcation diagram	65
4 3 6 1	Bifurcation at constant voltage	68
4 3 6 2	Bifurcation with voltage and flow	68
4 3 7	Bubbling regimes in terms of dimensionless numbers	70
<b>5.</b>	<b>Application &amp; Implementation.....</b>	<b>78</b>
5 1	Periodicity identification	78
5 1 1	Statistical modeling	79
5 1 2	Neural network models	79
5 1 3	Periodicity pattern detector	..81
5 2	Regime targeting of bubbling with electrostatic potential	..... 83
5 3	OGY Control ..	.... 90
5 3 1	Calculations	.. .90
5 3 1 1	Identifying the unstable fixed point	. 91

5 3 1 2	Calculating the manifolds	91
5 3 1 3	Calculating the eigenvalues	94
5 3 1 4	Shift vector.	96
5 3 2	Results	96
5 3 3	Entrainment studies	99
5 4	Summary	104
<b>6.</b>	<b>Conclusions &amp; recommendations.....</b>	<b>105</b>
	<b>References.....</b>	<b>108</b>
	<b>Appendices.....</b>	<b>113</b>
Appendix A	Progressive time return maps at constant flow rate and increasing electrostatic potential for a representative data set	114
Appendix B	Screen shot of the Bubble Toolbox for Chaotic Analysis	125
Appendix C	Screenshot of the Automation Workbench for Labview	126
Appendix D	Rotameter calibration curve at 10psig	127
Appendix E	Nomenclature	128
<b>Vita.....</b>		<b>129</b>



## ***List of figures***

2 1	Phase space trajectories and the Poincarè section	11
2 2	OGY control algorithm	14
3 1	Experimental schematic	24
3 2	Nozzle construction details	.29
3 3	Multivariate statistical techniques used to predict the bubbling regime from the period of formation data	34
3 4	Real time identification and fault identification	36
4 1	Pressure trace in gas inlet line, upstream of the nozzle	39
4 2	'Shoulders' in pressure time series	41
4 3	Pressure trace for period-1 bubbling	43
4 4	Power spectrum distribution for period-1 showing a single fundamental peak	43
4 5	Phase space for period-1 bubbling showing a single-loop	43
4 6	High speed images of slow bubbling	44
4 7	Pressure trace for period-2 bubbling	46
4 8	Power spectrum distribution for period-2 showing two fundamental peaks.. ..	46
4 9	Phase space for period-2 bubbling showing two-loops .	. 46
4 10	High speed images of period-2 formation of bubbles	47
4 11	Pressure trace for period-4 bubbling . . . . .	50
4 12	Power spectrum distribution for period-4 showing three fundamental peaks .	50

4 13 Phase space for period-4 bubbling showing four-loops	50
4 14 Pressure trace for chaotic bubbling	53
4 15 Power spectrum distribution for chaotic bubbling	53
4 16 Chaos in phase space	53
4 17 Pressure traces for bubbling with varying applied electrostatic potential, at a constant flow rate of 334 cc/min	55
4 18 Pressure trace for 1mm ID nozzle at 0kV	57
4 19 Pressure trace for 1mm ID nozzle at 5kV	57
4 20 Pressure trace for 1mm ID nozzle at 7.5kV	57
4 21 Period of formation of bubbles against bubble number, with varying applied electrostatic potential at a constant flow rate of 334 cc/min	58
4 22 Time return maps with an increase in the applied electrostatic potential at a constant flow rate of 334 cc/min	60
4 23 Time return maps with an increase in the flow rate at a constant applied electrostatic potential of 10,000 V	61
4 24 Time return maps with an increase in the respective control variable	63
4 25 Chaotic strange attractor in a 3-d time return map	64
4 26 Phase space variations with varying applied electrostatic potential field strength, at constant flow rate of 334 cc/min	66
4 27 Power spectrum variations with varying applied electrostatic potential field strength, at constant flow rate of 334 cc/min	67

4 28 Bifurcation with applied electrostatic potential field strength, at constant flow rate of 334 cc/min	69
4 29 Position of a single run with respect to bifurcation with flow-rate and electrostatic potential in tandem	69
4 30 Bifurcation with flow and voltage . . . .	72
4 31 Bifurcation with flow and voltage against dimensionless axes	72
4 32 Bubbling regime plot in terms of the modified Weber number	73
4 33 Bubbling regimes in terms of Tsuge's flow rate number versus electric Bond number	75
4 34 Frequency mapped as a surface plot against dimensionless flow-rate and voltage	76
5 1 Performance of numerical model using partial least squares	80
5 2 Neural network performance for identifying the periodicity of bubbling	82
5 3 Period-1 identification with periodicity pattern identifier	84
5 4 Period-2 identification with periodicity pattern identifier	85
5 5 An drift of 220cc/min in the disturbance (flow-rate), compensated by voltage to track a set point of constant bubbling frequency (0.05s) . . . .	87
5 6 Negative step change of 235cc/min in disturbance (flow rate) tracked by voltage for a set point of 0.05s . . .	88
5 7 Positive step change of 220cc/min in disturbance (flow rate) tracked by voltage for a set point of 0.05s . . . . .	89
5 8 Sorting fixed points on the 45° line on the time return map to find a true fixed-point	92

5 9	Identifying the stable and unstable manifold directions	93
5 10	OGY control attempt with electrostatic potential as the single control variable	98
5 11	Frequency distribution of zero crossings before control is turned on (region b)	100
5 12	Frequency distribution of zero crossings after control is turned on (region $c_1$ )	101
5 13	Frequency distribution of zero crossings after control is turned on (region $c_2$ )	102
5 14	Frequency distribution of zero crossings after control is turned off (region d)	103

## Chapter 1

# Introduction

---

*In all chaos there is a cosmos, in all disorder a secret order*

Carl Jung

Effervescence and bubbling have always been thought of as one of the simple phenomena, which make life interesting to look at. But beneath this innocuous visage lies a system so complex that the last decade has produced a flurry of papers investigating the interplay of bubbles. From numerical modeling of bubbles to studying the effect of sounds of bubble formation, numerous research thrusts have been made to try and capture this phenomenon in its entirety. Control of bubbles is one such aspect. Several attempts have been made to control bubbles, to tame them from a spectrum of sizes to a single file of pearls. But till date no successful attempts have been reported not only because of the spatio-temporal behavior, but also the sensitivity of the bubbling experiments to external noise. Yet it is the same simplicity of the experimental arrangements with bubbling experiments, which have made chaotic analysis

through bubbles a favorite. It is certainly easier to study chaos in a bubble column than to simulate it in earthquakes!

This research was carried out with two objectives

- 1 To identify a new control variable for bubbling
- 2 To tame chaos in bubbling by using the new control variable

These were two disjoint research directions. The first involved understanding the bubbling from the fluid mechanics point of view and studying the dynamics associated with the system. Once the system was quantified in terms of bubbling regimes and dimensionless numbers, the next step was to integrate the system information with control equations and set-up a scheme to implement the control. The latter phase of implementing the control algorithm was the most challenging. And it is this phase, where previous experience had showed, maximum investment was to be made.

Data acquisition and automation techniques were employed to generate large volumes of data for study. For the characterization studies of the bubble system, data analysis tools were built for data mining from the experimental data sets. Development of data analysis tools spurred study of statistical techniques like principal component analysis and wavelets to the bubbling data. Finally, to employ the control algorithm, real time computing modules were built for online analytical processing and simultaneous control. All of the software tools built for this experiment were in conjunction with Oak Ridge National Laboratory (ORNL) and are available through ORNL for evaluation. The reader is encouraged to contact the Duane D. Bruns research group at the University of Tennessee, Knoxville for an evaluation copy of the BUBBLE Toolbox for Chaotic Analysis© (Sarnobat, 2000) and the BUBBLE Automation Workbench© (Sarnobat, 2000) along with sample data for research purposes.

This research project has been documented in three parts, one as a part of this Master's thesis, a second as research papers submitted at the University of Tennessee, Knoxville and third as software releases through Oak Ridge National Laboratory

In the present thesis, the first chapter gives an introduction to the overall project. The second chapter updates the reader with concepts from research in bubbles and chaos control. The third chapter describes the experimental and data analysis techniques used. The fourth chapter presents the results and analysis from the identification of the bubbling system. The fifth chapter has results from the attempt to control chaos by using a well-known control algorithm. The sixth and final chapter details the conclusions and recommendations.

## Chapter 2

# **Background**

---

*The world that we have created thus far creates problems which cannot be solved at the same level we created them*

Albert Einstein

### *2.1 Electrostatic potential as an additional bifurcation variable*

Though a seemingly simplistic phenomenon, bubbling involves complex interactions between the gas and the liquid in play. The production of bubbles by various means is used in a plethora of technical applications, especially in the chemical and environmental engineering fields. Water treatment, metallurgy, froth flotation, fermentation, fluidization, and distillation are some widespread examples. Efficient gas-liquid processes introduce the gas in the form of small bubbles, since the greater interfacial area increases interphase heat and mass transfer. In an ideal



gas-liquid system, the bubbles are uniformly sized for even and predictable process performance, however, in reality, gas-liquid systems generally have a broad bubble-size distribution and complex dynamics (Kikuchi & co-workers, 1997, Femat 1998, Luewisutthichat & co-workers, 1997)

Bubble formation in a liquid from a submerged orifice has been the subject of numerous scientific studies, primarily aimed at theoretical prediction and experimental measurement and correlation of bubble size for prediction of interfacial area (Deshpande & co-workers, 1991, Terasaka & co-workers, 1992, Tsuge, 1986, Longuet-Higgins, 1991) Notable among these works is the development of an understanding that bubble size and bubbling frequency is influenced in a complex way on the interactions between consecutively formed bubbles At low gas flow rates, bubbling is regular and periodic, while at increasing flow rates bubble formation becomes irregular In their classic paper, Davidson and Schuler (1960) were perhaps the first to illustrate, through high-speed photography, the interaction between leading and trailing bubbles that leads to coalescence at higher flow rates Subsequently, several investigators have identified different regimes of bubbling, defined by dimensionless groups and characterized by different amounts of interactions between forming bubbles (Miyahara & co-workers, 1984, Tsuge & co-workers 1986) Models for the prediction of bubble volumes have been developed that incorporate the interaction between a primary bubble and subsequent bubbles at higher gas flow rates (Deshpande & co-workers, 1991)

With the availability of the advanced experimental equipment and the advent of the science of nonlinear dynamics, progress has been made recently in the understanding of bubbling Leighton and co-workers (1990) illustrated the complex hydrodynamic phenomena

present in bubbling through both high-speed imaging and acoustic signatures. Chaos in bubbling patterns was first reported by Tritton and Edgell (1993), who reported a period-doubling bifurcation with gas flow rate in bubbling of air from a single submerged orifice into water-glycerol mixtures. Mittoni and coworkers (1994), reported deterministic chaos in a similar system under a range of conditions by varying chamber volume, injection nozzle diameter, liquid viscosity and gas flow-rate. Similar results were obtained for bubbles by Tufaile & Sartorelli (2000). Nguyen and co-workers (1996), have demonstrated the spatio-temporal behavior of bubbles in single train of rising gas bubbles in a liquid column.

In the above studies, chaotic bubbling was studied primarily with flow rate as the bifurcation variable. Significant effects of external forces on bubbling, such as pulsing a flowing liquid (Fawkner and co-workers, 1988), and application of sound perturbations (Cheng, 1996, Tufaile & Sartorelli, 2000) have been demonstrated. Most notably, Tufaile & Sartorelli (2000) reported the capability to transform a chaotic bubbling state to a periodic state by the application of a synchronized sound wave.

The aim of the present study is to explore whether an applied electrostatic potential can be used as an additional bifurcation variable in bubbling dynamics. If successful, then electrostatic potential can be employed for control.

Zaky and Nossier (1977) first reported the effect of an electric field on bubbling, noting a decrease in bubble size and an increase in pressure upstream of the nozzle with increasing voltage for bubbling of air into transformer oil and n-heptane through an electrified needle. Further studies by Ogata et al (1979, 1985) and Sato et al (1979, 1980) showed that by the application of a few kilovolts, bubble size can be reduced from a few mm to less than 100  $\mu\text{m}$  in

many liquids, including nonpolar fluids like cyclohexane and polar compounds such as ethanol and distilled water. Sato and coworkers (1993) reported similar results for liquid-liquid systems in which the time scale of electrical charge relaxation (i.e., permittivity/conductivity) of the injected fluid is greater than that of the continuous fluid. This type of dispersion has been termed "inverse electrostatic spraying" (Tsouris et al. 1998) to differentiate it from the well studied "normal" electrostatic spraying (Grace and Marijnissen 1994). Several practical applications have been suggested for this type of spraying, including generating fine bubbles for flow tracers (Sato et al. 1980), enhancing gas-liquid reactions (Tsouris et al. 1995), and producing uniform microcapsules (Sato et al. 1996).

Two main controlling mechanisms have been identified — electric stress and electrohydrodynamic flows. The electric stress acts directly at the gas-liquid interface of growing bubbles and is directed inward (Tsouris et al. 1994, Harris and Basaran 1995). This force is manifested by an increase in nozzle pressure with an increase in applied voltage. Above a critical voltage whose magnitude depends on nozzle geometry, electrohydrodynamic flows are induced in the bulk fluid (Sato et al. 1980, 1993, 1997). These toroidal flows have a significant velocity near the injection nozzle and are directed outward from the points of highest field gradient. Under conditions of electrohydrodynamic flow, a significant decrease in nozzle pressure is exhibited with increasing voltage (Tsouris et al. 1998). The dynamics of electrified bubbling are complicated by the interactions of these mechanisms. Sato (1980) described three regimes of bubbling: periodic bubbling, dispersed bubble production, and a high-voltage region characterized by sparking and larger bubble production. Similarly, Shin et al. (1997) outlined three bubbling modes — dripping, an erratic mixed mode, and a spraying mode. These modes were roughly characterized by flow rate using a Reynolds number, and by a combination of

electrical forces and buoyancy forces using a modified Weber number. To date, no detailed study of the dynamics of electrified bubbling has been conducted, for example, it has not been verified that the regimes characterized as periodic are truly periodic, nor are there any detailed analyses and/or means of prediction of the transitions from periodic bubbling. Beyond its intrinsic scientific value, such information would be highly valuable in guiding the production of monodispersed droplets/bubbles.

In the present study, the effect of an applied electrostatic potential on bubbling dynamics was determined experimentally. In these experiments, bubbles were formed in a sufficiently viscous liquid (glycerol) such that electro-hydrodynamic flows were negligible and the main electrostatic mechanism affecting bubbling was the electric stress at the gas-liquid interfaces of the forming bubbles. Deterministic chaos analysis was applied to signals of the temporal fluctuation of pressure in the injection nozzle during bubbling under controlled experimental conditions to probe the combined effect of flow rate and applied voltage on bubble formation dynamics.

## 2.2 *Chaos & feedback control*

Identification of electrostatic potential as an additional bifurcation variable provided the basis for further investigation into control of bubbling processes using electrostatic potential as the additional control variable. Study of chaos and understanding the chaotic patterns involved is necessary for implementing control on the bubbling process.

Since the classic paper by Ott, Grebogi and Yorke, (1990) controlling chaos in physical

systems has been investigated by many researchers (Ditto & co-workers, 1990,1995, Hunt, 1991, Roy et al, 1992, Garfinkel & co-workers, 1992, Rollins & co-workers, 1993, Petrov & co-workers, 1993) This section begins with an introduction to concepts of chaos, and then proceeds to develop the Ott, Grebogi and Yorke, (OGY) control algorithm for a 2-dimensional system (Ditto & co-workers, 1990) A development for multi-variate OGY control is also presented

## 2.2.1 Concepts of chaos

Dynamical systems can be represented by equations of motion, which can be written as

$$\dot{x} = F(x, p, t) \quad (1)$$

for continuous systems and

$$x = F(x, p, n) \quad (2)$$

for discrete systems In these equations, we have  $x \in \mathbb{R}^N$ , which are state variables,  $p \in \mathbb{R}^{N_p}$ , which are system parameters, and  $F(\cdot)$ , which is a set of  $N$  equations describing the behavior of the system The solution to equation for continuous systems moves in a  $N$ -dimensional space called the *phase space* and is usually solved numerically The basis of this space is given by the state variables  $x$ , i.e. the location of the state of the system is determined by taking all the state variables as orthogonal coordinates in the phase space The system starts out at a certain *initial condition*  $x_0 = x(t=0)$  in space From the initial condition, dynamical systems trace smooth trajectories in phase space as they proceed in time The shape in phase space that the trajectory approaches as  $t \rightarrow \infty$  is called the *attractor* of the system For periodic motions these

trajectories are loops that are traced repeatedly with every period of the system

Chaos can be termed as the superposition of a very large number of unstable periodic motions. A chaotic motion may dwell for a brief time on a motion that is very nearly periodic and then may change to another motion that is periodic with a period that is perhaps five times that of the original motion and so on. The constant evolution from one (unstable) periodic motion to another produces a long-term impression of randomness, while showing short-term glimpses of order (Ditto et al, 1995)

Sensitivity to initial conditions is a hallmark of a chaotic systems. For a chaotic system, there are a very large number of trajectories corresponding to each unstable periodic motion, which pass close together. A small perturbation can shift the system from one trajectory to another. Thus for small changes in the initial state, the subsequent behavior of a chaotic system can appear to be very different.

The phase space trajectories contain all the information necessary to predict the future dynamics of the system. But phase space plots can be complicated and Poincare sections of phase space plots, which are obtained by cutting through the phase space with a plane, are used for simplification (**figure 2.1**). The infinite numbers of points in the phase space are thus reduced and the information contained is more manageable. The number of points in the Poincare section reveals the underlying periodicity of the system. Usually any periodic system of period  $n$  has a section, which consists of a finite set of  $n$  distinct points, which reflect the fundamental periodicity of the system. However for chaotic systems, the superposition of infinite number of periodic motions causes infinite number of points in the section.

In general the evolution of a chaotic system converges to an extended geometric structure

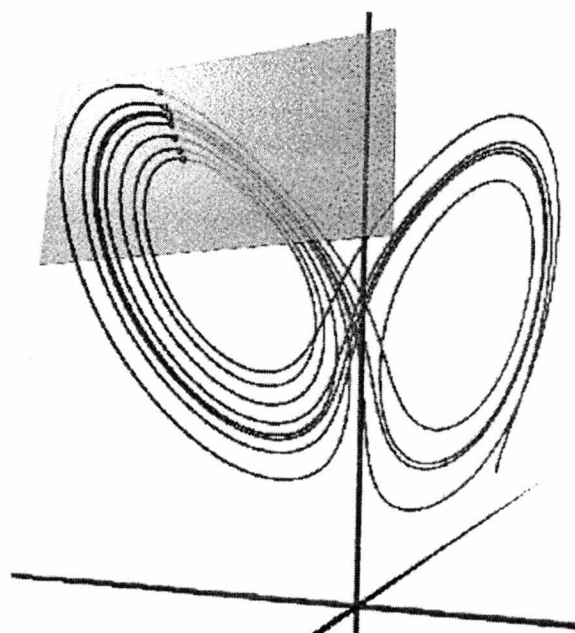


Figure 2.1. Phase space trajectories and the Poincaré section

*(Source: Van Goor, 1998)*

(the chaotic attractor), which is an infinitely long path (implying that it is not periodic motion), but at the same time does not completely fill up the state space, (implying non-random behavior, because a truly random system will have trajectories, which cover the entire volume of phase space available to the system)

In order to control chaos according to the OGY scheme it is only necessary to identify an unstable periodic point in the attractor, to characterize the shape of the attractor locally around that point and to determine the response of the attractor at that point to an external stimulus

The OGY scheme can replace the Poincare section by a delay coordinate embedding. This embedding depends on the recognition that information obtained by measuring all the system variables (position and momenta) at one given time may also be obtained by only one system variable obtained at several subsequent times. This system state vector (the set of all the positions and momenta,  $x_n = (x^1(t_n), x^2(t_n), \dots, p^1(t_n), p^2(t_n), \dots)$ ) is replaced by a delay coordinate vector,  $(x'(t_n), x'(t_n - \Delta t), x'(t_n - 2\Delta t), x'(t_n - 3\Delta t), \dots)$ , where the superscript I indicates on a particular experimental measurable and where  $\Delta t$  is some appropriately chosen delay. In other words the dynamics in full space can be reconstructed from measurements of just one time dependent variable and this time dependent variable carries sufficient information about all the others. For an N degree of freedom system with time series  $x(t)$ , the signals are plotted versus the delayed or advanced signals by a fixed time constant. The time series generates a trajectory  $p(t)$  in N dimensional space

$$p(t) = \{x(t), x(t + \Delta t), x(t + 2\Delta t), \dots, x(t + m\Delta t)\} \quad (3)$$

where  $m$  is the embedding dimension and  $k$  is the time delay or time lag. According to Takens'



theorem the rule of thumb for selecting time delay of lag involves satisfying the following criteria  $m > 2d + 1$ , where  $d$  is the actual dimension of the attractor (Takens, 1981) The choice of  $m$  and  $\Delta t$  are not crucial except to avoid a natural period of the system

The OGY control scheme requires the attractor to be characterized and an unstable fixed point on the Poincare section identified, about which control is desired Then the motion of the point representing the current system state along the stable and unstable directions is identified The stable and unstable directions on the map are the directions in the neighborhood of the unstable fixed point, in which the current system state is seen to approach and depart to the neighborhood of the fixed point These two directions form a saddle around the unstable point These directions (*eigenvectors*), along with the speed (*the eigenvalues*), with which the points approach the fixed point (or depart from the fixed point), characterize the shape of the attractor locally around the fixed point The OGY control algorithm uses this property of chaotic systems to identify the direction in which control is implemented These eigenvectors manifest themselves as stable and unstable manifolds on the time return map, which is a low dimension projection of a time delay embedding On the time return map, the unstable manifold lies along the tangent to the chaotic attractor evaluated at the location of the fixed point

## 2.2.2 OGY control

The OGY method waits for the system to land close to the desired fixed point Once the system is close to the fixed point, the control algorithm perturbs a parameter  $p$  such that the next iteration falls onto the stable manifold of the unperturbed system (**figure 2.2**) The system

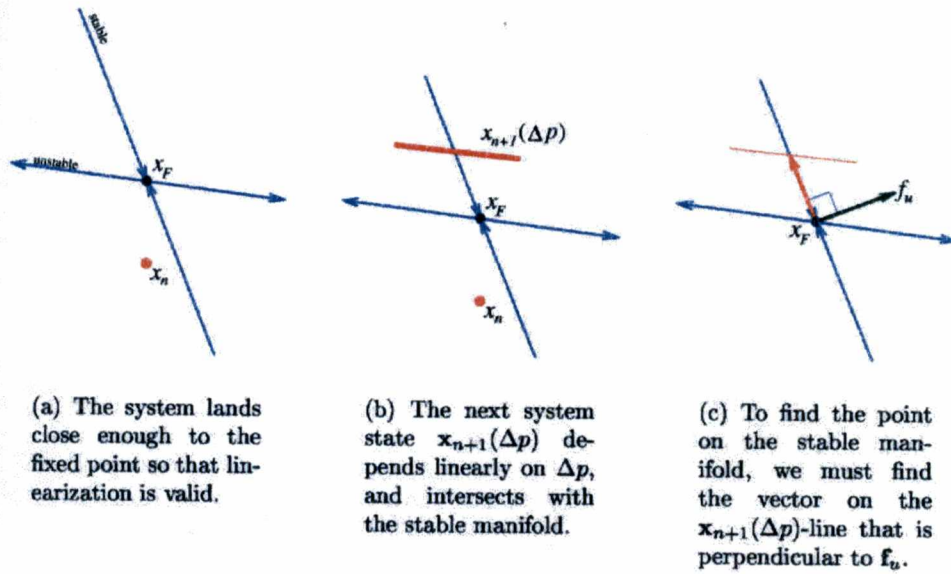


Figure 2.2. OGY control algorithm

(Source: Van Goor, 1998)

dynamics will then naturally draw the system closer to the fixed point. The derivation of the OGY algorithm is as follows. The algorithm is based on the linearization of the system close to the location of the fixed point, where the linearization is assumed to be valid. This is a reasonable assumption as the fixed point maps to itself. The linear dynamics can be expressed as

$$x_{n+1} - x_F(p) = M(x_n - x_F(p)) \quad (4)$$

where  $M \in \mathfrak{R}^{N \times N}$  is the mapping matrix. The mapping matrix  $M$  is characterized by its eigenvectors and eigenvalues

$$\begin{aligned} Me_u &= \lambda_u e_u \\ Me_s &= \lambda_s e_s \end{aligned} \quad (5)$$

where the subscripts  $u$  and  $s$  correspond to the unstable and stable directions respectively. The eigenvectors are normalized but may be non-orthogonal. The eigenvalues satisfy the condition,  $|\lambda_s| < |\lambda_u|$

Let us consider the space to be two-dimensional. For a two-dimensional map,

$$x = \begin{bmatrix} x_1 \\ x_2 \end{bmatrix} \text{ or } x^T = [x_1 \quad x_2] \quad (6)$$

In this two-dimensional space there is a map that depends on a parameter  $p$ .

$$x_{n+1} = f(x_n, p) \quad (7)$$

The fixed point for this map is also a function of the parameter  $p$

$$x_F = f(x_F, p) \quad (8)$$

Thus if the parameter is changed every iteration the fixed point also changes

$$x_F(p_n) = f(x_F(p_n), p) \quad (9)$$

The shift vector  $s$  for the estimation of the perturbed fixed point is given by

$$\begin{aligned} x_F(p_{n+1}) &\sim x_F(p_n) + (p_{n+1} - p_n)s, \\ s &\equiv \frac{d}{dp} x_F(p) \Big|_{p=p_n} \sim \frac{x_F(p_{n+1}) - x_F(p_n)}{p_{n+1} - p_n} \end{aligned} \quad (10)$$

In the vicinity of the fixed point, the map can be represented by a two dimensional square matrix for two-dimensional space

$$\begin{aligned} (x_{n+1} - x_F) &\sim M(x_n - x_F), \\ x_{n+1} &\sim x_F + M(x_n - x_F) \end{aligned} \quad (11)$$

If the current state is  $x_n$  state of the system after the next iteration depends on the value of the nominal parameter  $p_o$ , and the perturbation  $\Delta p$  we apply to it. To find an equation for  $x_{n+1}$ , we have,

$$x_{n+1} = x_F(p_o + \Delta p) + M(x_n - x_F(p_o + \Delta p)) \quad (12)$$

Expanding this into a first order Taylor series, we find

$$x_{n+1} = x_F(p_o + \Delta p) + s\Delta p + M(x_n - x_F(p_o) - s\Delta p) \quad (13)$$

The current state of the system is shown in figure 2 2(a). Equation (13) is shown as a red line in figure 2 2(b). To force the system towards the fixed point, state should be on the stable manifold. To express this condition mathematically, a change of basis is required with the new basis vectors,  $f_s$  and  $f_u$  defined normal to the unstable and stable manifolds respectively. In the new co-

ordinate system,  $(x_{n+1} - x_F)$  has to be orthogonal to the basis vector  $f_u$ , (which is in turn orthogonal to the stable direction  $e_s$ )

This can be expressed as

$$f_u^T (x_{n+1} - x_F) = 0 \quad (14)$$

The vectors  $f_s$  and  $f_u$  can be shown to be the left eigen vectors of  $M$ , and are defined as

$$\begin{aligned} f_u^T M &= \lambda_u f_u^T \\ f_s^T M &= \lambda_s f_s^T \end{aligned} \quad (15)$$

The left and the right eigenvectors are related through the relation

$$\begin{bmatrix} f_u \\ f_s \end{bmatrix}^T = [e_u \quad e_s]^{-1} \quad (16)$$

By replacing  $(x_{n+1} - x_F)$  we get

$$0 = f_u^T M(x_n - x_F(p) - s\Delta p) + f_s^T s\Delta p \quad (17)$$

By replacing  $M$  with its eigenvectors

$$0 = \lambda_u f_u^T (x_n - x_F(p) - s\Delta p) + f_s^T s\Delta p \quad (18)$$

Solving for  $\Delta p$  and substituting  $\Delta x_n = x_n - x_F(p)$ , we get the OGY formula

$$\Delta p = \frac{\lambda_u}{\lambda_u - 1} \frac{f_u^T \Delta x_n}{f_u^T s} = c \Delta x_n \quad (19)$$

**Comments**

The OGY control algorithm is basically a linear model, and it does two things

- 1 If the point is on the stable manifold, no action is taken
- 2 If the point is not on the stable manifold, it tries to push it onto the stable manifold

If the final formula is analyzed, it can be explained as the product of a gain, and a ratio of the current direction  $\Delta x$ , of the system to a base case,  $s$ . On the numerator, the factor  $f_u^T \Delta x$  gives the component of the system along the unstable direction. If the system is orthogonal to the unstable eigenvector and is along the stable eigenvector (assuming a 2-dimension space), and it will map to the fixed point and requires no external perturbation (dot product of orthogonal vectors is zero). After the point proceeds to the unstable direction the control output tries to force it onto the stable manifold and this is possible near the fixed point where the system is at its linear best. As the system goes away from the fixed point, the dot product increases and control output is maximum when the system moves along the unstable manifold trying to force it onto the stable manifold.

The basic assumption of linearity in the OGY control algorithm is that the eigenspace does not change for the system in vicinity of the fixed point. With a small perturbation in the fixed-point location, the stable and unstable manifolds change to orient themselves such that the eigenspace remains the same. This is true for linear systems only, but can be extended to non-linear systems when the change in the eigenspace is not large.

Equation (19) allows for only one system parameter to be controlled because the equation (12) has only one degree of freedom as shown in figure 2.2. The univariate OGY is based on

finding an intersection between the equation for the system state and the stable manifold. For univariate OGY to succeed, there cannot be more than one unstable direction as the control algorithm adjusts the placement of the saddle fixed point through small perturbations of the control variable. Thus, the number of independent control variables needed should be equal to the number of unstable directions. For multi-dimensional spaces, a multi-dimensional return map is plotted and information is extracted for multi-variate control.

### **Multi parameter OGY**

*The development of the multivariate OGY control algorithm has been presented by Van Goor, (1998)*

Rewriting equation for the system state,

$$x_{n+1} - x_F(p) = S\Delta p + M(x_n - x_F(p_o + \Delta p)) \quad (20)$$

where we now have a  $N$ -dimensional system with  $N_u$  unstable directions and  $N_s$  stable directions, ( $N = N_s + N_u$ ). In this equation,  $\Delta p \in \mathbb{R}^{N_p=N_s}$  and  $S \in \mathbb{R}^{N=N_u}$  is defined as

$$S = \begin{bmatrix} | & & | \\ \frac{\partial x_F}{\partial p_1} & \dots & \frac{\partial x_F}{\partial p_{N_u}} \\ | & & | \end{bmatrix} \quad (21)$$

Thus we have

$$x_{n+1} = Mx_n + (S - MS)\Delta p \quad (22)$$

If  $x_{n+1}$  is to be on the stable manifold, then  $\Delta x_{n+1}$  can be expressed as a linear combinations of the

stable eigenvectors of  $M$

$$x = V_s \alpha \quad (23)$$

where  $V_s \in \mathbb{R}^{N \times N_s}$  and  $\alpha \in \mathbb{R}^{N_s}$

Equating we have,

$$V_s \alpha = Mx_n + (S - MS)\Delta p \quad (24)$$

Rearranging,

$$J\Delta x_n = \begin{bmatrix} (S - JS) & V_s \end{bmatrix} \begin{bmatrix} \Delta p \\ -\alpha \end{bmatrix} \quad (25)$$

Solving for  $\Delta p$

$$\begin{bmatrix} \Delta p \\ -\alpha \end{bmatrix} = \begin{bmatrix} (S - JS) & V_s \end{bmatrix}^{-1} J\Delta x_n \quad (26)$$

Here only the first  $N_s$  elements of the left hand matrix need to be calculated  $\Delta x_n$  is multiplied with a fixed  $N_s \times N$  matrix to obtain the needed parameter perturbations to drive the system into the stable manifold

## 2.3 Summary

In this section, the literature survey for bubbling systems was presented. It was noticed that chaos in bubbles has been observed only in the past decade and that attempts to control bubbling concentrated on using flow-rate as the manipulated variable. The effect of electrostatic



potential on bubble/droplet formation has also been reported to be profound, both in terms of the bubble size and frequency. An introduction to chaos and development of a control scheme suggested by Ott, Grebogi & Yorke (1990), has been presented.

## Chapter 3

### **Methods**

---

*Perfect logic and faultless deduction make a pleasant theoretical structure, but it may be right or wrong,*

*The experimenter is the only one to decide, and he is always right*

L Brillouin, Scientific Uncertainty and Information, 1964

### 3.1. Experimental

#### 3.1.1. Introduction

This beauty of this experimental set-up was its pristine simplicity. All it consisted of was a single gas train, which culminated in a pearly column of bubbles. It is indeed fascinating to venture into the dynamics of a system as simple and discover and analyze details and patterns so complex. Not only were the results intriguing, the whole ordeal of obtaining the data soon became one of the riveting highlights of this experiment with The BUBBLE Automation WorkBench © (Sarnobat, 2000) for LabView™ and The BUBBLE Chaotic Analysis Toolbox © (Sarnobat, 2000) for MATLAB™. Screen shots have been provided in the appendix.

### 3.1.2. Set-up Details

A schematic of the experimental apparatus is shown in the **figure 3.1** The apparatus consisted of a gas flow and metering system, a data acquisition system, a pressure transducer for monitoring the response of the system and a high voltage power

supply for maintaining an electrostatic field between the nozzle and the ground electrode The high voltage power supply used was Bertan series 225, 0-50kV, regulated high voltage power supply, with remote analog high voltage programming, and remote analog high voltage & current monitoring, via a rear panel connector The high voltage power supply was interfaced with a PC-based controller through a data acquisition board and, controlled and monitored remotely A high voltage 'ripler'<sup>1</sup> was built in-house to add a +/- 450 V DC ripple to the output generated by the high voltage power supply This component was built because of the slow response time (1-4s) of the high voltage power supply to step from high voltage to low voltage The 'ripler' could respond to control moves at 500Hz

#### 3.1.2.1. The glass column

A square glass column of 4x4 cm cross-section and 28 cm in height was constructed The top of the glass column was sealed with a rubber gasket and plexiglass cover fitting with a fitting for attaching an outlet tube The plexiglass cover was also fitted with a ground electrode through a 1/8-inch Swagelok fitting The ground electrode was maintained at a depth of 2.5 cm in the glycerin The value was determined by carrying out various trials with different the electrode

<sup>1</sup> The author acknowledges the creativity of Boyce O. Griffith who was instrumental in the voltage 'ripler' being constructed

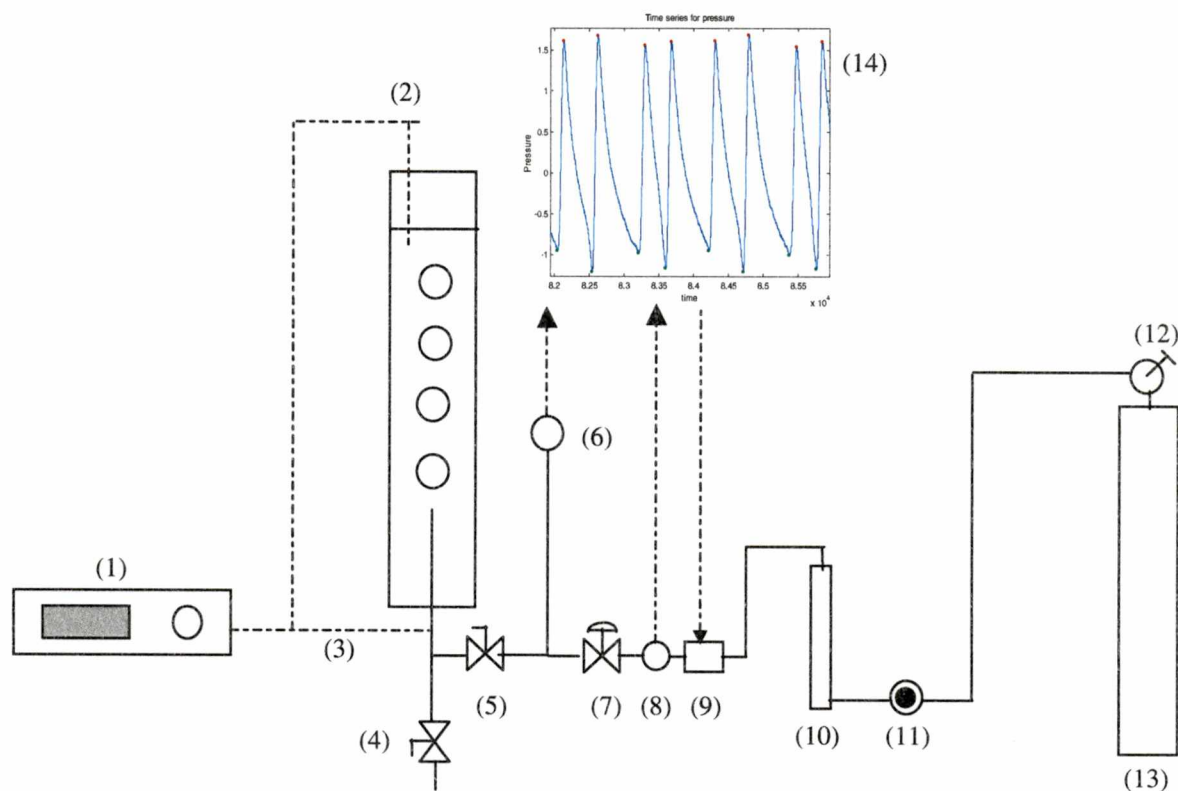


Figure 3.1. Experimental schematic:

(1) High voltage power supply (2) Ground electrode (3) Positive electrode (4) Drain valve (5) Stop valve (6) Pressure transducer (7) Needle valve (8) Flow meter (9) Piezo-electric valve (10) Rotameter (11) Pressure reducer (12) Pressure regulator (13) Nitrogen gas cylinder (14) Data acquisition system

inserted at different depths. It was found that for the trials with a greater surface area of the electrode exposed, the current through the liquid was higher, than it was when a lesser length of the electrode was inserted into the liquid. As a result of the greater current passing through the liquid, the power supply tripped at a lower voltage, thus reducing the range through which the voltage could be varied. With the selected length of the electrode, the power supply could be set to up to 13kV before the current exceeded the hardware limit of 0.3 mA.

Gas was injected into the column through a plastic nozzle with a metal cap orifice, which was electrified with the help of a copper wire passing through the plastic nozzle. The construction of the nozzle is discussed in further detail later in this section. A liquid solution consisting of 99.98% pure glycerin was normally maintained at 8.5 inches above the nozzle.

### *3.1.2.2. Gas flow and metering system*

The type of gas used was chosen so as not to react with the liquid. Nitrogen was found to be satisfactory; it did not contain significant amounts of moisture. Normal compressed air was not chosen because of the possibility of the liquid absorbing moisture from air, which would then change the conductive properties of liquid. Nitrogen was preferred over dry air because of its property of inertness. The liquid was found to be highly sensitive to moisture and so the column was always kept covered. The gas train used in the characterization experiments, consisted of a pressure regulator, a rotameter, a piezo-electric valve, a flow-meter, a flow control needle valve, a pressure transducer and a stop valve, which were all connected in series. A Brooks' model SHOR-RATE II of tube number R-2-15-D rotameter (6 inch) with stainless steel floats was used for measuring the gas flow rates covering a range of 10-500 cc/min. Since throttling at the control

valve tends to minimize fluctuations in the gas flow-rate upstream of pressure transducer, a fine NUPPO type needle valve located downstream of the rotameter was used to improve gas flow measurement. The key reason for using this needle was to keep the stability of the gas flow constant over the range of investigated flow rates and to minimize the volume between the valve and the nozzle. Without this valve variation of airflow was found at the rotameter due to bubble formation and also the detachment at the nozzle or the damping effect of the gas holdup section. For latter part of the experiments, this was replaced with a MaxTek MV-112 piezo-electric valve with a response time of the 70 microseconds. This valve was interfaced with the DAQ card and accepted a 0-5V, DC. A Cole-Parmer 8168 gas flow meter was used to return the flow rate of both as a digital display signal as well as a 0-5V DC output.

The gas inlet nozzle was equipped with a 0.75-mm internal diameter orifice, which was electrified by a copper wire passing through the nozzle. An elbow in the gas inlet tube prevented liquid buildup in the gas inlet line and residual liquid build-up could be drained periodically using a drain valve. Failure to remove these residual liquids resulted in erratic "burping" of the gas as the bubbles formed at the tip of the nozzle.

A pressure transducer (Setra Systems model 228, having a range from 0 to 1 psig) measured the inlet line gas pressure just before the stop valve. The output from the pressure transducer was a 0-5 V DC analog signal, which was fed to the data acquisition board through a signal amplifier, which was set at 10 $\times$  amplification. The drawback of this transducer was its relatively high time lag (1-3 ms). For latter control part of the experiments, an Endevco piezo-electric pressure transducer (range of 1 psig), was used for high accuracy and lower response time (70 micro-seconds). The signal was fed to a National Instruments' SC-2043-SG signal conditioning card, which provided the necessary excitation and was later fed to the data

acquisition card

### *3.1.2.3. Liquid selection*

Some researchers have shown that the bubbling systems can exhibit chaotic behavior by using low concentrations of glycerin and liquids other than glycerin Chakka (1994), investigated the influence of liquid density and viscosity on the dynamics of bubble behavior The results from this experiment suggested that glycerin exhibited the most regular behavior and the clearest apparent bifurcation sequence among three liquids, which were studied (i.e. glycerin, karo syrup and water) Apart from these factors, experiments conducted with electrostatic fields suggested that only glycerin allowed very high voltages to be applied without appreciable current passing through the liquid Glycerin with an assay of 99.98% (Fisher Chemicals) was chosen The high voltage power supply used in the experiment allowed a maximum of 0.3mA of current, before the supply tripped By adjusting the length of the ground electrode immersed in the glycerin, the power supply could withstand a maximum voltage up to 13kV, before the current exceeded the limit and the power supply tripped

Glycerin was found to be highly sensitive to moisture in the atmosphere It was also observed that the conductivity of glycerin increased with time, as electric voltage was applied to the liquid For consistent experimental conditions, fresh glycerin was used for each run, a run being defined as data taken at a constant flow rate, by changing the applied voltage in increments of 1000V from 0V to 10000V, with time intervals of 300s between successive readings, a reading being defined as a snapshot of data being taken for a certain length of time at a constant flow-rate and voltage

### 3.1.2.4. Data acquisition system

The data acquisition system consisted of a National Instruments<sup>TM</sup> PCI-MIO-16E-50 data acquisition board, (DAQ board) was used with a Pentium<sup>TM</sup> based PC. National Instruments<sup>TM</sup> Labview<sup>TM</sup> ver 5.1 was used as the data acquisition software. The DAQ board was configured for differential analog inputs (namely, pressure, current, voltage, output voltage monitor, flow), and differential analog outputs (namely, voltage output to the power supply, piezo-electric valve). The data was taken for 50s at 2000Hz or 5000 Hz, totaling either 100,000 or 250,000 data samples for each reading. For each flow-rate, 11 different voltage settings were used. The data was stored as spreadsheet files which were automatically loaded into MATLAB<sup>TM</sup> for data processing. The experiment was successfully automated through networking of two computers, with one computer handling the data acquisition and the other computer doing the data analysis as soon as the run was completed. Two separate configurations were used: one for the simple data acquisition runs and the real time simultaneous AI/AO. For the control aspect of the experiment, a LabView *vi*<sup>2</sup> was configured for simultaneous analog input and analog output from 125 Hz to 500 Hz. This aspect of the experiment has been described in detail in a separate report (Sarnobat, 2000).

<sup>2</sup>*vi* 'virtual instrument', jargon used by National Instruments for routines created with graphical programming interfaces in LabView<sup>TM</sup>

### 3.1.2.5. Nozzle construction

The nozzle was constructed keeping in mind two details (**figure 3.2**)

- 1) The orifice diameter
- 2) Chamber size



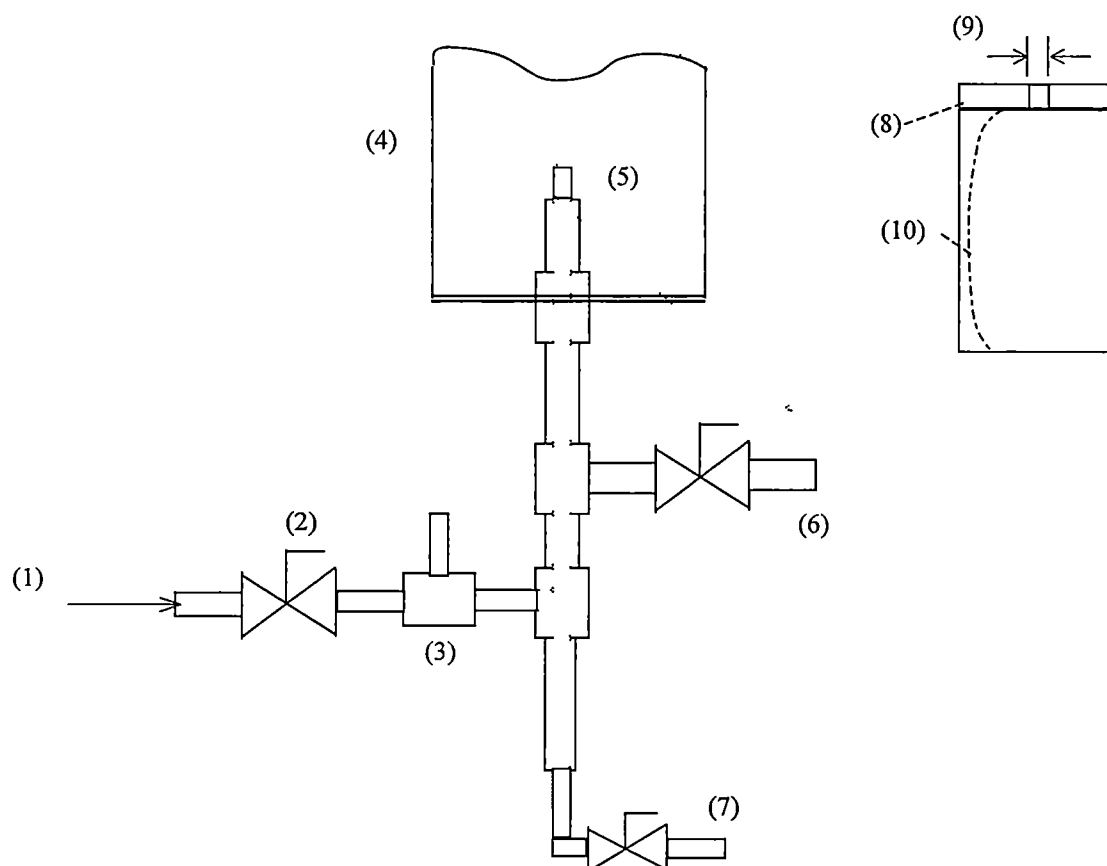


Figure 3 2 Nozzle construction details

(1) Gas inlet (2) Stop valve (3) Positive electrode connected to nozzle tip (4) Glass column (5) Nozzle tip (6) Column liquid drain (7) Drain for accumulated glycerin (8) Metal cap (9) 0.75mm ID orifice (10) Copper wire

Test runs were carried out in this investigation with a nozzle having a 1mm orifice diameter. The results from this plotted were plotted and rather 'strange-looking' return maps found. So, a slightly smaller orifice diameter & a larger chamber size than previous work (Cheng, 1996) was chosen. This was primarily based on the results obtained from test runs with the 1mm diameter nozzle. It was observed that the glycerin sometimes 'wepted' through the orifice and caused erratic 'burping' of the liquid, causing a renegade spike in the pressure signal. Increasing the chamber volume ensured that the liquid which wepted through could be drained via a tee-bend in the nozzle design.

*(The column should be drained prior to switching the gas supply off. In case the glycerin weeps into the gas inlet line, the line should be purged with acetone or methanol and then air/nitrogen keeping the drain open)*

### 3.1.3. Procedure

The experiments were carried out as a series of runs where the flowrate was held constant and the voltage gradually stepped up by increments of 1000V from 0V to 10,000V. The flow rate was varied from lowest permissible flow-rate of a slow period-1, and increased in steps of 5 absolute rotameter units to a highly chaotic bubbling regime. The experiment was automated using LabView and so a large number of runs could be carried out with high efficiency. The automation program varied the voltage, waited for stabilization of the bubbles, which was observed to be less than 300s, checked for instabilities in the high voltage and logged the data acquired as a text file with a record of the date, time, flow and voltage at which the data was recorded at. The rotameter flow rate had to be set manually. The data file contained pressure, voltage and current time series. The data was then preprocessed and variables stored as binary

files, which were later used in conjunction with an indigenously developed, GUI-based MATLAB Bubble Toolbox© to generate various plots for data analysis. The volume of data generated was very large as each run contributed to a data file cumulatively sized at 40MB.

## 3.2. Data analysis

Various approaches have been adopted for the data analysis of bubbling systems involving chaos. Fractal and deterministic chaos analyses have been adopted to analyze the complex dynamic behavior of multi-phase reactors. Hurst exponents from rescaled-range analysis, various types of fractal dimensions, Kolmogorov entropy and Lyapunov exponents have been used to characterize different hydrodynamic regimes and transitions among them (Kikuchi and co-workers, 1997, Ruzicha, 1997, Leuwisutthichat and coworkers, 1997).

This study was carried out to study the period doubling bifurcation route to chaos with electrostatic fields as the bifurcation variable. The following data analysis techniques were used for the characterization of chaotic bubble behavior.

### 3.2.1. Power spectra

The classical linear method for analyzing time series was used to transform the information into the frequency domain using Fourier analysis. Fourier analysis proved to be highly sensitive to changes in periodicity of the bubbling system. Femat & co-workers (1998), effectively used power spectra to study periodic-quasiperiodic-chaotic routes. Transitions from one regime to another could be very effectively identified as long as the system was not close to

chaos. When the system went chaotic, the regime could not be predicted conclusively, though it indicated the possibility of chaos. In this study, power spectrum distribution was used to identify the periodicity of bubbling in conjunction with a neural network.

### *3.2.2. Bifurcation and route to chaos*

Bifurcation plots have been widely used in literature (Martien & co-workers, 1985, Mittoni & co-workers, 1994, Tufaile & co-workers, 2000) to illustrate impending chaotic behavior in dynamical systems as a series of changes in the nature of the periodic motions as a result of a variation in some process input variable. For the bubbling process, the changes were quantified in terms of the period of formation of the bubble. Extensive 3-dimensional bifurcation plots were generated to compare and study the simultaneous effect of both electrostatic potential and flow rate on the system.

### *3.2.3. Time return maps*

Time series signals give all the information one needs to observe the dynamics of a system. But the nature of the information can be simplified with the help of time return maps or a Poincare map, without loss of the information about the dynamics of the system. Time return maps were used to transfer all the information of a non-linear time series of pressure measurement and give a visual aid to determine the exact fundamental periodicity of the system (Moon, 1992). For generating a time return map, a period of formation vector was generated by measuring either the peak-to-peak time distance or the time distance between the troughs.

Another method often cited in literature (Nguyen and co-workers, 1996), is used in conjunction with a zero crossing distance of the waveform. For the control aspect of the experiment, zero-crossings were used with the advantage of faster implementation.

### *3.2.4. Phase space reconstruction*

A classical phase space trajectory plotting of a dynamic system of  $N$  dependent variables requires  $N$  dimensions with orthogonal coordinate directions in order to represent each dynamical variable. But, this is limited by the amount of data available for analysis (Takens, 1981). For a system governed by an attractor, the dynamics in the full phase space can be reconstructed from measurements of just one time dependent variable, and this time dependent variable carries sufficient information about all the others (Takens, 1986). Phase space plots were used to conclusively establish the existence of chaos and identify the periodicity of the system.

### *3.2.5. Multivariate statistical techniques*

The periodicity of the bubbling process was modeled using statistical techniques such as regression, principal component analysis, linear and non-linear partial least squares (Sarnobat & Hines, 2000). This was an innovative approach to modeling the bubbling using a data based approach to attempt a numeric model for real time periodicity identification. The input data used was a histogram plot of the period of formation of the bubbles, which was 'regressed' onto a 'regime vector' (**figure 3.3**). The output of the model returned a number (from 1 through 16), which indicated the regime of the bubbling as perio-1, -2, -4 or chaos. Numbers higher than 4 indicated the existence of chaos. Numbers between any two states indicated the extent to which

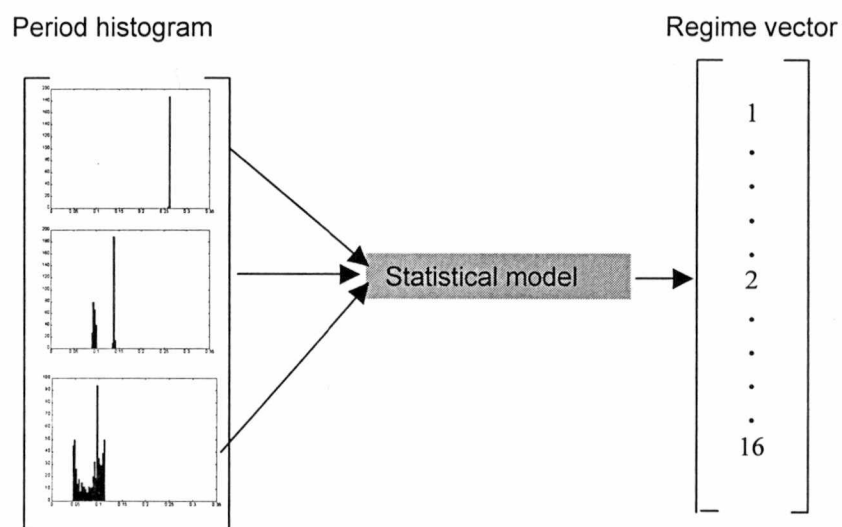


Figure 3.3. Multivariate statistical techniques used to predict the bubbling regime from the period of formation data.

the system corresponded to each regime. The training data used was generated manually by visually inspecting the entire data set for the regime the system was in. Results from this analysis are referenced in a separate paper by Sarnobat & Hines (1999).

### *3.2.6. Neural network model for regime identification*

A neural network model was trained by linear vector quantization (Tsoukalas, L H, and co-workers, 1997) for identification of the periodicity of the bubbling. Information about the bubbling regimes was extracted by frequency domain analysis using power spectra and identifying fundamental peaks. The fundamental bubbling frequency, (average bubbling frequency), was fed into the neural network along with 5 characteristic peak heights. The neural network used a Kohonen map, (Tsoukalas, L H, and co-workers, 1997) to cluster the data and the output was the cluster the input belonged to. The network could have discrete outputs of 1,2,4 and chaos. A scheme for real time identification of bubbling periodicity and change in periodicity was identified (**figure 3.4**), (Sarnobat & co-workers, 1999).

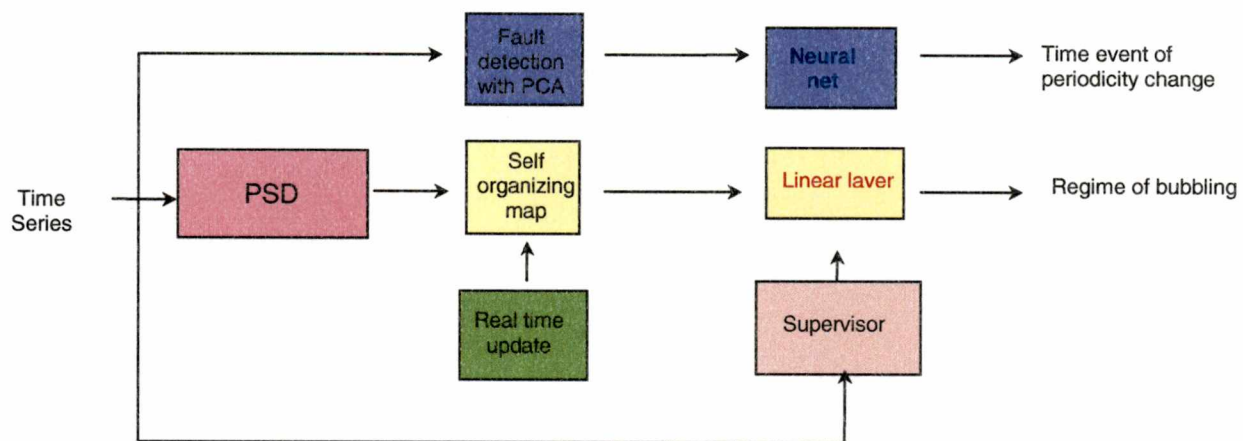


Figure 3.4. Real time identification and fault identification



## Chapter 4

# ***Modification & Analysis***

---

*What will prove altogether remarkable is that some very simple schemes to produce erratic numbers behave identically to some erratic aspects of natural phenomena*

Mitchell Feigenbaum, 1980

Visually, the bubbling experiment was really beautiful to observe. From a single steady train of pearly bubbles at higher periodicities, to a sequence of alternating bubble sizes and finally a flurry of bubbles when the system goes into chaos. The dynamics of this system needed to be understood and analyzed before trying to control the bubbling phenomenon. This called for visualizing the system in various subspaces, reading the underlying order of the bubble sizes and finally crystallizing all the observations into a control algorithm. This section deals with the deductions made from the experimental data.

### ***4.1. Formation of a single bubble***

As a bubble is produced, the pressure in the gas inlet upstream changes. Therefore the line pressure in the gas stream can characterize bubbling. The output of the pressure transducer

measuring the pressure upstream of the nozzle was fed to the computer through a DAQ card and the pressure trace seen with LabView in real-time as the bubble is being formed. As a bubble is formed, the pressure in the gas inlet begins to decrease. A typical bubble formation pressure trace is shown in the **figure. 4.1**

It is observed that the pressure rises rapidly, reaches a peak and then begins to fall off at a much slower rate than the rate of pressure increase. When a bubble is just beginning to form, the nozzle orifice is covered with a film of liquid which seals the orifice and thus does not allow the gas to form the bubble (figure 4.1, region 1). The surface tension forces prevent the seal from breaking and so the pressure in the gas inlet line rises. When the pressure in the gas line exceeds the surface tension forces of the liquid, the seal breaks and the bubble begins to form. As the liquid seal breaks (figure 4.1, region 2), the gas pressure drops and as the bubble begins to grow (Figure 4.1, region 3), the gas pressure drops even further. The bubble grows up to a point when the buoyancy forces exceed the surface tension forces holding the bubble down to the nozzle face. Once the buoyancy force exceeds the surface tension forces (figure 4.1, region 4), bubble release occurs and a liquid seal forms at the nozzle orifice. This marks the formation of another bubble and the whole cycle repeats again. So the bubble starts forming when the pressure in the line is maximum. The pressure slowly starts falling as the bubble is formed and when bubble release occurs, pressure is at the lowest point in the line. It can be observed that the initial rate of decrease of pressure is much higher than the rate of decrease of pressure near bubble release. This happens because the initial rate of growth of the bubble is rapid and as the bubble reaches the maximum volume dictated by the surface tension of the liquid, the growth of the bubble is inhibited and is slower.

Another phenomenon which was observed was that of 'shoulders' in the experimental data. It was found that the pressure time series peaks were 'interrupted' with smaller shoulders which has

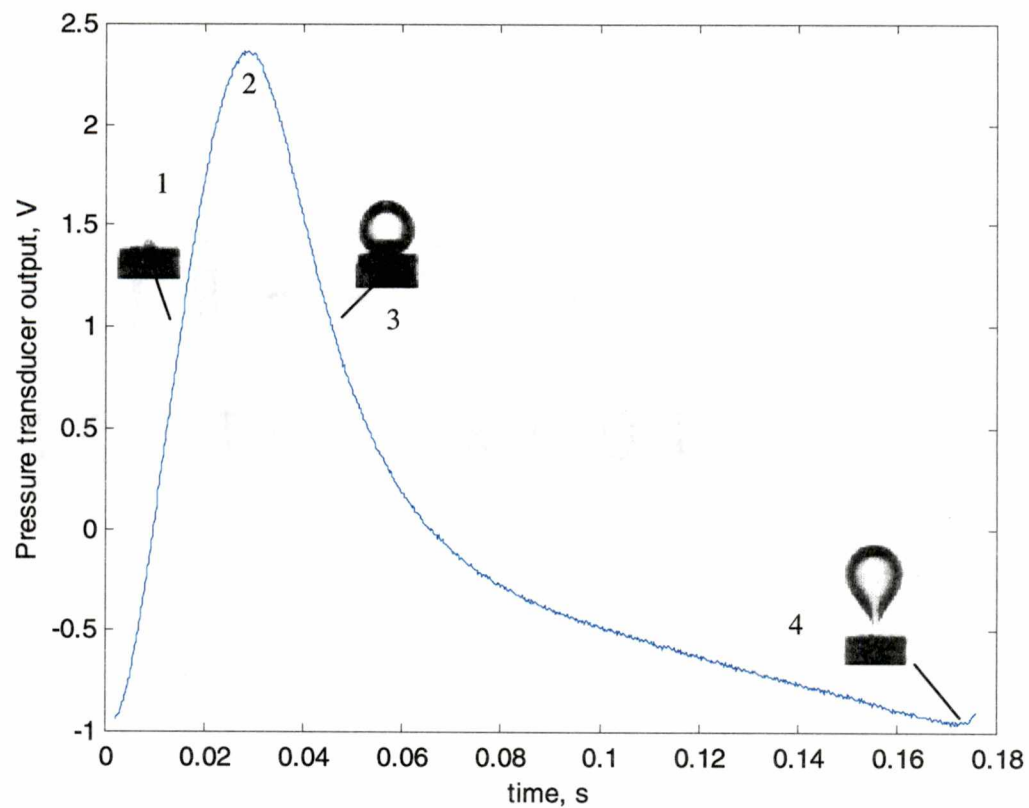


Figure 4.1. Pressure trace in gas inlet line, upstream of the nozzle. (1) surface tension forces are larger than the pressure in the nozzle, preventing bubble growth; (2) pressure in nozzle equals surface tension forces; (3) bubble growth occurs; and (4) buoyancy and inertial forces overcome surface tension, causing bubble detachment.

lower peak heights, but could not be neglected in the period calculations. A typical 'shoulder' occurrence is shown in **figure 4.2**

On further investigation with high-speed imaging, it was found that there is indeed a physical phenomenon associated with the occurrence of these shoulders. It can be seen from figure 4.2 that the 'shoulder' occurs after a series of medium to large sized bubbles. When the bubble just before the 'shoulder' leaves the nozzle tip, due to its large size the bubble creates a wake around itself. This causes the succeeding bubble to get sucked into the wake and causes it to leave before it matures into a larger bubble. This prematurely released bubble then coalesces with the preceding bubble, after which the next bubble does not get affected by any wake and thus is large. The phenomenon of shoulders was mainly predominant near period-4 regime, close to the occurrence of chaos. The 'shoulders' were ignored in analysis because the peak-finding algorithm was configured to detect major peaks only.

## 4.2. *Regimes of bubbling*

With a single train of bubbles, bubbling regimes having periodicities of 1 through 8 have been reported before entering the regime of chaotic bubbling. With glycerol solutions, bubbling regimes of 1,2,4 and 8 have been reported (Cheng, 1996). With the present study, bubbling regime of 8 was not observed. This is attributed to the larger size of the nozzle used as compared to previous investigation by Cheng (1996), where a nozzle diameter of 1mm ID was used. The bubbling system was seen to undergo a period doubling bifurcation into chaos. This section reproduces results by previous workers by observing the bifurcation sequence of bubbling with increase in flow rate.

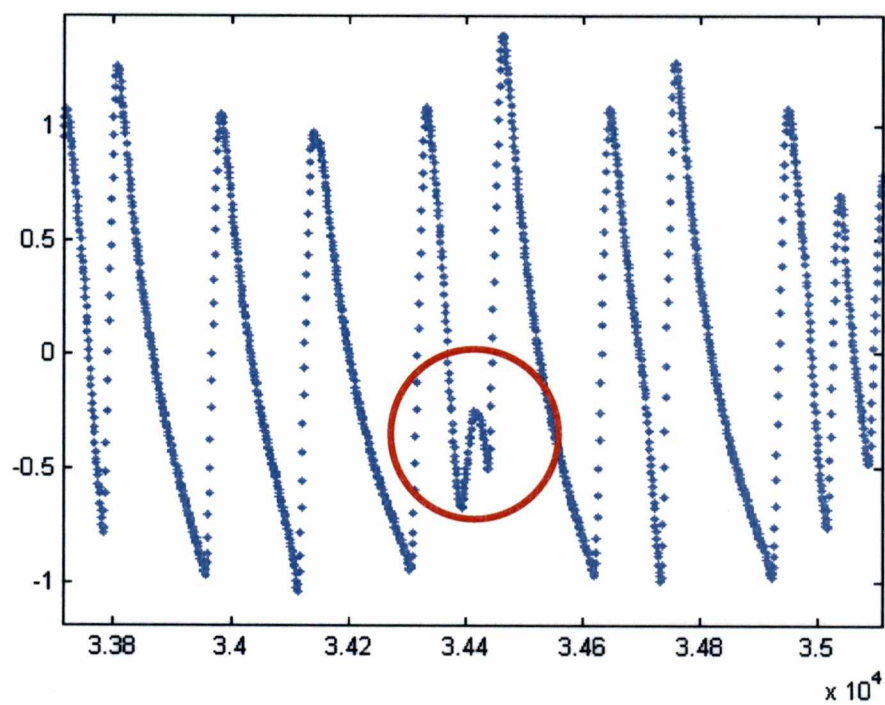


Figure 4.2. 'Shoulders' in pressure time series

### 4.2.1. *Period-1 bubbling*

Period-1 bubbling is when the system is at its linear best. All bubbles produced are of the same size and a pearly string of bubbles emanates from the nozzle. This is observed at relatively low values of flow rate and voltage when there is minimal interaction between the succeeding bubbles.

**Figure 4.3** shows typical pressure trace of period-1 bubbling at low flow rates. Approximately 8 peaks are observed in 2 seconds giving a frequency of about 4Hz. In this plot the pressure traces are seen to be identical to each other with equal peak heights and peaks occurring regularly, equal distances apart in time. At low flow rates it is observed that a single train of bubbles is produced. All the bubbles in the train are equally sized and the train of bubble is seen to rise slowly, with all of the bubbles rising at the equal velocities. There is uniform interaction between the bubbles and bubble formation. The pressure trace output obtained for this case of bubbling is a series of identical peaks.

With a slight increase in flow rate or increase in voltage, the frequency of bubbling increases. A similar train of bubbles as the earlier case is seen only that the sizes of bubbles are different. But even now no interaction is seen between the bubbles (**figure 4.6a**).

When the control parameter is increased further, the frequency of bubbles increases further. But now interaction is observed between the bubbles and bubbles of two different sizes can be seen with the naked eye (**figure 4.6b**). The larger bubble is seen to be the leading bubble and the smaller bubble is seen to be the trailing bubble. This marks the transition from period-1 to period-2 regime.

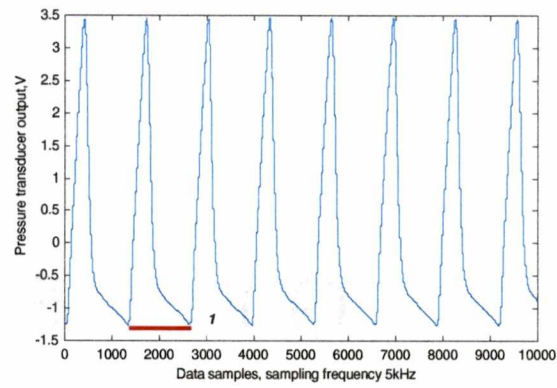


Figure 4.3. Pressure trace for period-1 bubbling

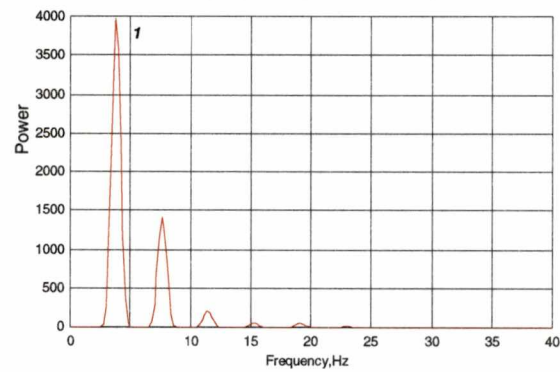


Figure 4.4. Power spectrum distribution for period-1 showing a single fundamental peak.

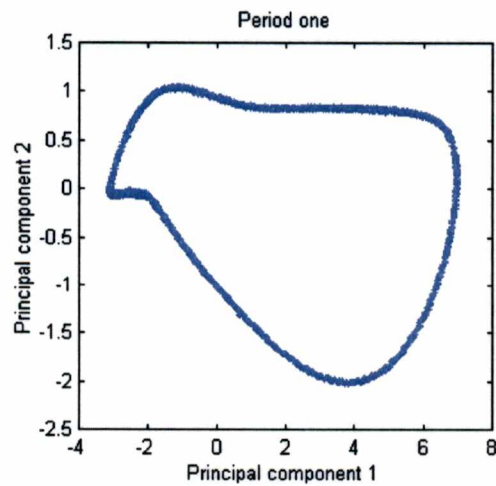


Figure 4.5. Phase space for period-1 bubbling showing a single-loop

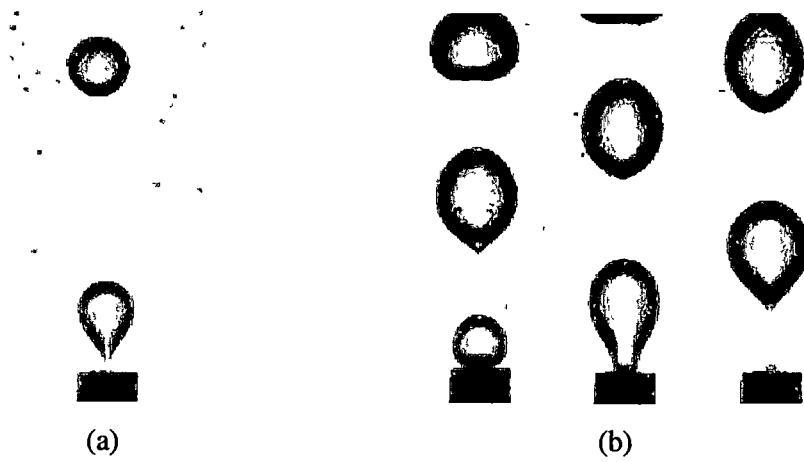


Figure 4.6 High speed images of slow bubbling  
(a) Period-1 bubbling. No interaction observed (b) Period-2 bubbling. Subtle interaction between bubbles observed



**Figure 4.4** shows the power spectrum distribution for period-1 bubbling. A peak at 3.8 Hz is seen to be prominent. This gives the frequency of period-1 bubbling. This is the dominant frequency and the other smaller peaks seen in figure 4.5 at 7.6 Hz, 11.4 Hz and so on are the harmonics of this dominant frequency. If the period of the bubbles is calculated, the mean calculated period is 0.2615 s, which gives a frequency of bubbling as  $1/0.2615 = 3.8246$  Hz.

When the time-embedding algorithm is used to perform principal component analysis on the pressure trace time series, and the first two principal components plotted against each other, the result is a single loop in phase space. The system has a periodic component, which retraces itself in phase space as the system proceeds further in time. This is a characteristic of period-1. **Figure 4.5** depicts the phase space for period-1.

#### 4.2.2. *Period-2 bubbling*

In period-2 bubbling, the bubbles produced are alternately large and small in size. This mainly occurs because of the inter-bubble interactions. **Figure 4.7** shows a period-2 bubbling pressure trace.

Peaks of two distinctly different heights are observed. These correspond to the two different sizes of bubbles. The larger peak implies that the gas pressure forces in the nozzle along with the buoyancy forces needed to overcome the surface tension forces are larger and so a larger bubble is formed before bubble release occurs. The smaller peak suggests that resultant upward forces are stronger and overcome the surface tension forces faster, resulting in a smaller bubble and causing faster bubble release. The main reason period-2 occurs is the drag reduction caused by the wake left behind by the leading bubble, which sometime causes coalescence of the leading and the trailing bubble (**figure 4.10**). So now two different periods of bubble formation are

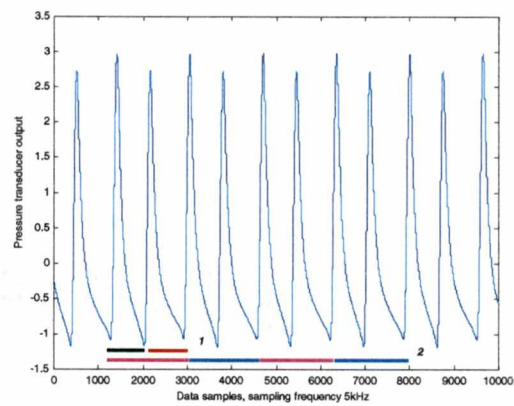


Figure 4.7. Pressure trace for period-2 bubbling

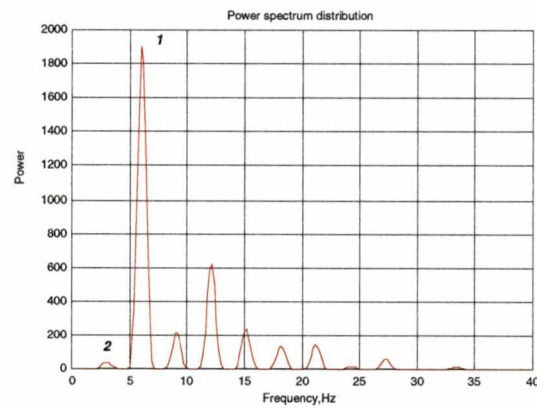


Figure 4.8. Power spectrum distribution for period-2 showing two fundamental peaks

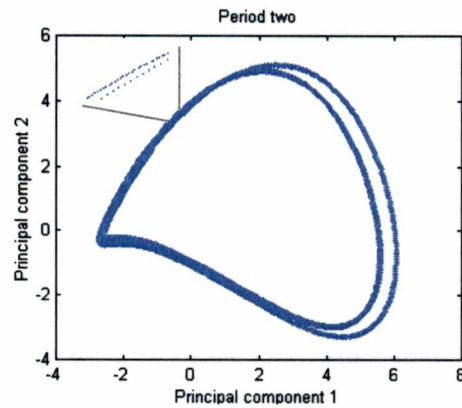


Figure 4.9. Phase space for period-2 bubbling showing two-loops

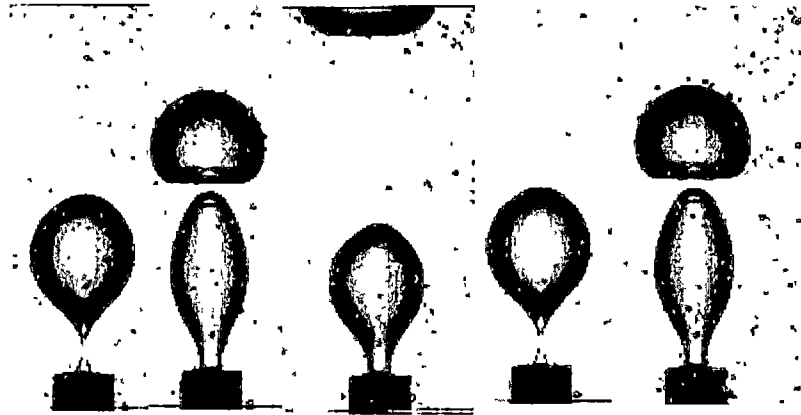


Figure 4 10. High speed images of period-2 formation of bubbles Leading large bubble causes wake which forces an early release of the trailing bubble

observed. Comparison of this pressure trace with the one for period-1 bubbling shows that the peak-to-peak time intervals in the pressure trace for period-2 is smaller than that for period-1 due to higher flow-rate and bubble interaction. This is because the frequency of bubbling is higher in case of period-2 than in case of period-1. The plot shows about 12 peaks formed in 2 seconds giving a frequency of about 6Hz.

**Figure 4.8** shows a plot of the power versus the frequency of period-2 bubbling. Here we observe two different principal frequencies. One dominant peak is seen at 6Hz and another dominant peak is seen at 3 Hz.

The average period of the bubbling was calculated to be 0.1803s (5.5458Hz) for the larger bubble and 0.1494s (6.6937Hz) for the smaller bubble. But in the power spectrum, contrary to expectations of two peaks at the respective frequencies, only one peak at 6Hz, which is the average of the two bubbling frequencies, is observed. This is because the calculated period is the time of formation of bubble. But the maximum power occurs at the frequency at which both the events of bubble formation occur, which is the average of the two frequencies. The whole cycle of formation of bubbles of two different sizes is occurring at one half the frequency at which the event for formation of the individual bubbles is occurring.

The Fourier transform sees the pressure trace as two separate period-one bubbling patterns occurring alternately, and a period-two bubbling pattern occurring at half the average bubbling frequency of the period-1 bubbles. This is illustrated in the pressure trace (figure 4.7) with the two individual period-1's shown by red and black bars, and the period-2's being indicated by pink and blue. (Note that pink and blue bars are used to show the same pattern).

To summarize, period-2 is characterised by two peaks in the power spectrum distribution, the higher of which corresponds to the frequency at which the bubble formation occurs and the

other peak corresponds to the frequency at which the pattern of bubbling repeats itself. The average frequency of bubble formation is equal to the reciprocal of the average period between the bubbles and the frequency at which the period-2 bubbling pattern repeats itself is half of the average frequency. The maximum power occurs at the average frequency of bubble formation and the power at the frequency of the bubbling pattern is comparatively much lower.

Chaotic systems are best studied in phase space where bifurcations can be identified as soon as they occur. **Figure 4.9** depicts the trajectory in phase space the system follows in period-2 bubbling. The trajectory is seen to comprise of two loops. Even though the loops seem to merge as one at certain parts on the phase plot, the distinctness of the two loops is maintained, though a magnified scale is required to observe them.

### 4.2.3. *Period-4 bubbling*

Period-4 bubbling can be thought of as a combination of two-period-2 bubbling patterns juxtaposed next to each other to form an overall sequence of four bubbles.

**Figure 4.11** shows the pressure trace for period-4 bubbling. Four distinctly different peaks are seen in the pressure trace. As the control variable is increased from period-2, the bubbling increases in frequency and consequently the period reduces. Further increases in the flow-rate lead to period-4 bubbling. A pattern of four different bubbles with alternate leading (large) and (trailing) small bubbles repeats itself. Here the pattern of 4 different peaks is subtle and special analysis tools like time return maps have to be used. It can be seen that the peak to peak height has reduced considerably and the frequency of the bubbles has increased. Approximately 18 peaks can be counted within the 2s time interval shown and the frequency of the bubbles is about 9Hz.

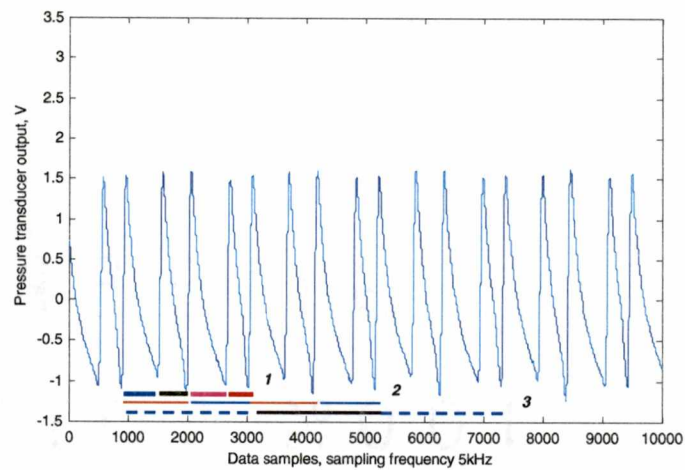


Figure 4.11. Pressure trace for period-4 bubbling

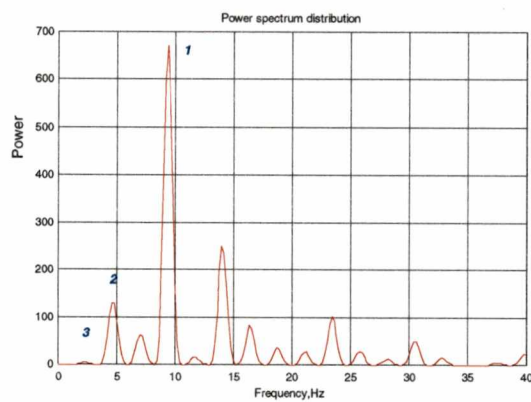


Figure 4.12. Power spectrum distribution for period-4 showing three fundamental peaks

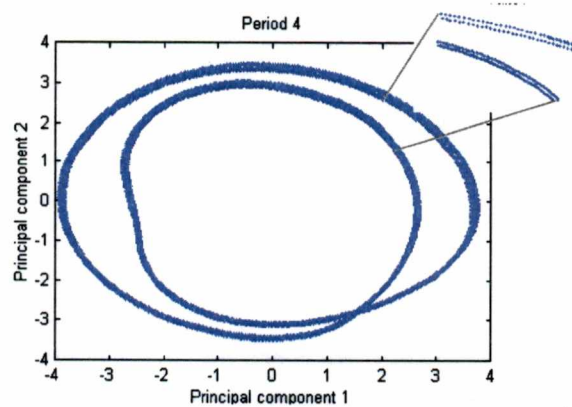


Figure 4.13. Phase space plot for period-4 showing four loops

**Figure 4.12** shows the plots for the power spectrum distribution for period-4 bubbling. In the power spectrum distribution, the dominant peak occurs at 9.4 Hz, (peak 1) with two smaller peaks at 4.6 Hz (peak 2), and 2.3 Hz (peak 3). The peak at 7.1 Hz, and the rest of the peaks occurring in the spectrum are harmonics of these three frequencies. Period-4 bubbling occurs with formation of four bubbles of different sizes. So, the frequency of the formation of these four different bubbles dominates and is seen as a peak at 9.4 Hz. But within each period-4 bubbling pattern, two period-2 bubbling patterns are observed.

Each of the two period-2 patterns are different from each other and this gives rise to period-4. The average bubbling frequency of each of the two bubbling patterns shows up as the peak at 4.6 Hz. These period-2 bubbling patterns occur faster than the whole cycle of period-4 bubbling and are slower than the frequency of the individual bubbles. The whole bubbling pattern of period-4 bubbling occurs at a frequency which is one half the frequency of period-2 bubbling and shows up as a very small peak at 2.3 Hz.

Period-4 is thus characterised by three peaks in the power spectrum distribution. The highest of the peaks corresponds to the frequency of bubble formation. This frequency is equal to the reciprocal of the averaged period between the bubbles. The lowest of the peaks corresponds to the frequency at which the overall bubbling pattern repeats itself. This frequency is equal to the reciprocal of the period of each cycle of four bubbles. The middle peak corresponds to the frequency at which the period-2 bubbling within period-4 bubbling repeats itself. This frequency is double the frequency of period-4 bubbling.

The phase plot for period-4 bubbling is shown in **figure 4.13**. On close examination, it can be seen that there are four distinct loops in the phase plot, which could be mistaken for only 2

loops due to low resolution. The system traces each of the four loops as the bubbling proceeds. At least four peaks are required for the bubbling to close four loops in phase space.

#### 4.2.4. Chaotic bubbling

The description 'deterministically chaotic' (or chaotic, for short) is assigned to that class of physical and mathematical systems that exhibit bounded, irregular behavior due to sensitive dependence on initial conditions. Visually, chaotic bubbling is a regime wherein no truly repeating pattern can be traced. **Figure 4.14** shows the non-linear pressure time series for observations for chaotic bubbling.

**Figure 4.15** shows the power spectrum distribution of chaotic bubbling. To fully appreciate the spectrum of chaotic bubbling, a larger window size of 16,384 was used to reveal the details in the distribution, versus a window of 8,192 in earlier calculations. A similar window size was tried for each of the cases of periodic bubbling, but no significant difference in the power spectrum distribution was observed. In chaotic bubbling, bubbles of different sizes are formed in an aperiodic yet deterministic manner. So a spectrum of different bubbling frequencies exist and it becomes difficult to uniquely characterize chaos via power spectral analysis. But a qualitative indication of chaos can be obtained from the power spectral distribution, and possible chaotic behavior of bubbling can be predicted from the spectral observations. From the figure 4.15 we observe that now the peaks become less distinct and the bubble frequencies start to spread throughout the range of possible bubbling frequencies. Also, the power at the fundamental frequencies starts to decrease, indicating a larger spreading of power among other bubbling frequencies. It is important to note that certain frequencies were favored, and these frequencies show a distinct signature of period-4 bubbling.



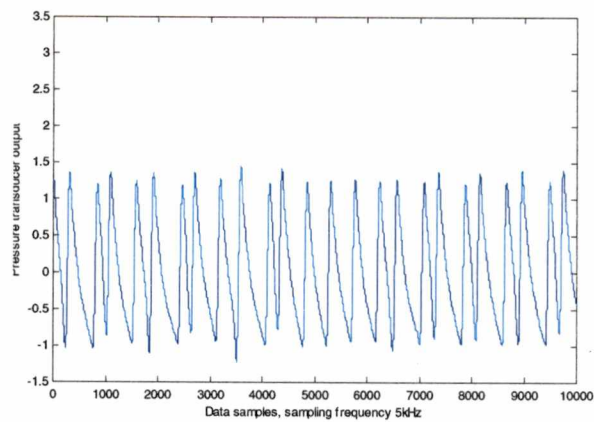


Figure 4.14. Pressure trace for chaotic bubbling

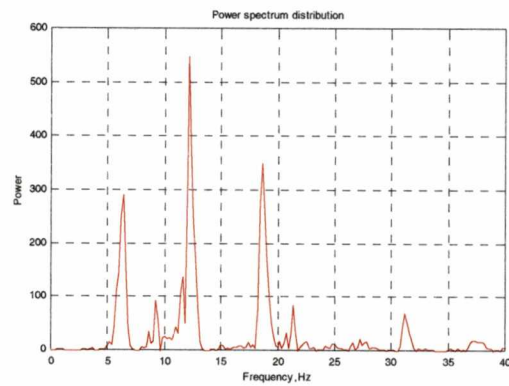


Figure 4.15. Power spectrum distribution for chaotic bubbling

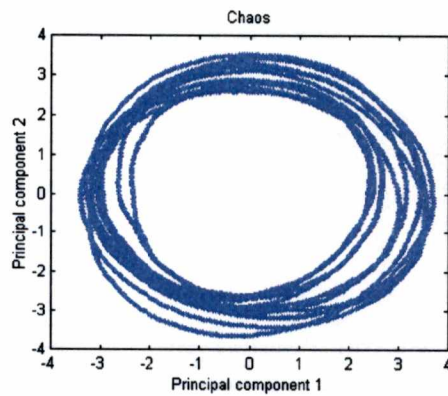


Figure 4.16. Chaos in phase space

In phase space (**figure 4.16**), the chaotic bubbling traces independent multiple loops, which outline a so-called strange attractor (unlike random systems which fill up the whole of the phase space)

In summary, periodicity can be diagnosed by analysis of the power spectrum distribution. Qualitative indication of chaotic bubbling is also possible, but the effectiveness of the power spectrum as a qualitative tool diminishes as chaos increases.

### 4.3. *Effect of electrostatic potential on bubbling*

To illustrate the effect of electrostatic potential on bubbling, a sample 'data slice' at a nitrogen gas flow-rate of 334 cc/min was chosen. The data slice was taken at a *constant* flow rate increasing the voltage from 0 to 10,000 V in increments of 1000V. Each of the runs was plotted in a unique color with respect to the whole database, which was defined by an RGB (red-green-blue) vector formed by a constant, fraction of maximum voltage and fraction of maximum flow rate (RGB vector-[frac max voltage frac maximum flow-rate 1]). All plots in this section have been plotted on the same scale for easy comparison.

#### 4.3.1. *Pressure traces*

The non-linear pressure time series is the raw variable, available for analysis of the bubbling process. **Figure 4.17** shows pressure traces for bubbling at constant flow rate, but at various voltages. The data samples were taken at 2kHz, and a data length of 1 s has been shown. The voltage for each of the pressure traces has been mentioned as the title for each of the

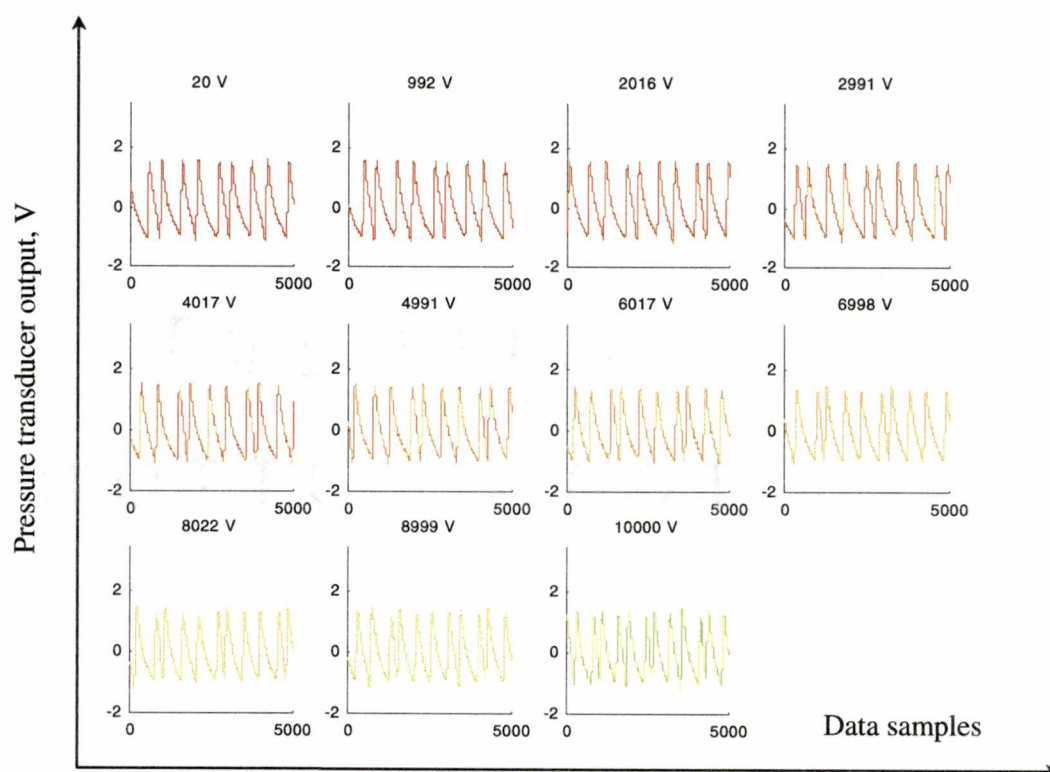


Figure 4.17. Pressure traces for bubbling with varying applied electrostatic potential, at a constant flow rate of 334 cc/min.

subplots The voltage increases from left to right, and from top to bottom The ordinate shows the output from the pressure transducer and the abscissa shows the data sample number

A subtle difference in the pressure traces can be observed by visual inspection The number of pressure trace peaks increase with an increase in applied electrostatic potential It can be seen that the frequency of bubbling increases as the voltage increases

*Note The variation of pressure traces with increase in voltage is highly dependent on the nozzle diameter In test runs carried out on with a nozzle diameter of 1mm internal diameter, a greater effect of electrostatic voltage was manifest (figure 4.18-20) This was attributed to the lower internal pressure in larger bubbles, allowing them to be distorted more by electrostatic forces*

### 4.3.2. Periods of formation

Shifts in bubble formation period appear to be consistent with the onset of bifurcations Using the pressure time series, the distance between the peaks was calculated and the corresponding time distance computed and plotted against the bubble index

**Figure 4.21** illustrates the effect of applied electrostatic potential on the period of formation of bubbles It can be observed that at the start of the run, the system is just into period-4 In the first plot, we observe three clearly distinct bubble periods, while closer inspection reveals that the longest period is actually split into two that are very close together. As the voltage is increased, period of formation of bubbles begins to decrease The difference between the periods of formation also increases This gives rise to four

distinctly different, but faster bubbles Another interesting observation is that the smaller bubbles explain for most of the change in bubble size spectrum with change in electrostatic potential This

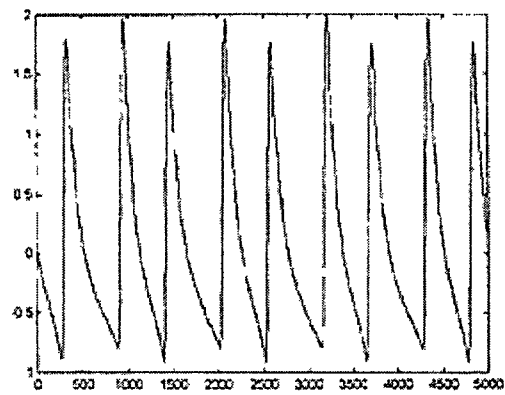


Figure 4 18 Pressure trace for 1mm ID nozzle at 0kV

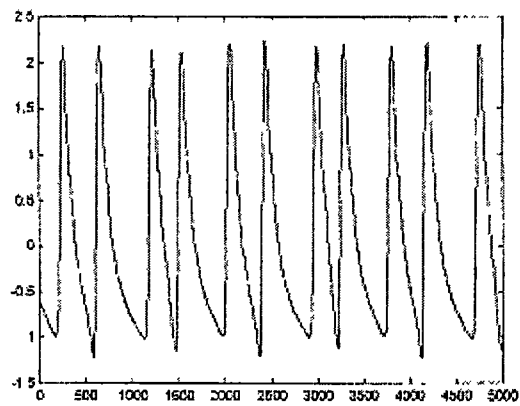


Figure 4 19 Pressure trace for 1mm ID nozzle at 5kV

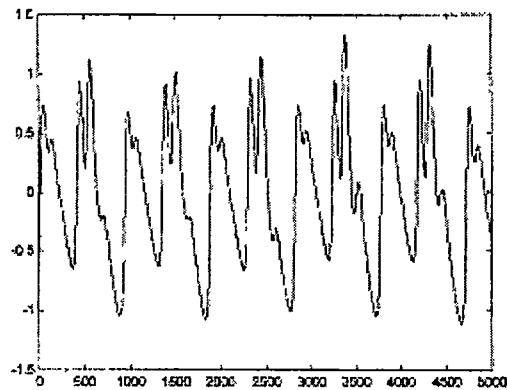


Figure 4 20 Pressure trace for 1mm ID nozzle at 7.5kV

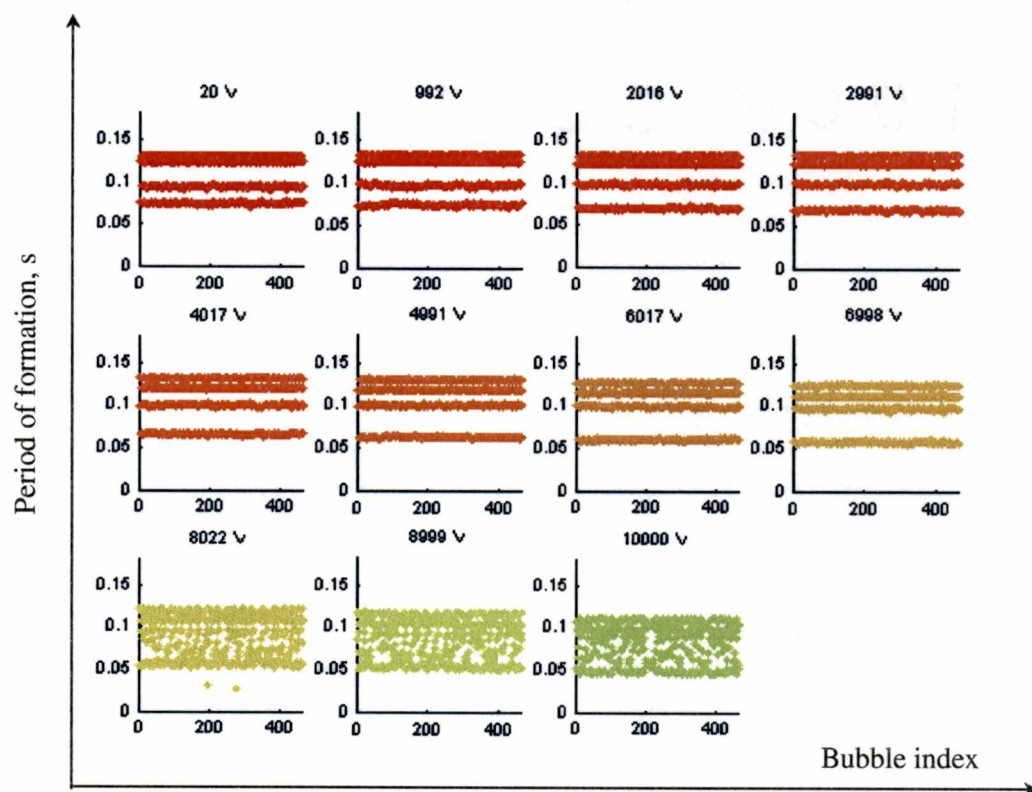


Figure 4.21. Period of formation of bubbles against bubble number, with varying applied electrostatic potential at a constant flow rate of 334 cc/min.

is because increase in electrostatic potential causes smaller bubbles to be released faster as compared to larger bubbles

When the voltage is approximately about 3000V, four distinct bands of periods of formation are seen. As the voltage is increased further, the periods continue to get smaller and the bands move away from each other. Here it can be seen that the main difference occurs in the period of formation of the larger bubbles, which are seen at the top of the plots. So, from voltages from about 3000V up to 6000V, the system is said to be into well-defined period-4 bubbling.

At about 7000V, the bubbling system is seen to be on the verge of transitioning into more complex behavior approaching chaos. At this state when the system is extremely sensitive to ambient conditions and any disturbances however subtle are enough to affect the regime of the system in an exponential manner, either to cause the bubbling to revert to period-4 or to push it into chaos.

When the system approaches chaos, the periodicity of the system is lost and the bands seen in the period of formation plot become more and more fuzzy as the system approaches chaos. But during the transition into chaos, the system bears a signature of the earlier bubbling regime. Here (figure 4.21 subplot for 8022v) we can see that though the system enters chaos, there is a persistent memory of the original period-4.

### 4.3.3. *Time return maps*

Time return maps are used for visualizing transitions in periodicity and chaos. In a time return map, the period of every bubble is plotted against the period of the succeeding bubble.

**Figure 4.22 & figure 4.23** illustrate the change in the periodicity of bubbles with an increase in the applied electrostatic potential at a constant flow rate, and vice versa. (For

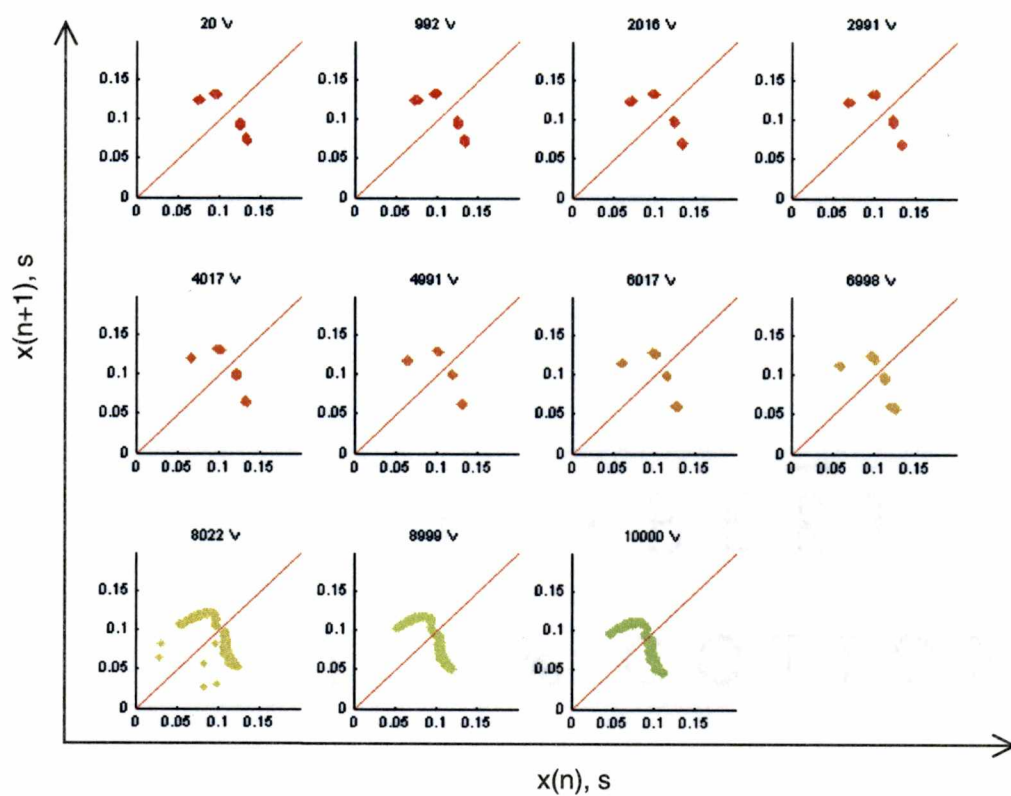


Figure 4.22. Time return maps with an increase in the applied electrostatic potential at a constant flow rate of 334 cc/min.



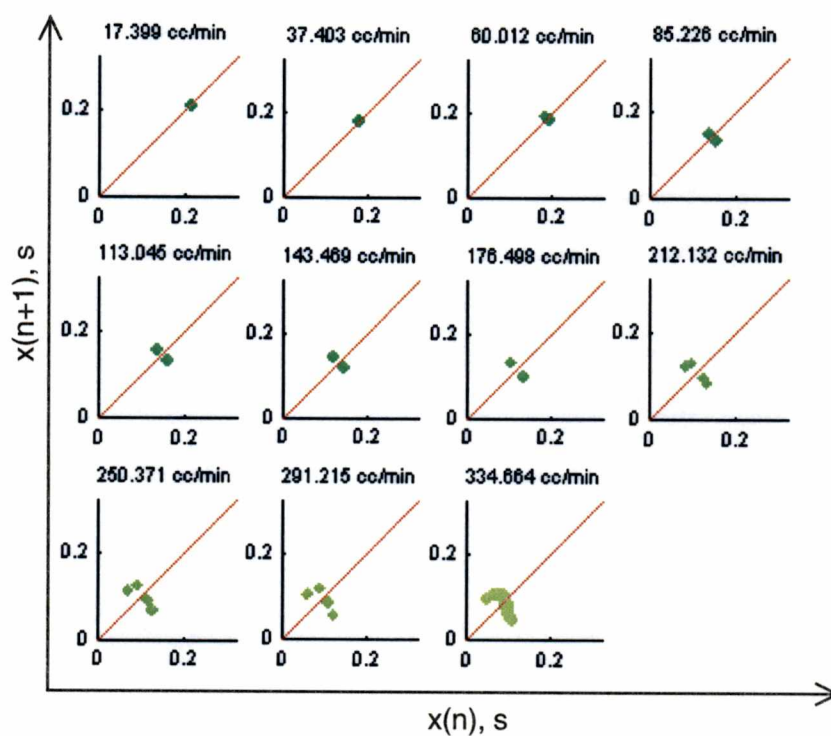
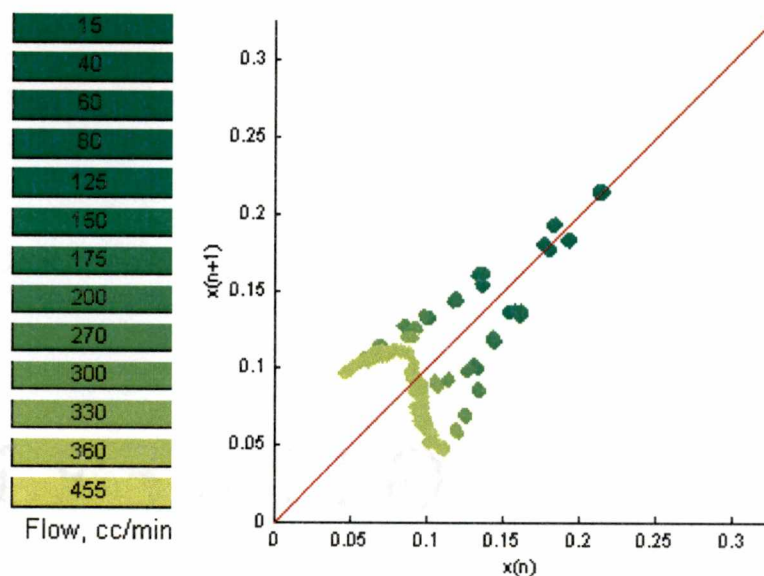


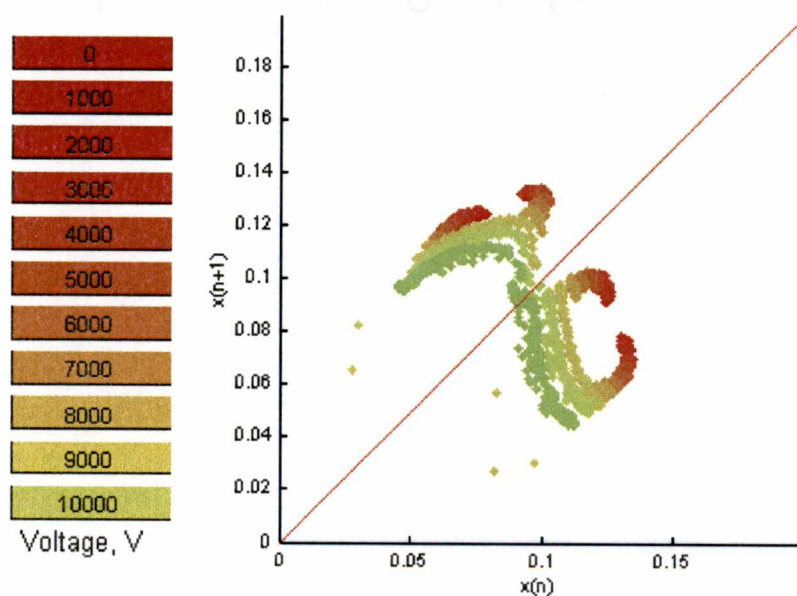
Figure 4.23. Time return maps with an increase in the flow rate at a constant applied electrostatic potential of 10,000 V.

comparison of the effect of electrostatic potential with the effect flow on the bubbling, **figure 4.24** shows all the plots from figure 4 22-23 on the same graph) At low values of applied electrostatic potential, the bubbling system is seen to have just bifurcated to a period-4 condition (indicated by the four distinct points on the plot) As the voltage is increased, the points on the time return map are seen to diverge from each other, indicating a shift into better-defined period-4 This happens because now the system has distinctly different periods of formation of bubbles Between 3000-6000V, the system is seen to be in well-defined period-4 conditions In the region from 3000-6000V, the change in either control variable, (flow rate or applied electrostatic potential), have to be substantial before the periodicity is changed (Note: Progressive time return maps of an entire dataset are presented in appendix A)

At higher voltages, the system becomes more and more unstable and bifurcates into chaos at voltages beyond 7000V and higher As the system bifurcates into chaos, the return map begins to fill in with the four distinct points becoming more and more indistinct When the system is fully chaotic, all the points lie along a narrow ribbon-like strange attractor The shape of the attractor is a system dependent phenomenon and characterizes a deterministic mapping relationship between successive bubble events **Figure 4.25(a)** illustrates the time return map in 3 dimensions It is worthwhile to note that the system reached this chaotic state at a *constant* flow rate, with an increase in the applied electrostatic potential The return map plotted in this figure also gives information about the number of times the system revisited various regions on the return map The colors vary directly with the intensity of points, with the lighter end of the spectrum indicating a maximum return frequency and darker colors indicating a minimum The frequency distribution plot indicating the percentage of the total number of bubbles is shown in figure 4.25b



(a) Increase in flow-rate at constant voltage (10 kV)



(b) Increase in voltage at constant flow-rate (334 cc/min)

Figure 4.24. Progressive time return maps with an increase in the respective control variable

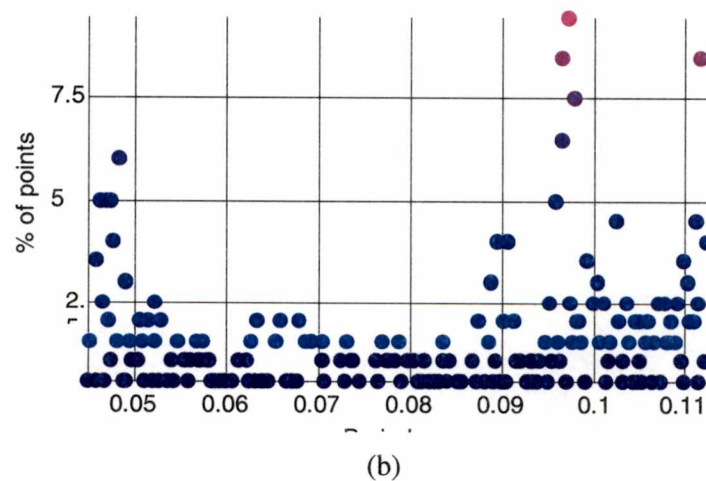
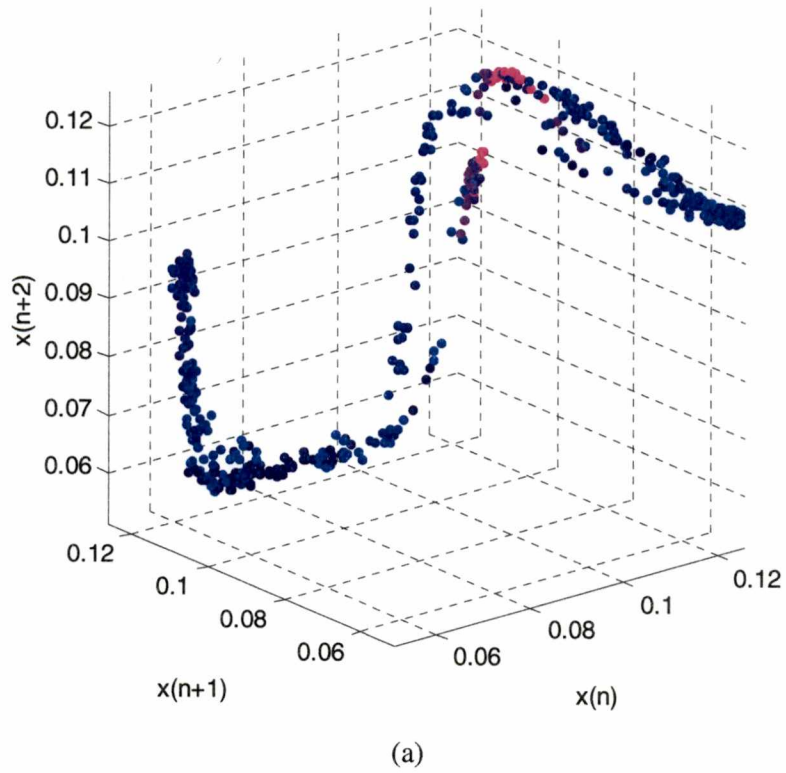


Figure 4.25.(a) Chaotic strange attractor in a 3-d time return map. The plot is presented as in intensity plot (b) with the lighter colors indicating greater number of visits.

#### 4.3.4. *Phase space analysis*

At lower applied voltages, four distinct loops are seen in the phase space. As the system moves towards chaos, the phase space plot becomes more complex and less distinct. When chaotic, the system moves along several non-repeating trajectories in phase space, which are seen as a tangle of separate loops (**figure 4.26**)

#### 4.3.5. *Power spectrum distribution*

Power spectrum analysis (**figure 4.27**) reveals power in a narrow range of frequencies at lower voltages when the system has higher periodicity. As applied voltage increases, the broadening bubble size distribution causes the peak height reduction, suggesting more distribution of power along a wider range of frequencies. An increase in the frequency of the dominant peak suggests an increase in the average bubbling rate. At bubbling regimes in chaos and near chaos, the power is spread along a range of frequencies causing an increase in the power at lower frequencies. As with flow changes, the power spectrum distribution though can only qualitatively suggest the occurrence of chaos.

#### 4.3.6. *Bifurcation diagram*

Bifurcation diagrams illustrate the effect of the control variable on the periodicity of the system. By studying bifurcation plots, the dynamic state of the column can be qualitatively predicted and one or more parameters correspondingly adjusted to target a specific bubbling regime. Bifurcation analysis was used mainly to decide the optimum system state at which to employ control.

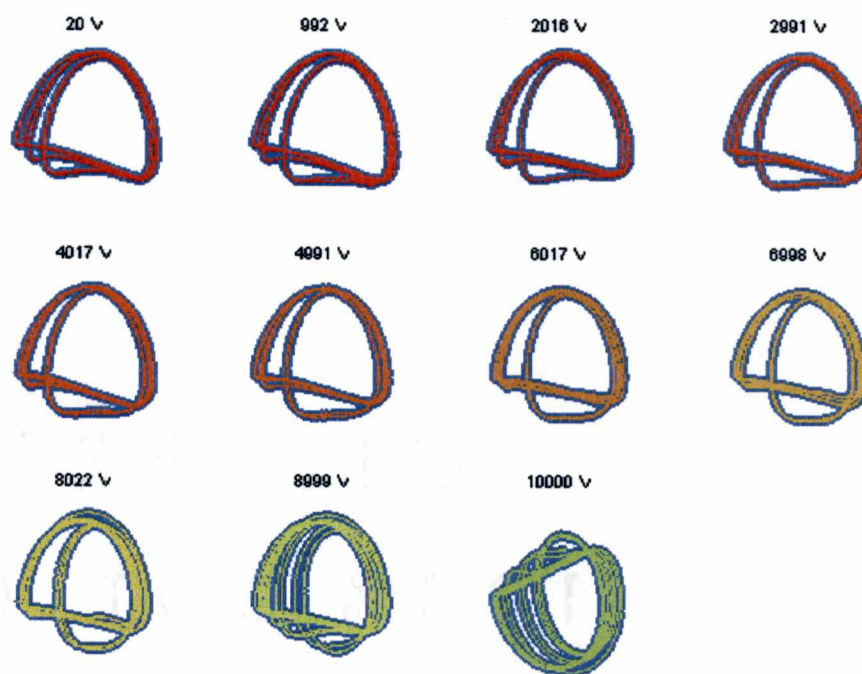


Figure 4.26. Phase space variations with varying applied electrostatic potential field strength, at constant flow rate of 334 cc/min (*note: All plots are on the same scale*)

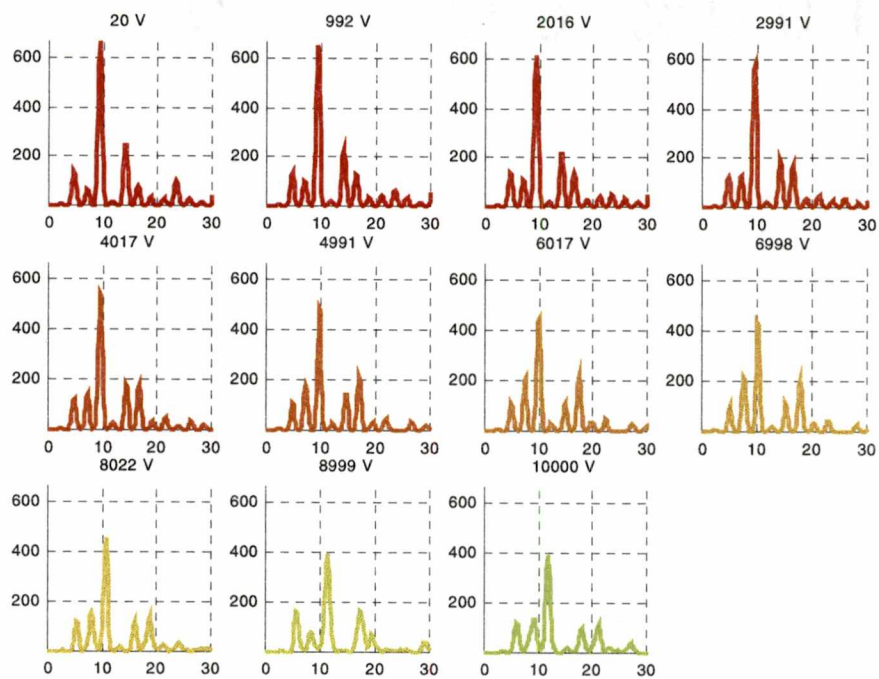


Figure 4.27. Power spectrum variations with varying applied electrostatic potential field strength, at constant flow rate of 334 cc/min

#### *4.3.6.1. Bifurcation at constant voltage*

In **figure 4.28**, the flow rate has been kept constant at 334 cc/min, and the voltage was gradually increased in steps of 1000 volts from 0 to 10,000 V. Bifurcation of the bubbles with increase in electrostatic potential control variable is evident from this plot. At low values of the applied electrostatic potential, the system exhibits period-4. With an increase in voltage from left to right, the period of formation of bubbles decreases and at the same time the size distribution of the bubbles increases. Now, the system has four distinctly different bubbles forming. At higher values of applied voltage, the system starts bifurcating into chaos. When the system is chaotic, the periods of formation are almost continuously distributed along a wide band.

#### *4.3.6.2. Bifurcation with voltage and flow*

In non-linear dynamics literature bifurcation maps involving changes to only one control parameter have widely been used. To analyze the effect of electrostatic potential in tandem with flow rate, similar bifurcation plots were made at different flow rates and plotted on the same plot to generate 3-dimensional bifurcation plots. It is seen that electrostatic potential alters the dynamics of the bubbling by decreasing the periodicity of the system. **Figure 4.29** gives the bifurcation of the system along the two axes and also marks the specimen system state to be studied in blue. This state is also highlighted in **figure 4.28**. It can be observed that with flow, the system is at a much higher value of



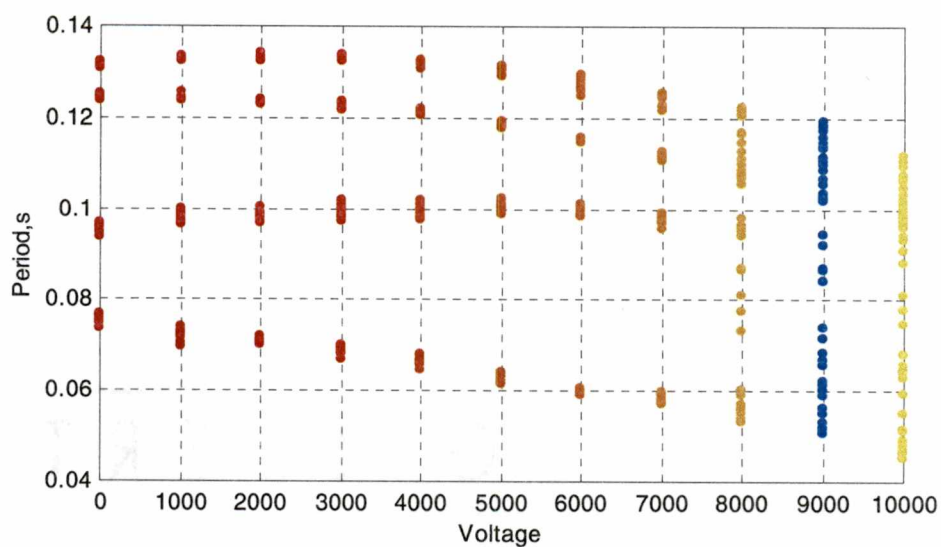


Figure 4.28. Bifurcation with applied electrostatic potential field strength, at constant flow rate of 334 cc/min

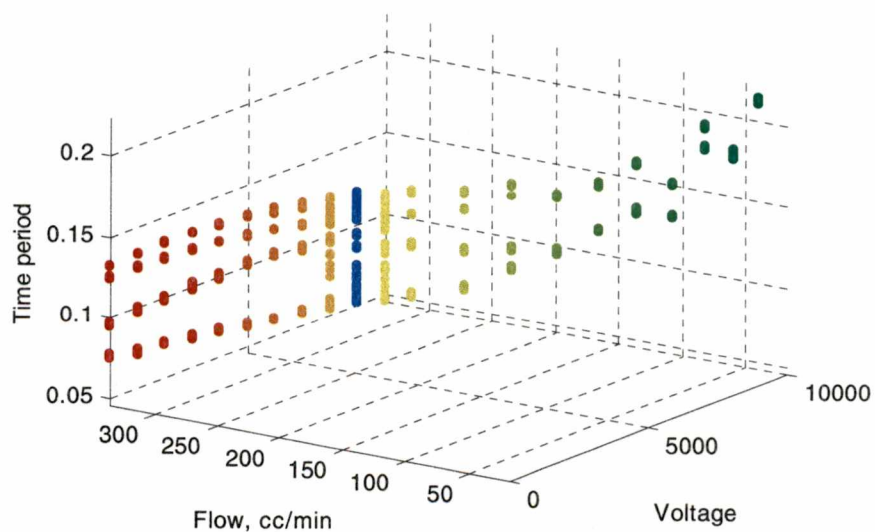


Figure 4.29. Position of a single run with respect to bifurcation with flow-rate and electrostatic potential in tandem

bubble formation at the top right corner of figure 4.29. Voltage on the other hand is much more subtle in its effect, which is manifest on the voltage axis.

### 4.3.6.3. Bubbling regimes in terms of dimensionless numbers

Studying bubbling regimes in terms of dimensionless numbers give the operating conditions a more universal flavor. The dimensionless numbers chosen for study are the Tsuge flow-rate number (Tsuge, 1984) and the electric Bond number (Harris & Basaran, 1995, Shin & coworkers, 1997).

Tsuge's flow rate number is defined as

$$N_w = Bo \cdot Fr^{0.5} \quad (1)$$

where

$$Bo = \frac{D_i^2 \rho g}{\sigma} \quad (2)$$

$$Fr = \frac{u^2}{D_i^2 \rho} \quad (3)$$

The Tsuge flow-rate number is a ratio of the buoyancy forces characterized by  $Fr$  and the surface tension forces, characterized by  $Bo$ .

Electric Bond number is defined as

$$Be = \frac{d, \epsilon_a E^2}{\sigma} \quad (\text{Harris \& Basaran, 1995}) \quad (4)$$

The electric Bond number is a ratio of the electrostatic forces and the surface tension forces

In order to study the collective effect of electrostatic and buoyancy forces, Shin and co-workers,(1997) suggested a modified Weber number which was the ratio of the sum of the electrostatic forces as compared to surface tension forces. This number is an indication of the total upward forces, which seek to release the bubble, as compared to the surface tension force which prevents the bubble release.

Modified Weber number is defined as

$$We = \frac{d_i \varepsilon_a E^2 + u^2 d_i \rho_a}{\sigma} \quad (5)$$

The period of formation has been plotted against the voltage and the flow-rate in **figure 4.30** while in **figure 4.31** the electric Bond number and Tsuge flow-rate number is used. One important observation in these two figures is that while the plots appear to be continuous in **figure 4.30**, a significant break in data is seen when the numbers are plotted on dimensionless axis in **figure 4.31**. This is because the dimensionless number definition contains a 'squared' term for the electrostatic field and flow rate for each of the two axes. This causes the values to shoot up as the absolute value increases. This also implies that the change in system state will be higher per unit change in control variable at higher values of the control variable.

The modified Weber number suggested by Shin and co-workers illustrates the combined effect of electrostatic potential and flow rate on the bubbling regimes (**figure 4.32**). Here the red markers indicate chaotic regimes and the colors with lower temperature indicate higher periodicity. The regime identification was done by an empirical 'regime-identifier' algorithm, which used ratios of peaks from the power spectral analysis. It is seen that period-1 is only seen

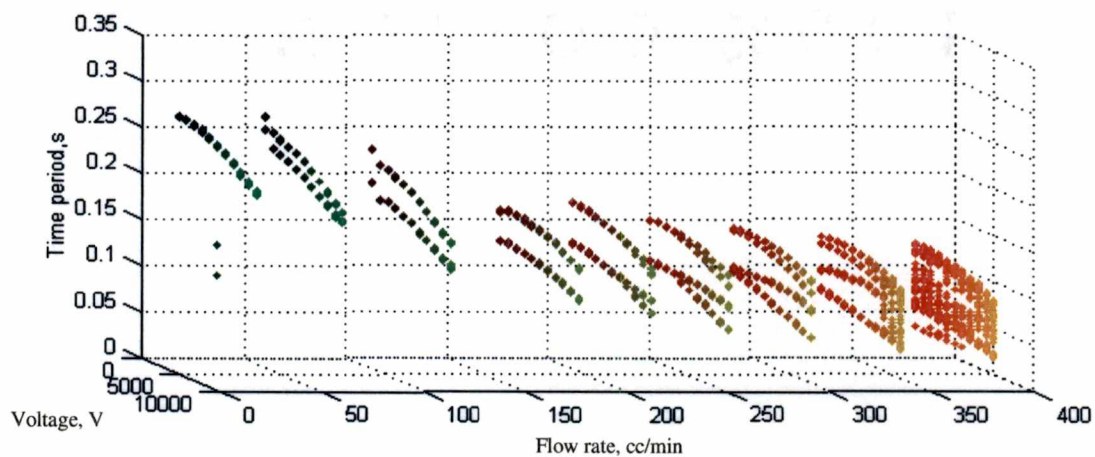


Figure 4.30. Bifurcation with flow and voltage

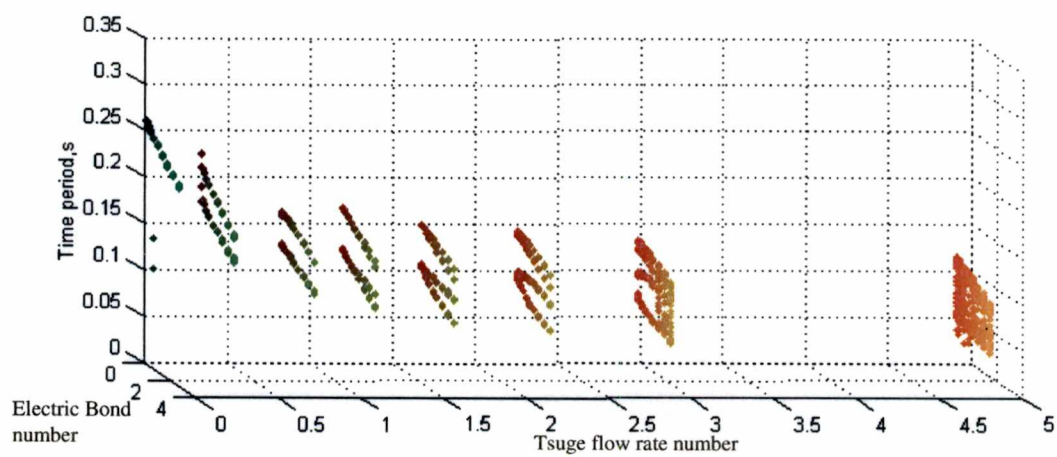


Figure 4.31. Bifurcation with flow and voltage against dimensionless axes

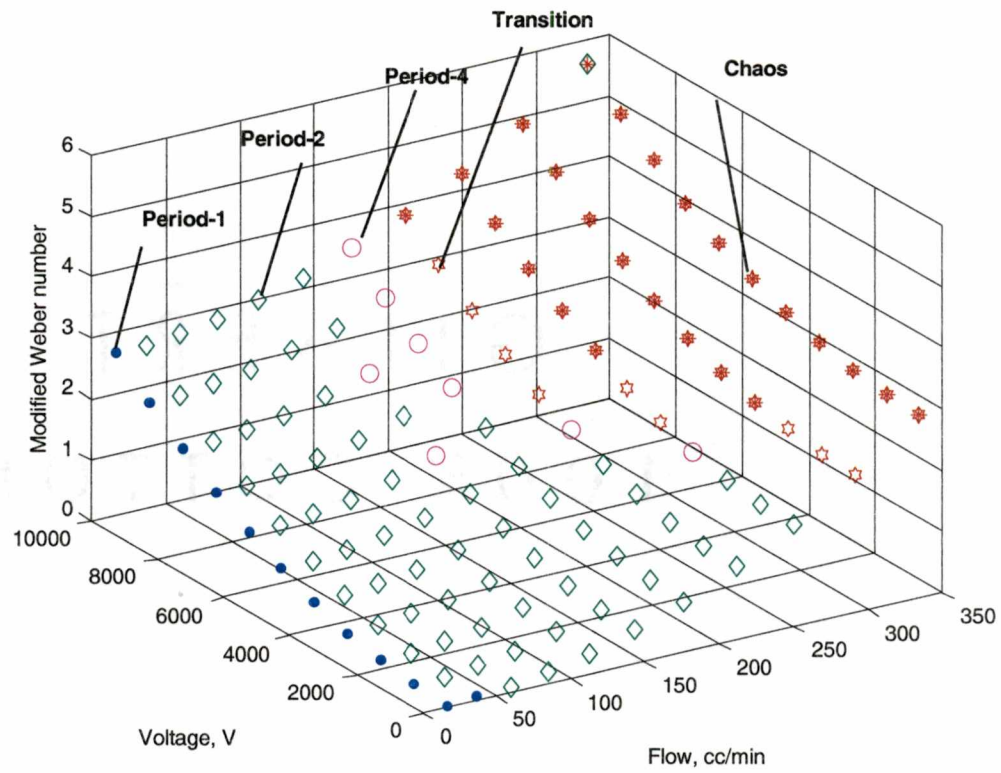
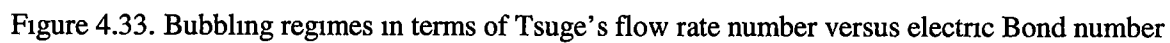


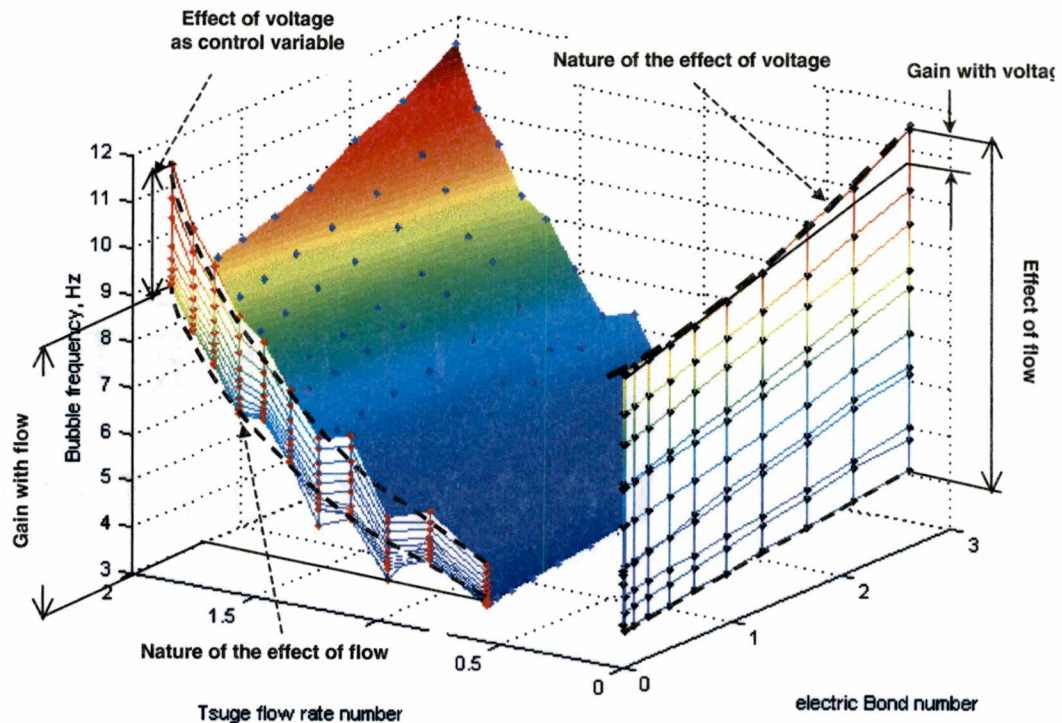
Figure 4.32. Bubbling regime plot in terms of the modified Weber number

at the low voltages and low flow rates. As either of the variables is increased, the bubbling regime passes through a period-2 and four before bifurcating into chaos. The bubbling regime cannot be predicted using the modified Weber number alone as the regime is also based on the ratio of the electrostatic and buoyancy forces; however, the figure does show a clustering of regimes according to the modified Weber number.

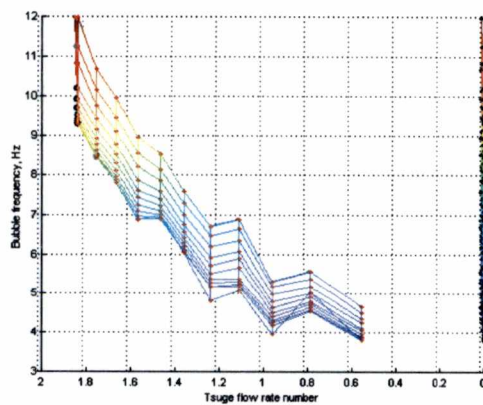
The effective regimes of bubbling in terms of periodicity can be identified in **figure 4.33**, which gives the periodicity of the system in terms of the dimensionless flow rate number and electric Bond number. From figure 4.33, it can be observed that the increase in electric Bond number has a greater effect on the regime at values of higher Tsuge flow-rate numbers. At the Tsuge flow-rate number of about 1.7, increase in the electric Bond number causes change in bubbling regimes from period-2 into period-4 and finally into chaos.

The frequency of bubbling is affected by both the flow rate and the electrostatic potential. **Figure 4.34** shows the surface plot of the bubbling frequency as a function of the flow rate number and the electric Bond number. The plot also shows the projection of the surface plot onto the flow rate axis and the electrostatic axis, which can be termed as operating lines. The projection gives a qualitative idea about how the individual control variable impacts the frequency of bubbling. The projection on the flow axis shows the effect of the electrostatic potential. The linearity of the operating lines suggests the nature of the effect of the flow. The electrostatic potential shifts the operating line from the lower extremity to the upper extremity, as the bubbling frequency increases with an increase in electrostatic potential. The linearity of the operating line is not affected to a large degree. This indicates that the electrostatic forces have a smaller effect on bubbling behavior than changing flow rate. The difference between the two operating lines gives the gain, which can be harnessed as a result of electrostatic potential as an additional control variable.

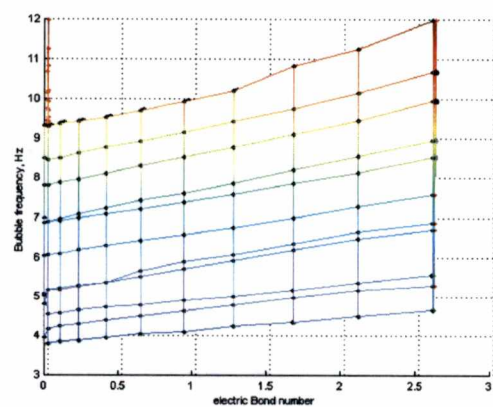




(a)



(b)



(c)

Figure 4.34. Frequency mapped as a surface plot against dimensionless flow-rate and voltage. (a) Surface plot of frequency of bubbling against dimensionless flow-rate and electrostatic potential (b) Projection of surface plot onto the flow-rate axis (Note: Abcissa is reversed) (c) Projection of surface plot onto the electrostatic potential axis



On the other hand, the operating lines on the electrostatic axes are affected by flow rate in stronger way. The operating line at low flow rates is close to being linear, whereas at higher flow rates the operating line is curved suggesting more non-linear characteristics. Again the difference in the operating lines is the gain due to flow rate as the control variable.

Figure 4.34 suggests that to obtain maximum gain for control, the values of flow and electrostatic potential should be at the upper operating limit. But this also implies that the system will be chaotic and so any small changes in either of the control variables will be amplified exponentially. Well, that's where engineering and chaotic analysis comes together.

## Chapter 5

# ***Application & Implementation***

---

*The world is what it is and I am what I am This out there and this in me, all this, everything, the result of inexplicable forces A chaos whose order is beyond comprehension*

Henry Miller, Black Spring

Electrostatic potential was shown to dramatically affect the bifurcation sequence of chaotic bubbling. An increase in electrostatic potential caused an increase in the average bubbling at a constant flow rate. This has provocative implications wherein the effect of electrostatic potential can be harnessed to optimize and control the entire bubbling phenomena. The emphasis in this research was on closed loop control enhancements to process performance.

### ***5.1. Periodicity identification***

The bubbling periodicity identification was the initial step to controlling bubbling. This identification was to be done in real time so that dynamic calculations could be utilized to control the bubbling.

### 5.1.1. Statistical modeling

An initial approach was modeling the bubbling periodicities as a function of the frequency distribution of the periods of formation using various regression techniques (Sarnobat & Hines, 1999). The results were not satisfactory because of the non-linearity and extreme sensitivity of the bubbling process to perturbations, as against the least squares approach adopted by most of the regression analysis. A sample of the model performance is shown in **figure 5.1**. The model performance degraded when the system changed from higher periodicities to lower ones. Near chaotic conditions, the model could not discriminate between any of the regimes.

### 5.1.2. Neural network models

It was found that power spectrum analysis could be used to extract the significant information (section 4.2). The fundamental peak gives the average frequency of bubbling (say  $x$ ) and peaks observed at  $0.75x$ ,  $0.5x$ ,  $0.25x$  give information about the periodicity regimes of the bubbling (figures 4.4, 4.7, 4.10, 4.13). A non-zero peak height at  $0.5x$  suggests period-2 and a peak at  $0.25x$  indicate period-4. The peak at  $0.75x$  is a harmonic of frequencies at  $0.25x$ , but also gives a qualitative indication about the existence of chaos. The peak heights of these peaks along with the average bubbling frequency are all that are required to characterize the bubbling periodicity. A neural network was constructed to map periodicity regimes of bubbling (Sarnobat and co-workers, 1999). The neural network was designed to have 5 inputs and one output. Four of the five inputs were the peak heights at multiples of  $1x$ ,  $0.75x$ ,  $0.5x$ ,  $0.25x$ , where  $x$  is the fundamental frequency in the power spectrum distribution of the time series. The fifth input was the value of the fundamental frequency itself. The neural network had one output, which was the periodicity of the system. A periodicity of 16 was assigned to the class when the system was in deterministic chaos. A Kohonen based neural network was used and the training was conducted

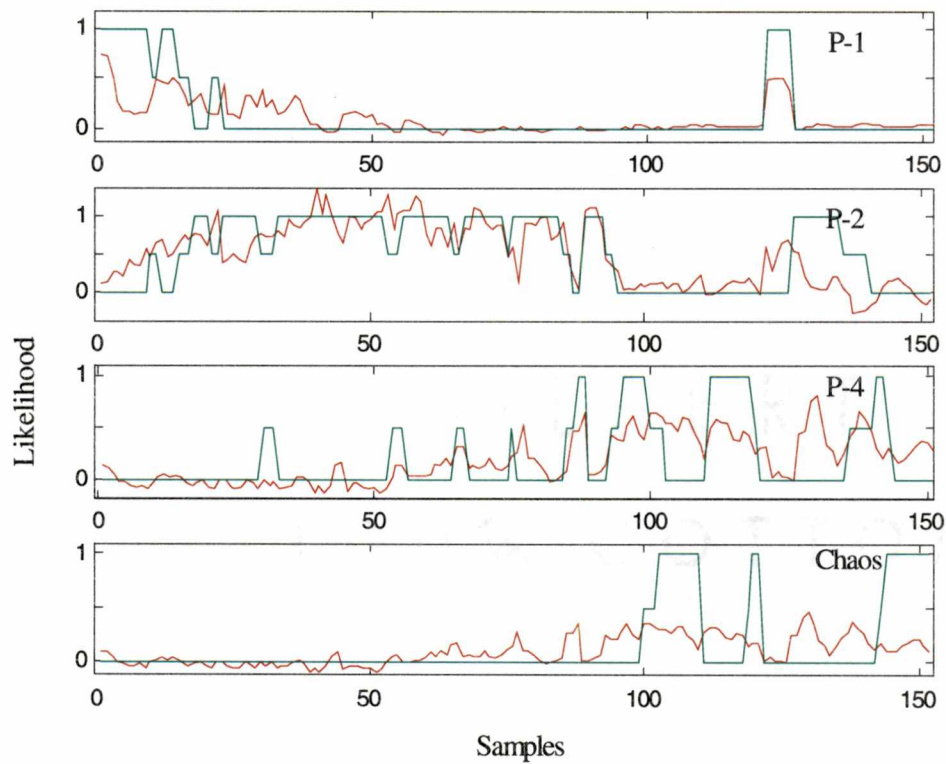


Figure 5.1. Performance of numerical model using partial least squares. Input data are the frequency distribution of the periodicity and the output is a 'state' vector, which indicates the likelihood of the bubbling regime. Each of the periods was assigned a 'likelihood' between 0-1 which indicated the extent to which the system corresponded to that state. (The green line indicates the target and the red line is the estimated state)

with linear vector quantization, (Tsoukalas & Uhrig, 1996, Sarnobat & co-workers, 1999) The performance of the neural network model is shown in **figure 5.2** The model performance was found to be satisfactory, but implementation in LabView for real time calculations was difficult Also for the neural network large amounts of training data were required and the model would only be valid if the operating regimes were all comprehensively represented in the training data This was a big factor in considering other techniques for real time identification

### 5.1.3. *Periodicity pattern detector*

An important constraint on the real time periodicity identification is the adaptability of the algorithm to LabView implementation A real time simultaneous input/output vi was designed to calculate the periods of formation This was a software timed data acquisition and hence all the calculations were done within a 10ms loop between data points The disadvantage of this method was that any memory usage of by the operating system reflected in the timing loops being longer than the 10ms This caused a outliers in the zero-crossings because the time between zero-crossings also included the additional processing time required by LabView The effective rate of data acquisition was 100Hz at the 'worst' operating condition, which took maximum length of time to process the data The periods of formation were dynamically plotted as a time return map, which clearly indicated the periodicity of formation

A simple 'pattern-identifier' routine was set up to identify the bubbling regime It was based on the observation that regular patterns are formed in periodic regimes and in chaos no pattern can be detected For period-1 formation, every bubble is of the same size, for period-2 every third bubble and for period-4, every fourth bubble In chaos none of the bubbles form a pattern A target array of every second, third & fourth bubble set up The value of the period of formation of the current bubble was subtracted from each of the array elements and the averaged differences are compared against a tolerance A moving window based approach was used keeping

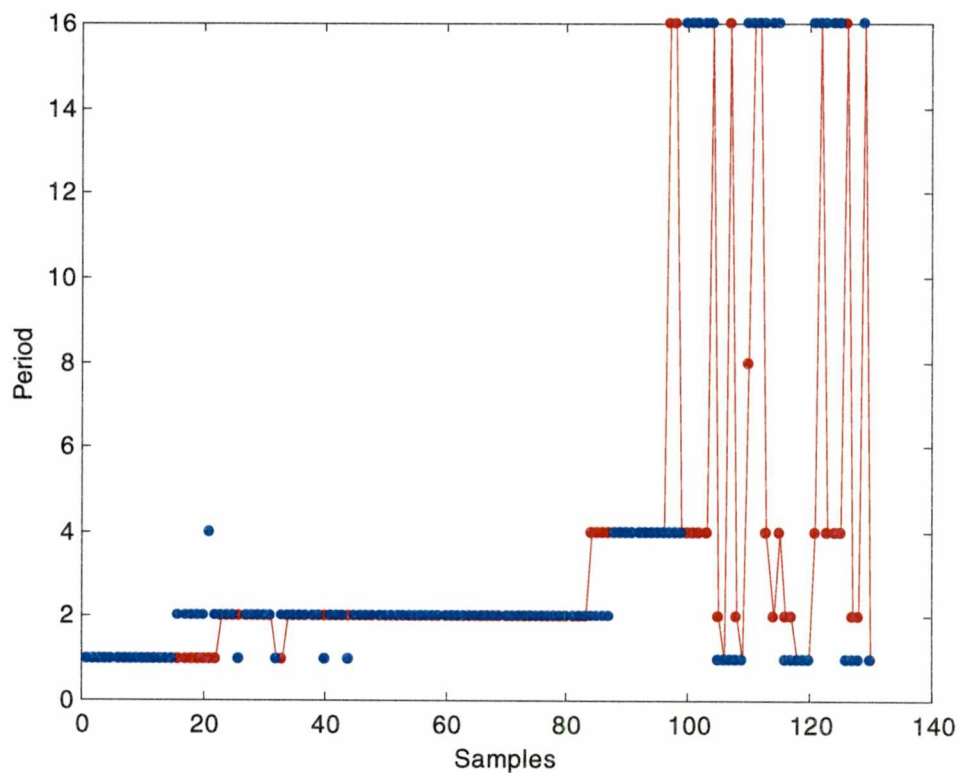


Figure 5.2. Neural network performance for identifying the periodicity of bubbling. A Kohonen map was used and the network trained by linear vector quantization. The inputs were the fundamental peak heights extracted from the power spectrum distribution and the average bubbling frequency. (The red dots indicate the target and the blue dots indicate the estimated state).

$\{Bubble(3)-Bubble(0)\} < tolerance$	$\{Bubble(2)-Bubble(0)\} < tolerance$	$\{Bubble(1)-Bubble(0)\} < tolerance$	Regime
0	0	0	Chaos
0	0	1	?
0	1	0	Period-4
0	1	1	Period-1
1	0	0	Period-4
1	0	1	?
1	1	0	Period-2
1	1	1	Period-1

Table 5 1 Truth table for bubble regime identification (Key Y=1, N=0)

the last 32 bubbles in the history array. Longer windows can be used to decrease the oversensitivity of the identifier to changes in periodicity. Depending on which elements are below the tolerance, a truth table is set-up for the regimes of bubbling.

The results (figure 5.3, 5.4) suggest that this regime identifier can be used with confidence for detecting period-1 and period-2. But, when the bubbling regime enters period-4, the measurement error due to either computational limits reached by LabView or due to external noise, causes erratic results because this identifier compares the bubble sizes and any error will cause a misclassification of period-4.

This identifier was used for feedback control to ensure regime of bubbling. A simple P-I controller can be implemented for manipulating the flow-rate and/or voltage to achieve the required regime of bubbling. Presently this is limited by computational requirements for control into either of the regimes.

## 5.2. Regime targeting of bubbling with electrostatic potential

Electrostatic potential was shown to affect the frequency of bubbling in a manner similar to increasing the flow rate. In the frequency plot of figure 4 34, it can be seen that for a single

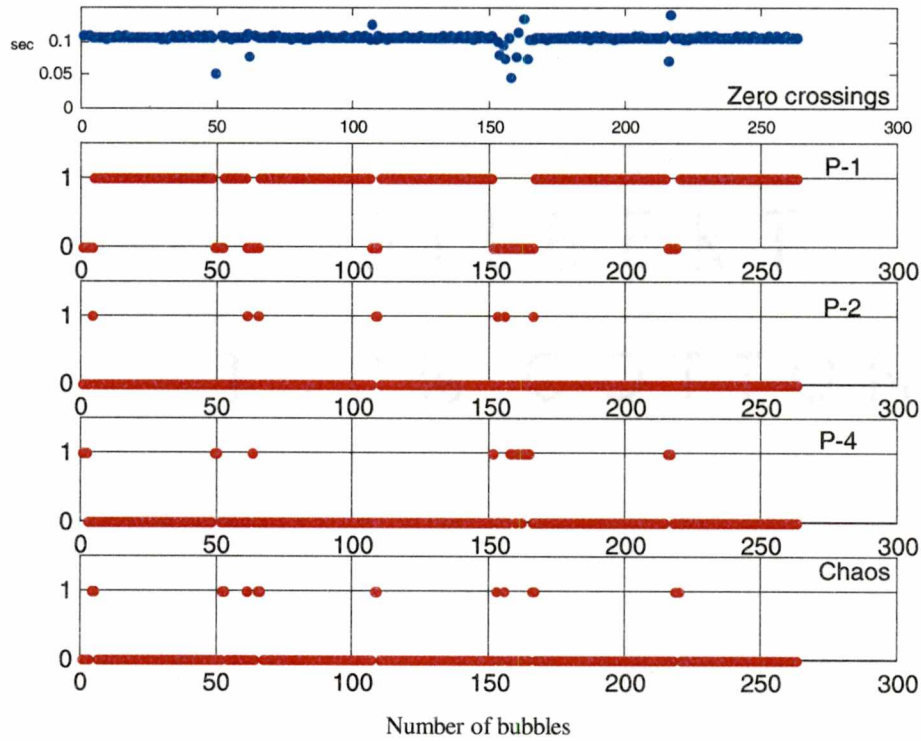


Figure 5.3. Period-1 identification with periodicity pattern identifier. Blue plot is the zero-crossings (in units of seconds), plotted against the bubble indices. The red plots are the flags for each of the periodicities. This plot shows that the identifier captures period-1 satisfactorily (P-1).



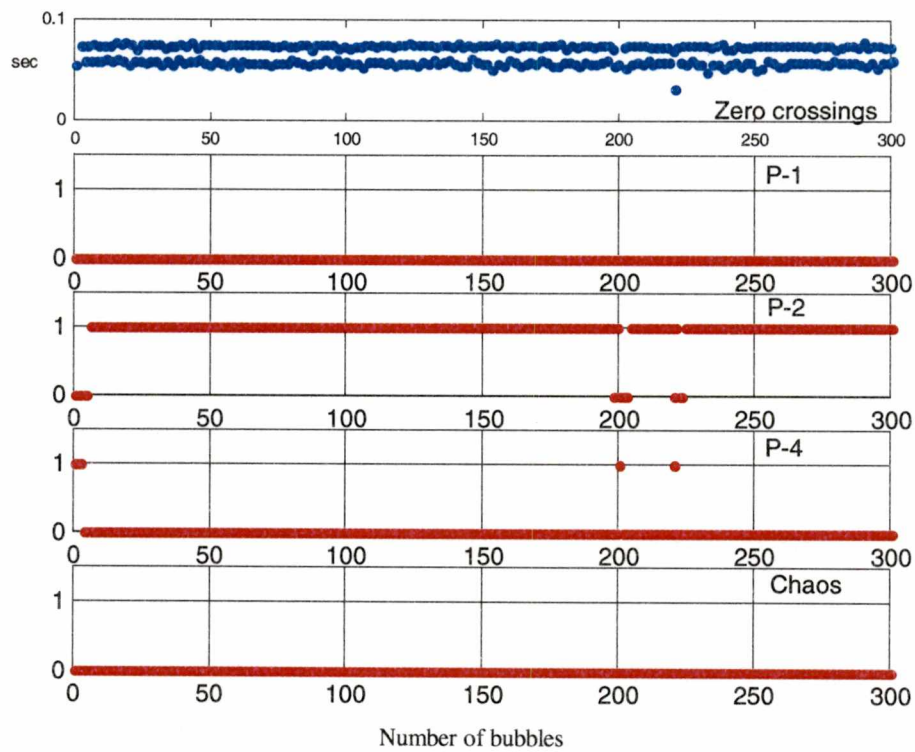


Figure 5.4. Period-2 identification with periodicity pattern identifier. Blue plot is the zero-crossings (units in seconds), plotted against the bubble indices. The red plots are the flags for each of the periodicities. This plot shows that the identifier captures period-2 satisfactorily (P-2).

frequency of bubbling, an operating line can be determined. This suggests that voltage and flow can be used in tandem to maintain constant bubbling frequency. An increase in flow rate can be compensated by a corresponding decrease in electrostatic potential, or vice versa.

A simple PI-controller loop was used with voltage as the manipulated variable, flow rate as the disturbance and the average bubbling frequency as the process variable to be held at a set-point. The average bubbling frequency was calculated by taking the mean of the previous 20 bubbles. The control moves were implemented after multiples of 20 bubbles (~1s) to give the system time to stabilize before implementing the next control move. Results are shown in **figures 5.5-5.7**.

**Figure 5.5 (a)** shows the response of the system to a gradual increase in the disturbance (flow rate). The period for formation, manipulated variable (electrostatic potential) and flow-rate are plotted against the number of bubbles. Before the disturbance was introduced into the system, the system was at a steady period 1 bubbling with the electrostatic potential at 10kV. The flow rate was gradually varied in a series of small increments from 200cc/min to 420 cc/min. The set point was set to the average bubbling frequency before the disturbance was introduced. The aim was to get the controller to manipulate voltage to match the bubbling frequency before the disturbance was injected.

From figure 5.5, it can be seen that the controller steps down the voltage so maintain a constant bubbling period of formation (0.05s). The plot for the flow rate is noisy on the right hand side because the flow rate varies as the pressure at the nozzle varies with the formation of each bubble. **Figure 5.5 (b)** shows the return maps before and after the disturbance. Before the disturbance is injected, the system is in a 'noisy' period-1. After the controller has compensated for the disturbance, the bubbling frequency is maintained at the set point, but now the system is into a noisy period-4.

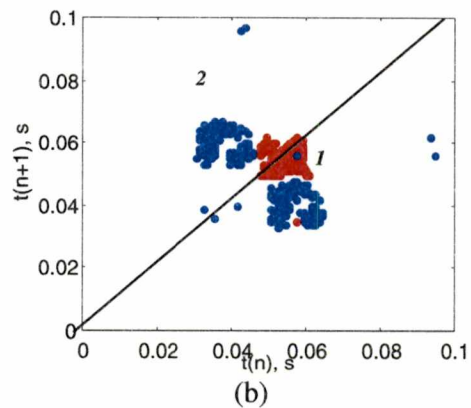
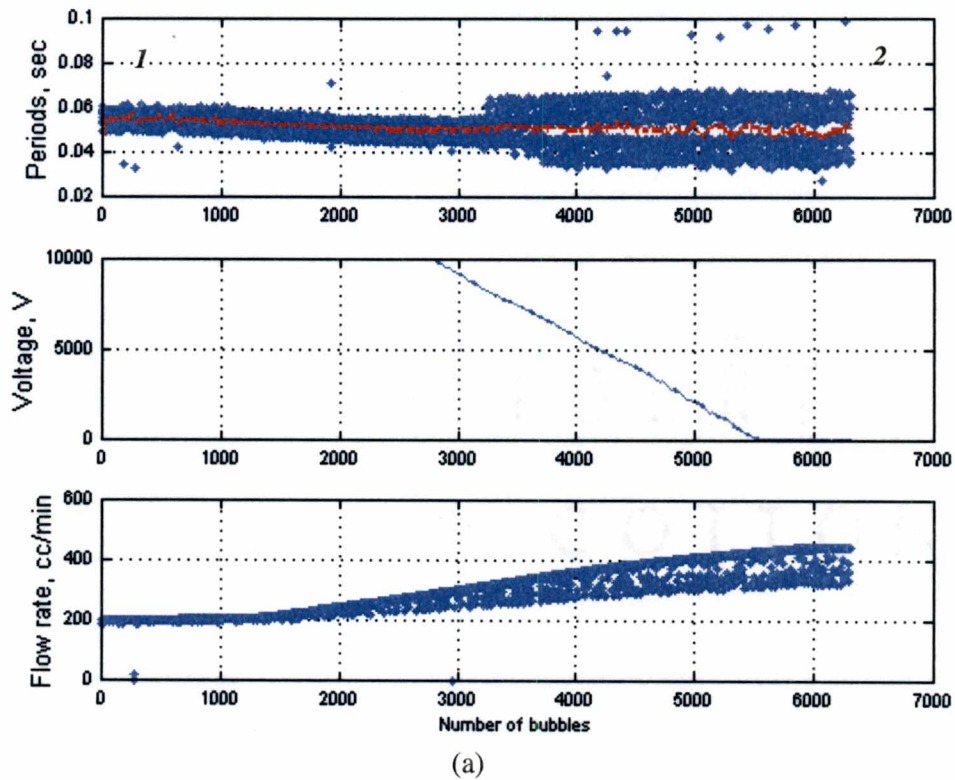


Figure 5.5. (a) An drift of 220cc/min in the disturbance (flow-rate), compensated by voltage to track a set point of constant bubbling frequency (0.05s). (b) System goes from noisy period-1 at state '1' to period-4 at state '2'

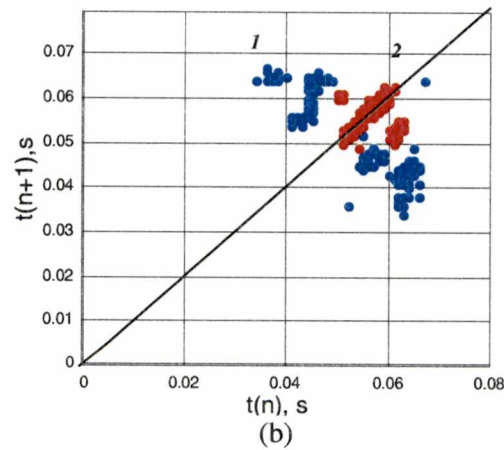
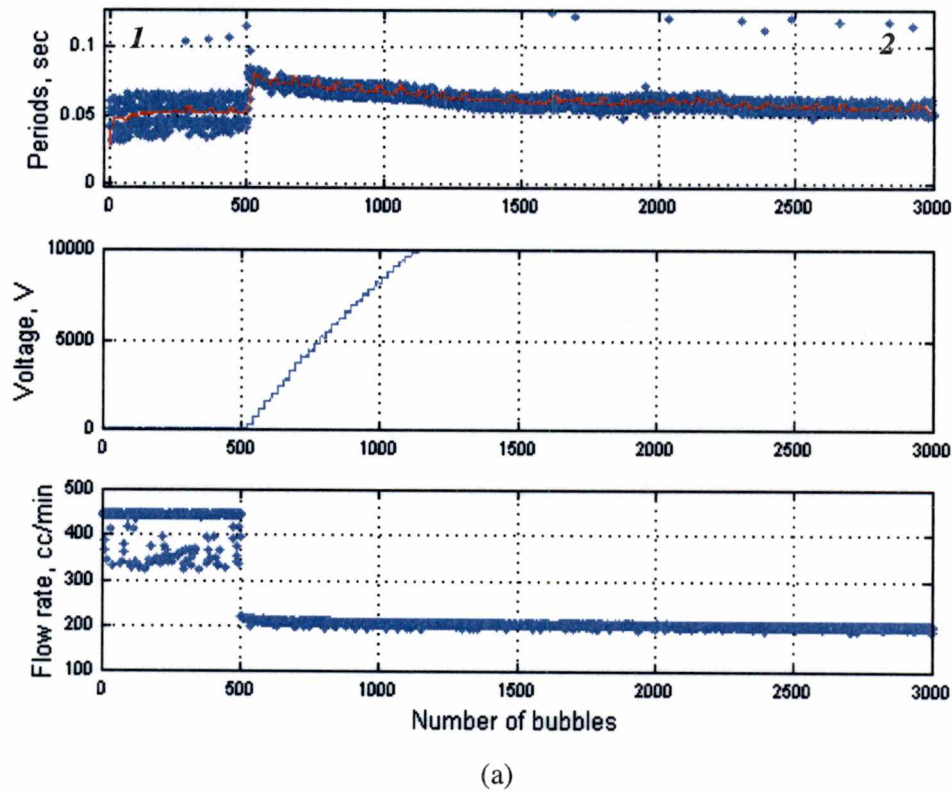
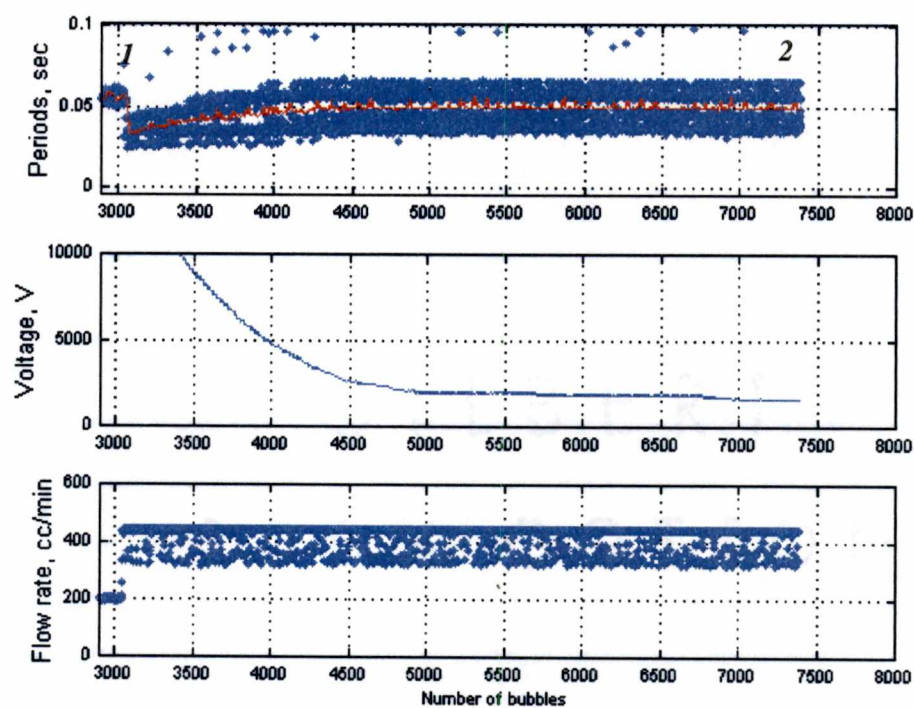
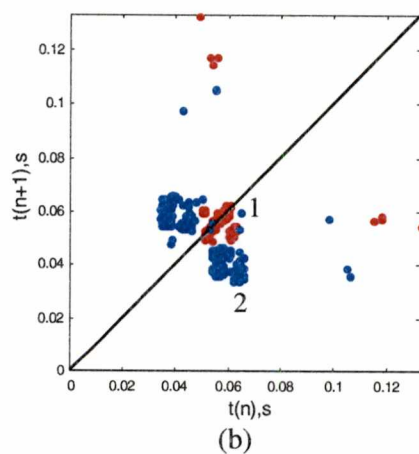


Figure 5.6. (a) Negative step change of 235cc/min in disturbance (flow rate) tracked by voltage for a set point of 0.05s. (b) System goes from period-4 at state '1' to noisy period-1 at state '2'.



(a)



(b)

Figure 5.7. (a) Positive step change of 220cc/min in disturbance (flow rate) tracked by voltage for a set point of 0.05s (b) System goes from noisy period-1 at state '1' to period-4 at state '2'.

**Figure 5.6** illustrates the effect of a negative step change of 235 cc/min in the disturbance. The controller compensates the disturbance and in effect the system goes from a period-4 to a noisy period-1.

**Figure 5.7** illustrates the effect of a positive step change of 220 cc/min in the disturbance. The controller action maintains the set point of 0.05s, but changes the periodicity of the system from a period-1 into period-4.

In figures 5.5-5.7, outliers are observed on the plot, which shows the zero-crossings. These outliers (at ~0.9-1.0s) are actually the formation times of two bubbles, which are caught because of a computing limitation of LabView. These do not cause a control loop problem as a moving window approach is adopted and an average past bubble period is used as the process variable. For the runs shown in the figures 5.5-5.7, a moving window of 20 bubbles was found to give satisfactory results.

### 5.3. OGY Control

The slow control regime targeting method described in section 5.2, demonstrates the effect of voltage and suggests that electrostatic potential can be used for control of individual bubbles at a higher frequency.

#### 5.3.1. Calculations

The crucial step for control is the extraction of information about system stability from the time return maps. This is because all the constants in the control law are calculated from the values of the stable and unstable manifolds and their corresponding eigenvalues, which in turn are

obtained from time return maps. The development of the OGY control algorithm has been presented in an earlier section (chapter 2)

There are four aspects to this calculation

- 1 Identifying the unstable fixed-point
- 2 Calculating the manifold directions
- 3 Computing the eigenvalues
- 4 Shift vector determination

The first two steps are shown in figure 5.8-5.9

### *5.3.1.1. Identifying the unstable fixed-point*

The unstable fixed-point can be thought of as a periodic trajectory onto which the system is to be stabilized. On the time return map, (which can be thought of as pseudo-phase space), the point moves along the stable manifold, mapping to the fixed-point, and continues to map to the fixed-point, until a perturbation causes it to continue along the unstable manifold to complete the sequence. For a chaotic attractor, each of the properties is necessary and sufficient. This means that all points which map to themselves are fixed-points and all fixed-points map to themselves.

### *5.3.1.2. Calculating the manifolds*

To calculate the stable and unstable manifolds, various methods have been suggested. A least square fitting method has been suggested in Cheng (1996), in which the mapping matrix  $M$  is calculated by least square approximation of the map data. This method though is fraught with errors and as the chaotic system is highly sensitive to the smallest

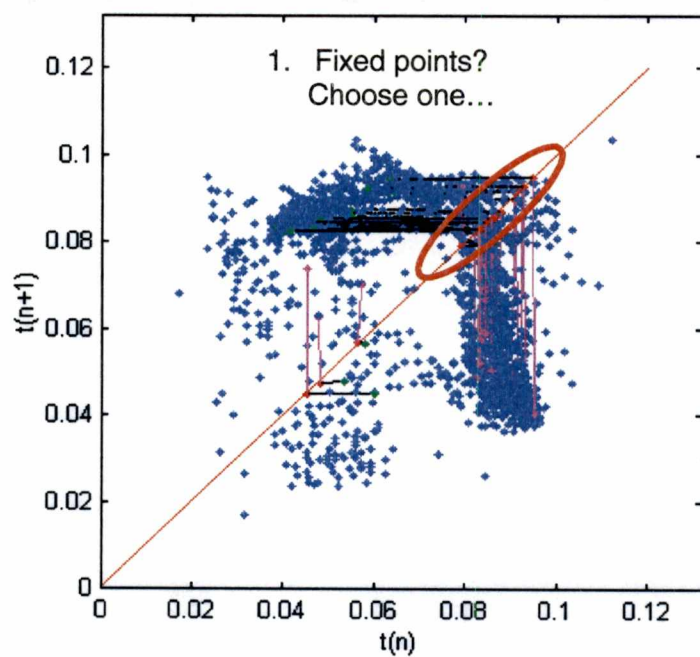


Figure 5.8. Sorting fixed points on the 45° line on the time return map to find a true fixed-point. (Flow-rate: 443 cc/min, voltage:10,000V)



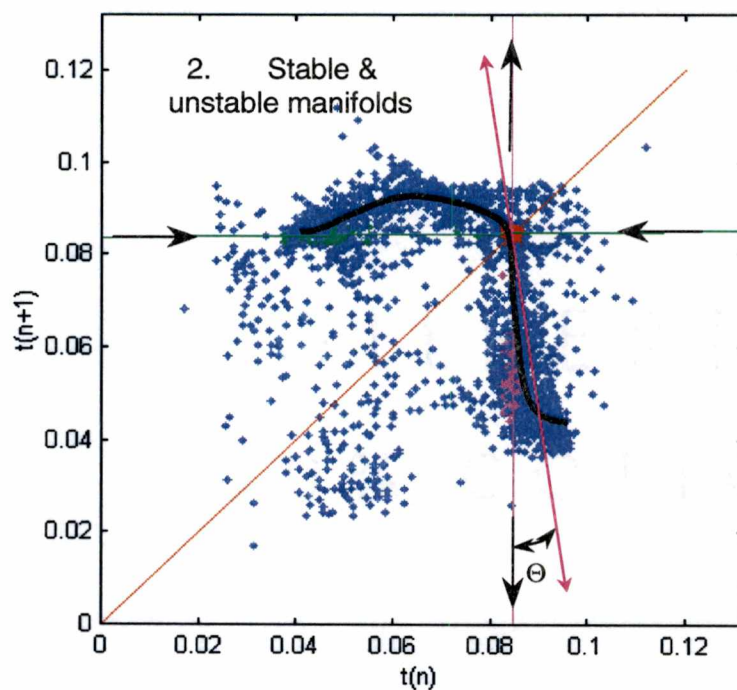


Figure 5.9. Identifying the stable and unstable manifold directions. The angle  $\Theta$  denotes the deviation of the calculated unstable manifold from the true unstable manifold, which is along the tangent to the attractor at the fixed point. The black line approximates the shape of the true attractor. (Flow-rate: 443 cc/min, voltage:10,000V)

perturbations (such as noise), the effectiveness of this method is greatly reduced. Another method suggested by Cheng (1996), uses cluster analysis to calculate the manifolds.

In this method, like other conventional fixed-point calculation approaches, a small tolerance is chosen to approximate a region around the fixed-point. Then the points, which map to that region are selected and the manifolds calculated. It was observed that in some cases the points map to the fixed-point, jump within the approximated tolerance and then jump out along the unstable manifold. In such cases, the movement of the fixed-point within the tolerance is neglected. But the location of the fixed-point has to be approximated first. This is tricky because the system has to 'hit' the fixed-point multiple times to be sure that it is the fixed-point. In experimental trials, due to presence of system noise, the chaotic system may map to the neighborhood of the unstable fixed-point a number of times before mapping to the fixed-point itself. A comprehensive dataset is required before enough information about the fixed-point location is acquired.

The direction of the unstable manifold is the tangent to the chaotic attractor at the fixed-point location (figure 5.9). Identification of the manifolds from experimental data is usually different from the direction of the manifold calculated from analysis of the time return map. To compensate from the error in manifold direction, the calculated unstable manifold direction was swept through an angle of  $15^\circ$  on either side to search the control law solution space.

### *5.3.1.3. Calculating the eigenvalues*

By knowing the manifold directions and hence the eigenvectors, one can calculate the corresponding eigenvalues based on the following procedure, (taken from Cheng, 1996). Consider two consecutive mapping points going to the fixed-point

$$p_1 = \begin{bmatrix} t_n & t_{n+1} \end{bmatrix}$$

$$p_2 = \begin{bmatrix} t_{n+1} & t_{n+2} \end{bmatrix}$$

The slope between these points is

$$m = \frac{t_{n+2} - t_{n+1}}{t_{n+1} - t_n}$$

Since they are located on the same eigenvector, the generalized solution for mapping points can be written in the form

$$t_{n+k} = \frac{\lambda^2 t_n - \lambda t_{n+1}}{\lambda t_n - t_{n+1}} = \frac{\lambda(\lambda - 1)}{(\lambda - 1)}$$

Taking the limit as  $\lambda \rightarrow 0$ , the eigenvalues around the fixed-point are equal to the slopes of the eigenvectors by L'Hospitals rule

$$m = \begin{cases} \lambda & \lambda \neq 1 \\ \lambda & \lambda = 1 \end{cases}$$

The following algorithm was used to calculate the fixed-point and the manifolds

- 1 After studying time return maps, a MATLAB™ routine was written to sort the points which map within a certain distance of each other. A single fixed-point was isolated by visual inspection of the walk-in states (Figure 5.8)
- 2 After choosing a tolerance around this fixed-point, points that mapped to this region were determined and the stable direction calculated as an average of many directions identified (figure 5.9)
- 3 Unstable manifolds were approximated as the direction along which maximum numbers of points leave the fixed-point location. This direction was then varied through 15° on either side of the approximated unstable manifold direction to compensate for the error in approximation

### 5.3.1.4. Shift vector

The shift vector is a measure of how much a unit change in the perturbation changes the location of the fixed point. It is calculated by calculating the fixed-point location from return maps at corresponding to two different conditions of the control variable and then observing the change in the fixed point. For the present experiment, the two return maps were plotted at 9500V and 10500V giving an effective perturbation of 1000v to the system. The change in the fixed point was found to be 0.001s. Thus the change in the return map per unit volt increase in the electrostatic potential is  $1e-5s$ .

The OGY control algorithm in its final form is

$$\Delta p = \frac{\lambda_u}{\lambda_u - 1} \frac{f_u^T \Delta x_n}{f_u^T s} = c \Delta x_n$$

and is implemented as

$$\Delta p = c_1 (c_2 \Delta x_1 + c_3 \Delta x_2) = c \Delta x_n$$

### 5.3.2. Results

Choice of the bubbling regime was based on the following observations

- 1 Control gain available with electrostatic potential was greater at higher voltages. From figure 4.34, it can be seen that the voltage gain has a non-linear behavior and changes in bubbling with unit changes in voltage are greater at higher voltages applied at the nozzle.
- 2 From the flow rate response, it can be seen that the flow rate affects the bubbling with an order of magnitude increase over electrostatic potential. To counter the effect of flow, a

comparatively large gain in electrostatic potential is needed (which is not possible with the limitations of current equipment) Consequently the minimum flow rate needed to ensure that the system was in chaos at the operating voltage was chosen

The goal was to bring the system back into higher periodicities, ideally to period-1. Several runs with the OGY parameters were carried out and manual tuning of the gain coefficients had to be done to ensure that the control moves were in operating limits. A scaling coefficient ( $c_1$ ) of the order of  $10^{-2}$  had to be added to get the calculated controller output to be in the permissible range of the voltage rippler which was  $\pm 490\text{V}$ . For the control trial carried out in **figure 5.10** the following constants were used:

- 1 Base voltage 10,000 V
- 2 Flow-rate 443 cc/min
- 3 Controller coefficients  $c_1=0.01$ ,  $c_2=-6.2e5$ ,  $c_3=0.084e5$
- 4 Data acquisition rate 100Hz

These constants were for the set of operating conditions unique to this experimental run. Time return maps and manifold calculations were carried out for every experimental run as the system information changed with every change in operating conditions.

The results of a representative OGY control attempt is shown in figure 5.10. In section (a), the system is nearly fully chaotic with no voltage being applied and with the application of electrostatic potential in (b), the system goes in to, what can be termed as, 'full-blown' chaos. Note that a remnant of a period-4 signature can be observed in (b). When the controller action is initiated at index 890 in section (c), it can be seen that though the system is still in chaos, the

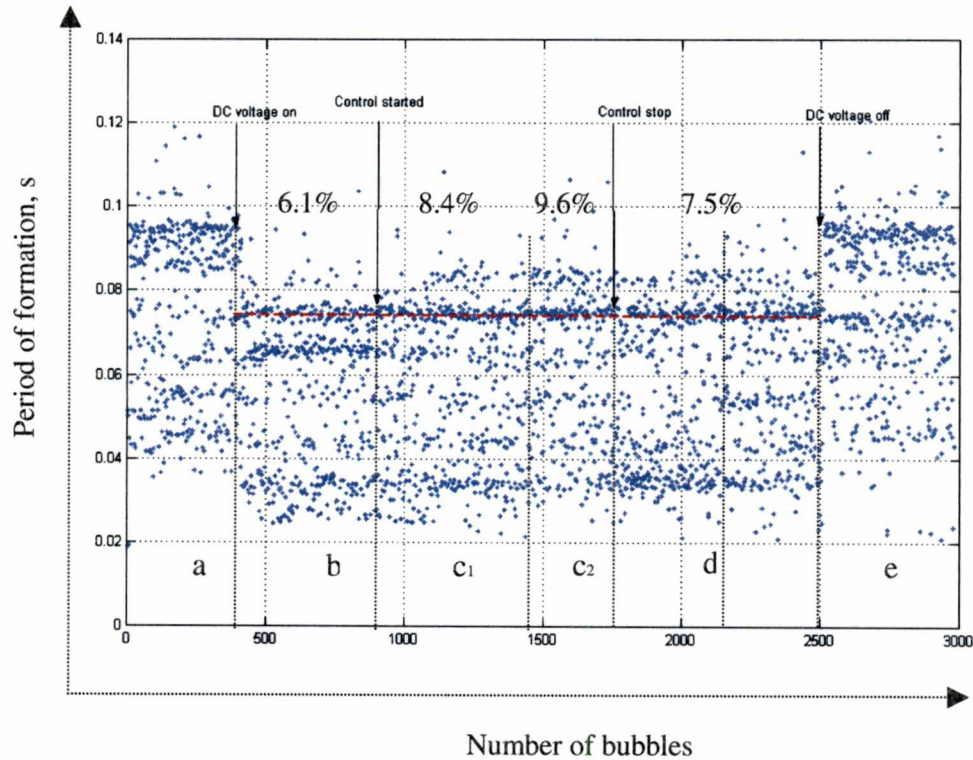


Figure 5.10. OGY control attempt with electrostatic potential as the single control variable. a) No DC voltage applied. b) 10kV DC voltage applied. c) Control initiated. d) Control stopped. e) DC voltage turned off. The red line indicates fixed-point location.

period-4 signature is less distinct. Instead an additional band is observed at the top where the system fixed-point location is calculated. In section (c<sub>2</sub>) it can be seen that there is only one band of bubbling. This is because the OGY control moves tend to '*push*' the system on the stable manifold and the points favor dwelling on the fixed-point. The red line indicates the fixed-point location. The control was turned off at the index 1750. Even after the control is turned off, the system is seen to be in a state of entrainment in section (d) and the entrainment is lost in section (e) where appearance of additional bands is seen. The voltage was again turned off at an index of 2500.

Tight control was not observed in controlling the bubbling to a periodic state from its open-loop chaotic behavior with control turned on, but a distinct effect of the control moves on the bubbles was obvious. The effect of the control scheme is better illustrated in a frequency distribution plot (**figures 5.11-5.14**). A progressive increase in the hits on the fixed-point can be seen when the control is turned on (figures 5.12-5.13), as opposed to when there is no control (figures 5.11, 5.14). After the control is turned off (figure 5.14), the number of fixed-point hits is observed to be higher than the number before the control was turned on (figure 5.11). This can be explained by the entrainment phenomenon in which a chaotic system maintains characteristics even after the perturbations are turned off.

### 5.3.3. *Entrainment studies*

In the present control experiments, tight control was not observed. It was surmised that the controller's gain of 490 V provided by the voltage 'ripple' was not sufficient. To confirm this assumption, entrainment studies were carried out (Cheng, 1996). The response of the bubbling to a square wave of  $\pm 490\text{V}$  amplitude at various frequencies was studied. No perceptible change

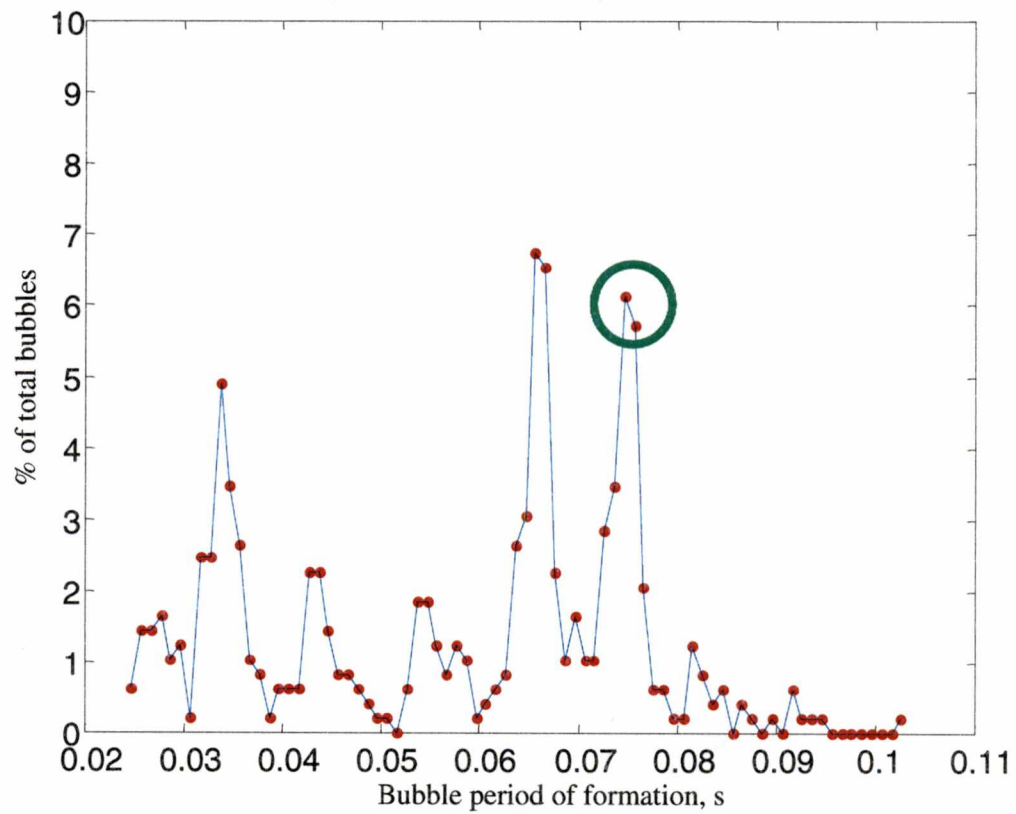


Figure 5.11. Frequency distribution of zero crossings before control is turned on (region b). Fixed point hits observed are 6.1% of the total number of bubbles



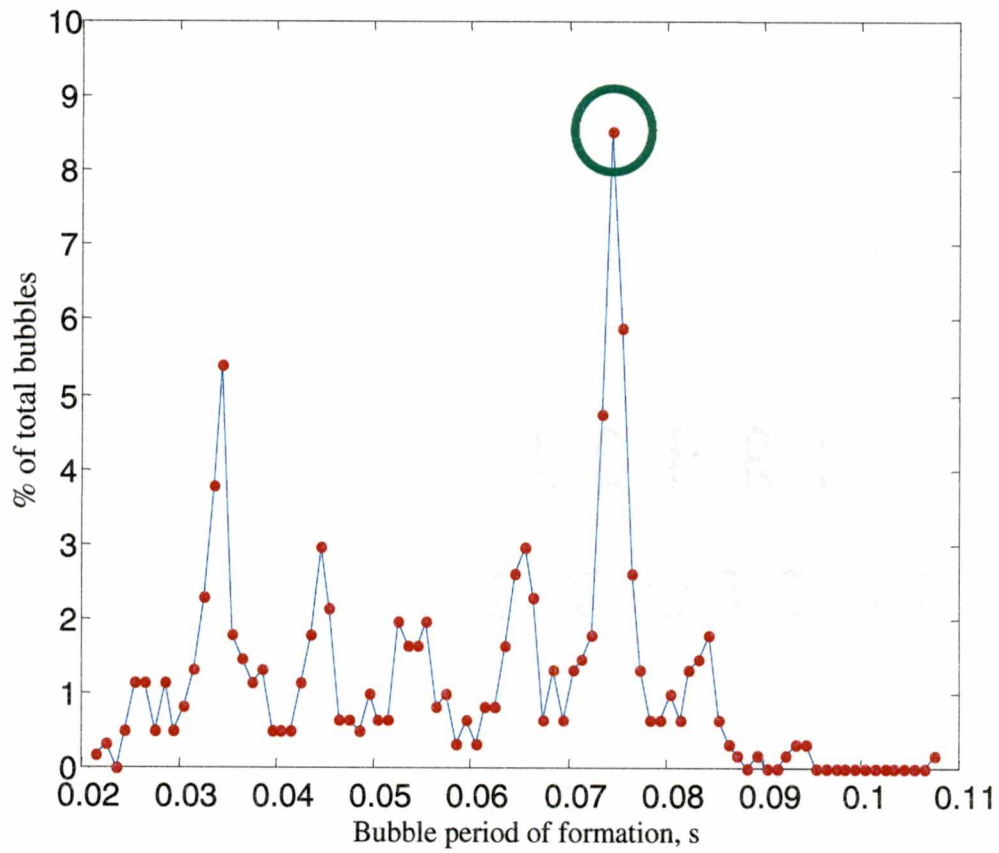


Figure 5.12. Frequency distribution of zero crossings after control is turned on (region  $c_1$ ). Fixed-point hits increase to 8.4% of the total number of bubbles

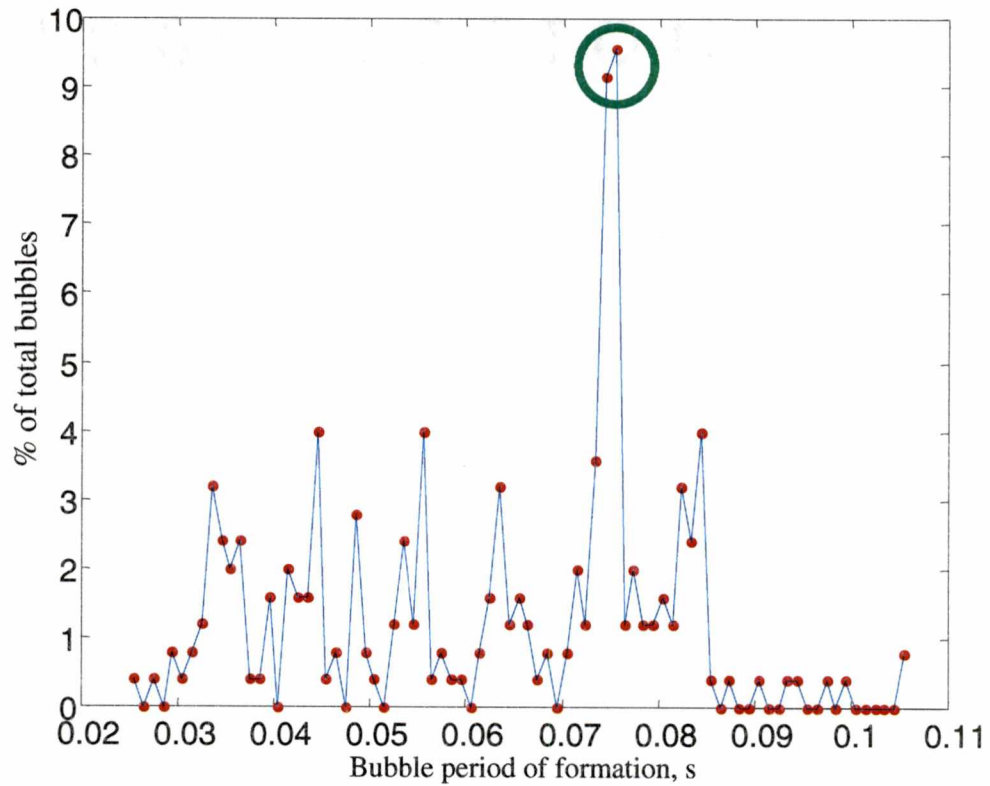


Figure 5.13. Frequency distribution of zero crossings after control is turned on (region  $c_2$ ). Fixed-point hits observed increase to 9.6% of the total number of bubbles.

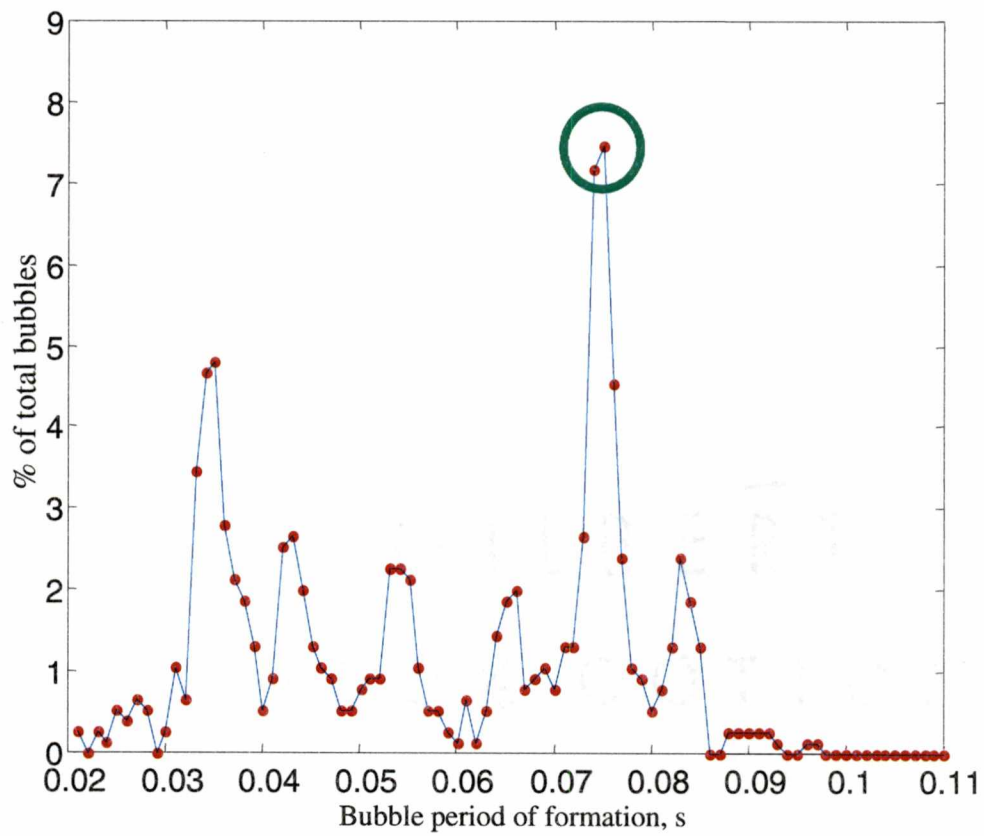


Figure 5.14. Frequency distribution of zero crossings after control is turned off (region d). Fixed-point hits decrease to 7.5% of the total number of bubbles

was observed in the pattern of the bubbles. This confirmed that the available gain was not sufficient to control the bubbling from chaotic bubbling to period-1. The present voltage swing available moves the fixed point by a distance of 0.001s. This is confirmed by the value of the shift vector which is  $1 \times 10^{-5}$  s/volts. To move the fixed point by a distance of 0.01s, rather than 0.001s, an amplification factor of 10x is required for the present voltage swing. This would approximately mean a voltage swing of  $\sim 5000\text{V}$ .

## 5.4. Summary

Real time identification of bubbling was attempted through statistical modeling techniques. Real time identification was shown to succeed for bubbling regimes of period-1 and period-2 with a scheme that compares the sizes of bubbles with a previous moving window history. Regimes of period-4 could not be identified mainly because of lack of faster computing resources and the sensitivity of the calculations to measurement errors. Electrostatic potential was harnessed to control bubbling to a constant average bubble period of formation as the set point, with an increase/decrease in the flow-rate as the disturbance. It was found that with changes in disturbance the regime of bubbling could be changed while maintaining a constant average bubbling rate. Electrostatic potential was also used as the control variable in the OGY chaos control algorithm to tame the chaos in bubbling with partial success.

## Chapter 6

# ***Conclusions & recommendations***

---

*Discovery, they believe, is inevitable*

Ian Malcolm, in Michael Crichton's *Jurassic Park*

The main objective of this research was to identify the modification of bubbling phenomena with electrostatic potential and then tame the chaos of bubbling with the newly identified variable

Electrostatic potential was identified as a bifurcation variable, which could be used to modify the periodicity of the bubbling. Extensive 3-d bifurcation plots revealed that the effect of electrostatic potential on the period of formation in comparison to flow-rate is similar. Surface contour plots, which mapped frequency of bubbling as a function of flow-rate and electrostatic potential suggested that effect of electrostatic potential on the bubbling frequency was non-linear with relatively greater effect on the bubbling at higher flow-rates. Electrostatic potential was discovered to modify bubbling to an extent where it could be used for control.

Flow control, which was carried out by previous researchers, was unsuccessful mainly because of the lack of fast valves. It was also felt that the dynamics of the change in the nozzle

chamber supply pressure to change in flow-rate also presents a challenge to using flow-rate as the manipulated variable. Electrostatic potential was identified as a control handle with better response dynamics (as compared to flow-rate) and thus was conjectured to promise relatively '*crisper*' control. The effect of electrostatic potential on bubbling regimes was studied at different flow parameters and the non-linear gain characteristics of electrostatic potential were identified. The bubbling regime at higher electrostatic potential was found to be more sensitive to unit change in voltage than at lower voltages. This investigation of chaos in bubbling led to development of several data analysis and automation tools (Sarnobat, 1999, 2000).

A real time bubbling regime identification module in LabView was successfully implemented to achieve simultaneous feedback control and real time return map updating with a moving window history. Regime control was demonstrated targeting a specific bubbling regime for period-1 and period-2. Electrostatic potential was successfully used as the manipulated variable to track a constant average bubbling frequency with flow-rate changes as the disturbance. Future work can include integration of the two control modules for maintaining a constant bubbling frequency within a constant regime. This is presently limited by sufficiently fast computing resources.

OGY control was attempted with partial success, limited by the small gain provided by the physical equipment ( $\pm 490$  volts). It is recommended that the same experiment be repeated with a higher voltage swing ( $\pm 5000$  volts) if a voltage '*ripler*' with a response time of greater than 40Hz can be built. It is also recommended that multivariate control with voltage and flow rate both as control variables is carried out with voltage as the fine-tuning parameter and flow control providing the rough tuning parameter. A real time OGY control module needs to be investigated into which can do dynamic fixed-point calculations and controller coefficient updates. This currently is limited by computer speed and memory. But that should not be a tight

constraint in the future. Alternatively, an OGY controller tuning search module can be implemented to fine tune the controller after the rudimentary manifold calculations. This is currently limited by the problem of running the column continuously for long periods of time, which causes an increase in the conductivity of glycerol with time.

Data analysis tools developed with MATLAB™ used multi-variate statistical techniques like principal component analysis to analyze bubbling. Wavelets and multi-scale methods were used with promising success and its potential as a chaos analysis tool are stressed.

Finally in the regime of bubbling and associated phenomena, in the present study the effects of electro-hydrodynamic (EHD) flows were assumed to be negligible and were not studied. Future study of bubbling can include study of EHD flows induced with different shapes of nozzles, various chamber sizes and changing the nozzle diameter. Changing the liquid selection is another avenue of investigation. The application of electrostatic potential to inverse spraying in liquid-liquid system holds bright prospects in light of this research.

## ***REFERENCES***



## References

- Chakka, P (1994) An experimental study of chaotic behavior of bubbles in liquid columns Masters Thesis The University of Tennessee, Knoxville
- Chang, Y , (1996) Characterization and control of chaotic bubble behavior Masters thesis The University of Tennessee, Knoxville
- Deshpande, D A , Deo M D , Hanson F. V , & Oblad A G (1992). A model for the prediction of bubble size at a single orifice in two phase gas-liquid systems *Chemical Engineering Science*, 47(7), 1669-1976
- Ditto, W L , Lindner, J F , Spano, M L (1995) Techniques for control of chaos *Phys D*, 86, 198-211
- Drahos J , Bradka F , & Puncochar M (1992) Fractal behavior of pressure fluctuations in a bubble column *Chemical Engineering Science*, 47(15/16), 4069-4075
- Dressler, U & Nitsche, G (1992) *Phys Rev Lett* 68, 1
- Fawcner R D , Kluth P P , & Dennis J S , (1990) Bubble formation at orifices in pulsed, flowing liquids *Trans Inst Chem Eng* , 68, Part A, January 1990
- Femat R , Alvarez-Ramirez J , & Soria A , (1998), Chaotic flow structure in a vertical bubble column *Physics Letters*, A 248, 67-79
- Grace, J M & Marijnissen, J C M. (1994) A review of liquid atomization by electrical means *J Aerosol Sci* 25, 1005-1019
- Harris, M T & Basaran, O A (1995) Equilibrium shapes and stability of nonconducting pendant drops surrounded by a conducting fluid in an electric field *J Colloid Interf Sci* 161, 389-413
- Kikuchi R , Yano T , Tsutsumi A , Yoshida K , Punchochar M , Drahos J., (1997) Diagnosis of chaotic dynamics of bubble motion in a bubble column *Chemical Engineering Science*, Vol 52, Nos 21/22, p3741-3745
- Leighton T G , Fagan K J , & Field J E , (1991) Acoustic and photographic studies of injected bubbles *Eur J Phys* , 12, 77-85

- Luewisutthichat W , Tsutsumi A ,Yoshida K , (1997) Chaotic hydrodynamics of continuous systems", *Chem Eng Sci* , 52, (21/22) p3685-3691
- Martien P , Pope S C , Scott P L , & Shaw R S , (1985) The chaotic behavior of the leaky faucet", *Phys Lett* , 110 A, No 7, 8
- Mittoni L J , Schwartz M P , & La Nauze R D , (1994) Deterministic chaos in the gas inlet pressure of gas-liquid bubbling systems *Phys Fluids*, 7,(4), April
- Neda Z , Bako B , & Rees E , (1995) The dripping faucet revisited *Chaos*, Vol 6, No 1, 1996
- Nguyen K , Daw C S , Chakka P , Cheng M , Bruns D D , & Finney C E A ,(1996) Spatio-temporal dynamics in a train of rising bubbles *Chem Eng J* , 65, 191-197
- Ogata, S , Tan, K , Nishijima, K & Chang, J -S (1985) Development of improved bubble disruption and dispersion technique by an applied electric field method, *AIChE J* 31, 62-69
- Ogata, S , Yoshida, T & Shinohara, H (1979) Small air bubble formation in insulating liquids under strong non-uniform electric field, *Jpn J Appl Phys* 18, 411-414
- Oguz, H N , & Prosperetti, A , (1993), Dynamics of bubble growth and detachment from a needle *J Fluid Mech.*, vol 257, pp111-145
- Pygras,K. (1992) Continuous control of chaos by self-controlling feedback *Phys Lett A* 170, 412-428
- Sarnobat, S U , DePaoli, D W , Bruns, D D ,(2000),"Enhanced Nonlinear Dynamic Bubbling", Draft manuscript for publication
- Sarnobat, S U , Hines, (1999),W J ,"Modeling periodicities of bubbling with multi-variate statistical techniques", Research paper, Department of Nuclear Engineering, The University of Tennessee,Knoxville Available through Oak Ridge National Laboratory, Oak Ridge ORNL/TM-2000/197
- Sarnobat, S.U , Hines,W J., Bruns, D D (1999),"Real-time periodicity identification of chaotic bubbles with a self-adapting Kohonen neural network model", Research paper, Department of Nuclear Engineering, The University of Tennessee, Knoxville Available through Oak Ridge National Laboratory, Oak Ridge ORNL/TM-2000/198
- Sarnobat,S U ,(2000),"The Bubble Automation Workbench", Automation application software for LabView™, Department of Chemical Engineering, University of Tennessee,

Knoxville

Sarnobat, S U, (2000), "The Bubble Toolbox for Chaotic Analysis", Data analysis software for MATLAB™, Department of Chemical Engineering, University of Tennessee, Knoxville

Sato M, Hatori H, & Saito M, (1997), Experimental investigation of droplet formation mechanisms by electrostatic dispersion in a liquid-liquid system *IEEE Trans Ind Appl*, vol 33, no 6, November/December

Sato M, Saito M, & Hatori T, (1993) Emulsification and size control of insulating and/or viscous liquids in liquid-liquid systems by electrostatic dispersion *J Colloid Interf Sci* 156, 504-507

Sato, M (1980) Cloudy bubble formation in a strong nonuniform electric field *J Electrostat* 8, 285-287

Sato, M, Hatori, T & Saito, M (1997) Experimental investigation of droplet formation mechanisms by electrostatic dispersion in a liquid-liquid system

Sato, M, Kato, S & Saito, M (1996) Production of oil/water type uniformly sized droplets using a convergent AC electric field *IEEE Trans Ind Appl* 32, 138-145

Sato, M, Kuroda, M & Sakai, T (1979) Effect of electrostatics on bubble formation *Kagaku Kogaku Ronbunshu* 5, 380-384

Sato, M, Saito, M & Hatori, T (1993) Emulsification and size control of insulating and/or viscous liquids in liquid-liquid systems by electrostatic dispersion *J Colloid Interf Sci* 156, 504-507

Shin, W -T, Yiacoumi, S & Tsouris, C (1997) Experiments on electrostatic dispersion of air in water. *Ind Eng Chem Res* 36, 3647-3655

Terasaka, K, & Hideki, T, (1993) Bubble formation under constant flow conditions *Chem Engr Sc* Vol 48, No 19, pp3417-3422

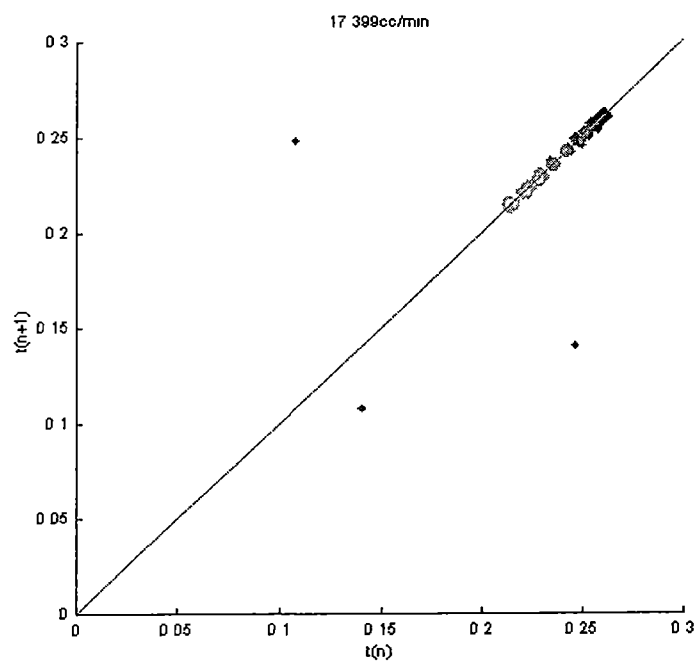
Tritton D J, & Egdell C., (1992). Chaotic bubbling. *Phys Fluids*, A 5(2), February.

Tsouklalas, L.H., Uhrig R.E, (1997) *Fuzzy and neural approaches in engineering*. John Wiley & Sons

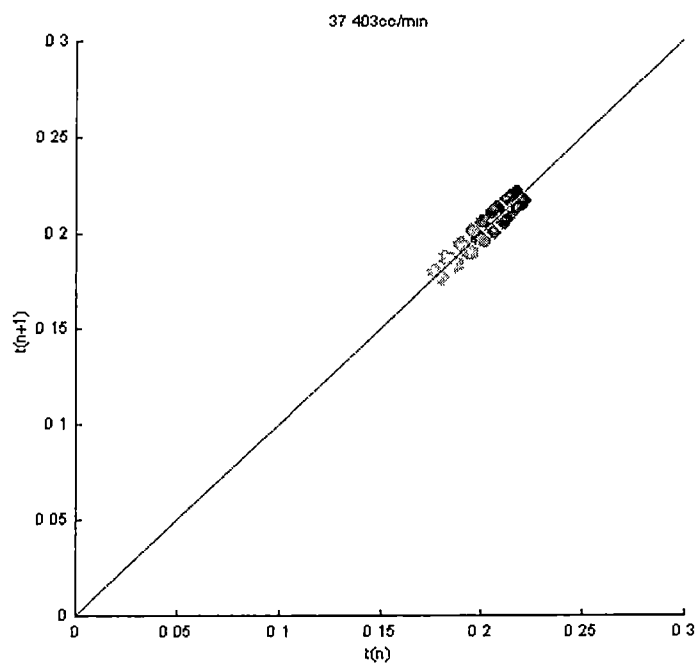
Tsouris C, Shin W, Yiacoumi S, (1998) Pumping, spraying and mixing of fluids by electric-fields *Canad J Chem Eng*, Vol 76, June

- Tsouris, C , DePaoli, D W , Feng, J Q & Scott, T C (1995) An experimental investigation of electrostatic spraying of nonconductive fluids into conductive fluids *Ind Eng Chem Res.* 34, 1394-1403
- Tsouris, C , DePaoli, D W , Feng, J Q , Basaran, O A & Scott, T C (1994) Electrostatic spraying of nonconductive fluids into conductive fluids *AIChE J* 40, 1920-1923
- Tsouris, C , Shin, W -T & Yiaccoumi, S (1998) Pumping, spraying, and mixing of fluids by electric fields *Canad J Chem Eng* 76, 589-599
- Tufaile A , Pinto R D , Goncalves W M , & Sartorelli J C ,(1999) Simulations in a dripping faucet experiment *Phys Lett , A* 225, 58-64
- Van Goor, N A (1998), Control of chaotic and nonlinear systems in influenced by dynamic noise Doctoral dissertation, University of Tennessee, Knoxville
- Zaky, A A & Nossier, A (1977) Bubble injection and electrically induced hydrostatic pressure in insulating liquids subjected to non-uniform fields *J Phys D* 10, L189-L191

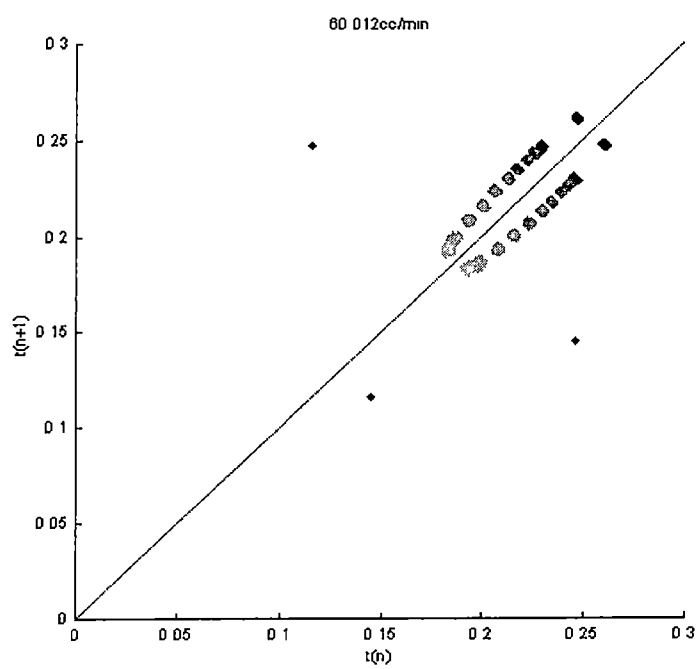
## ***APPENDIX***



Appendix A 1 Progressive time return map for constant flow-rate and increase in applied electrostatic potential from 0 kV to 10kV

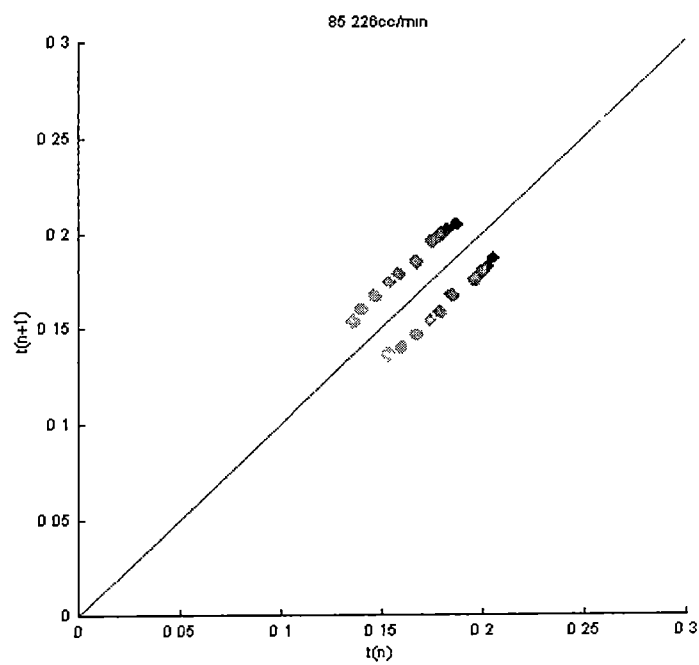


Appendix A 2 Progressive time return map for constant flow-rate and increase in applied electrostatic potential from 0 kV to 10kV

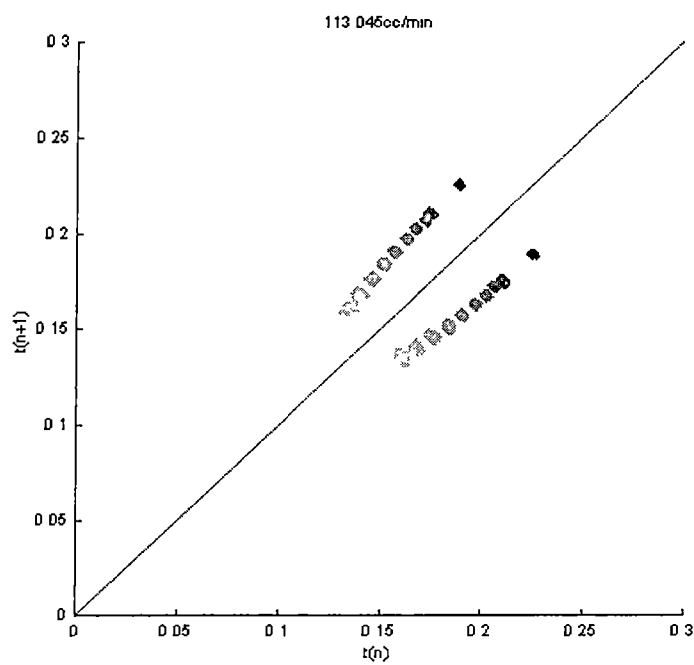


Appendix A 3 Progressive time return map for constant flow-rate and increase in applied electrostatic potential from 0 kV to 10kV

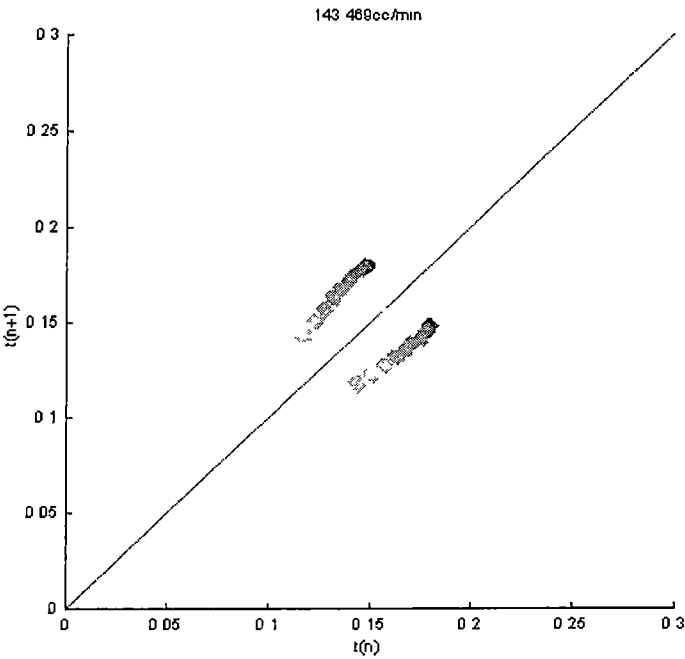




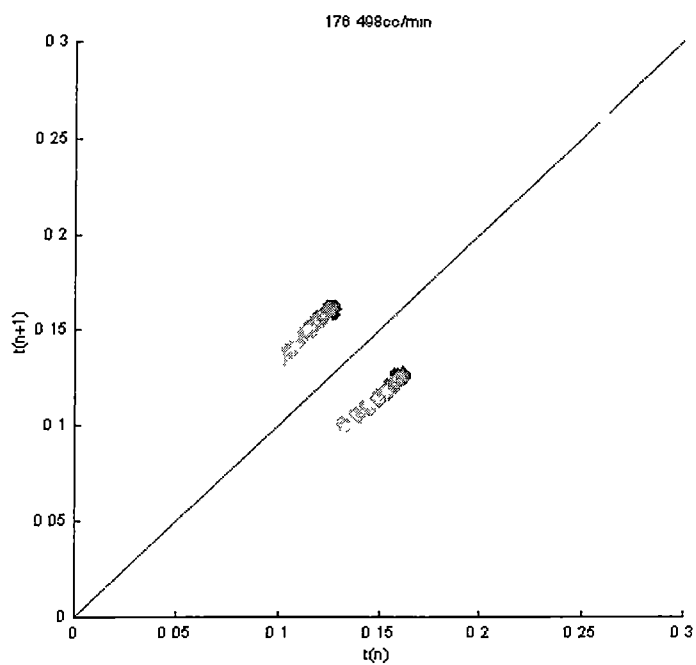
Appendix A 4 Progressive time return map for constant flow-rate and increase in applied electrostatic potential from 0 kV to 10kV



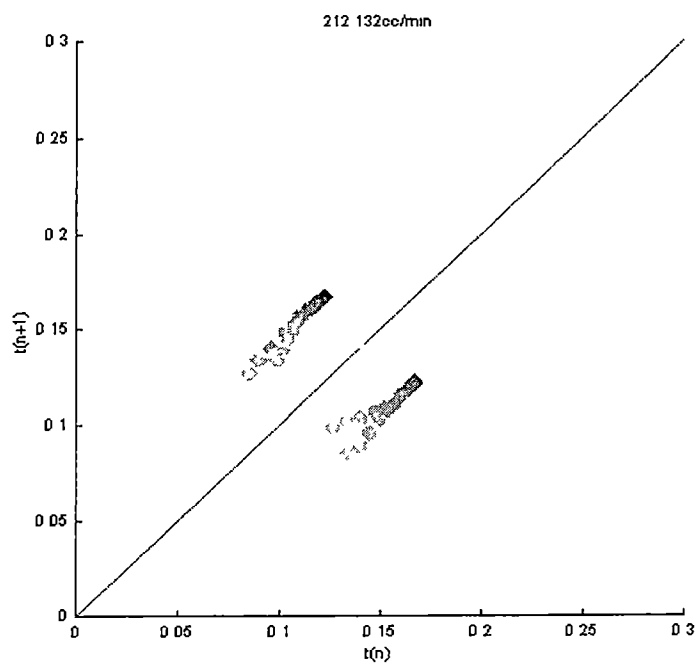
Appendix A 5 Progressive time return map for constant flow-rate and increase in applied electrostatic potential from 0 kV to 10kV



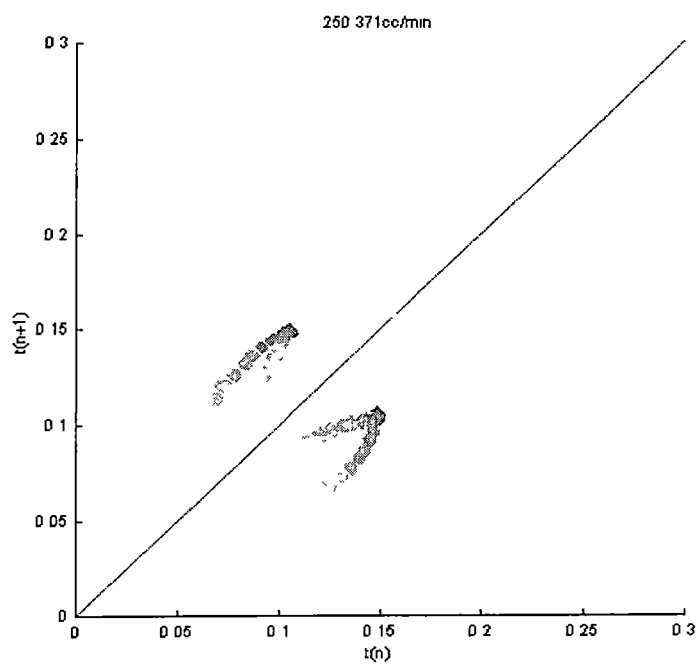
Appendix A 6 Progressive time return map for constant flow-rate and increase in applied electrostatic potential from 0 kV to 10kV



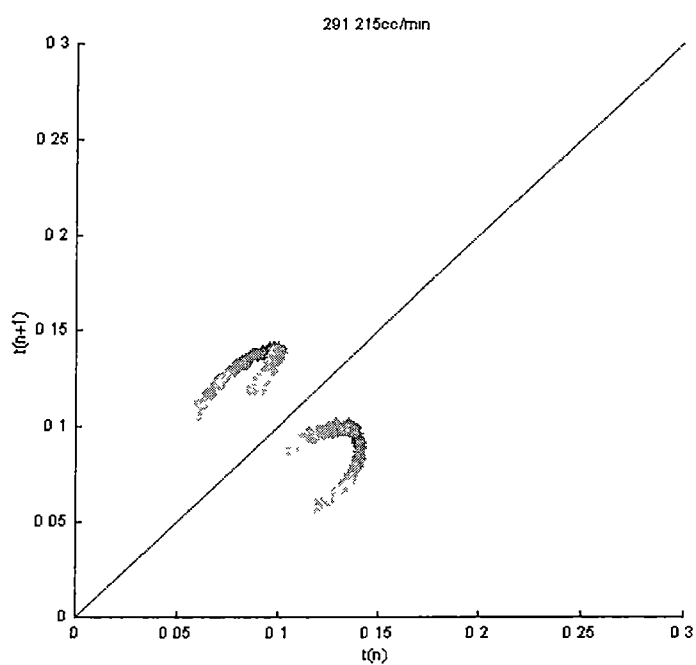
Appendix A 7 Progressive time return map for constant flow-rate and increase in applied electrostatic potential from 0 kV to 10kV



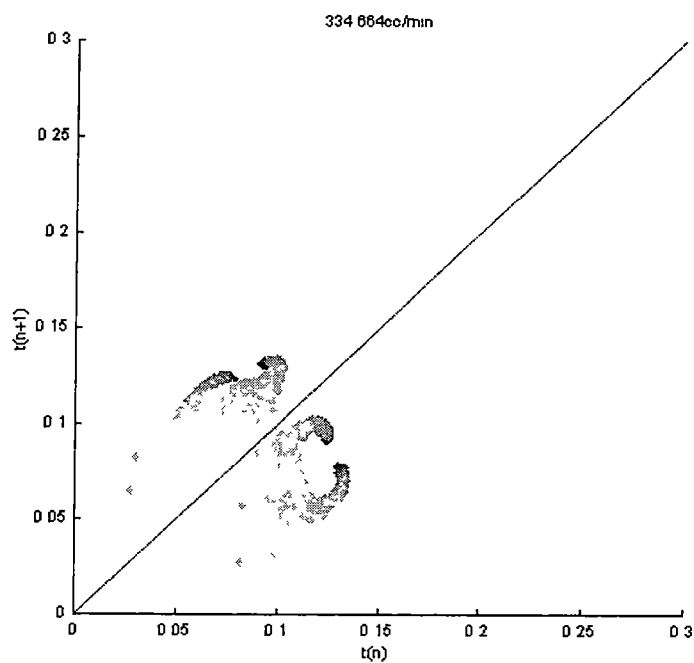
Appendix A 8 Progressive time return map for constant flow-rate and increase in applied electrostatic potential from 0 kV to 10kV



Appendix A 9 Progressive time return map for constant flow-rate and increase in applied electrostatic potential from 0 kV to 10kV

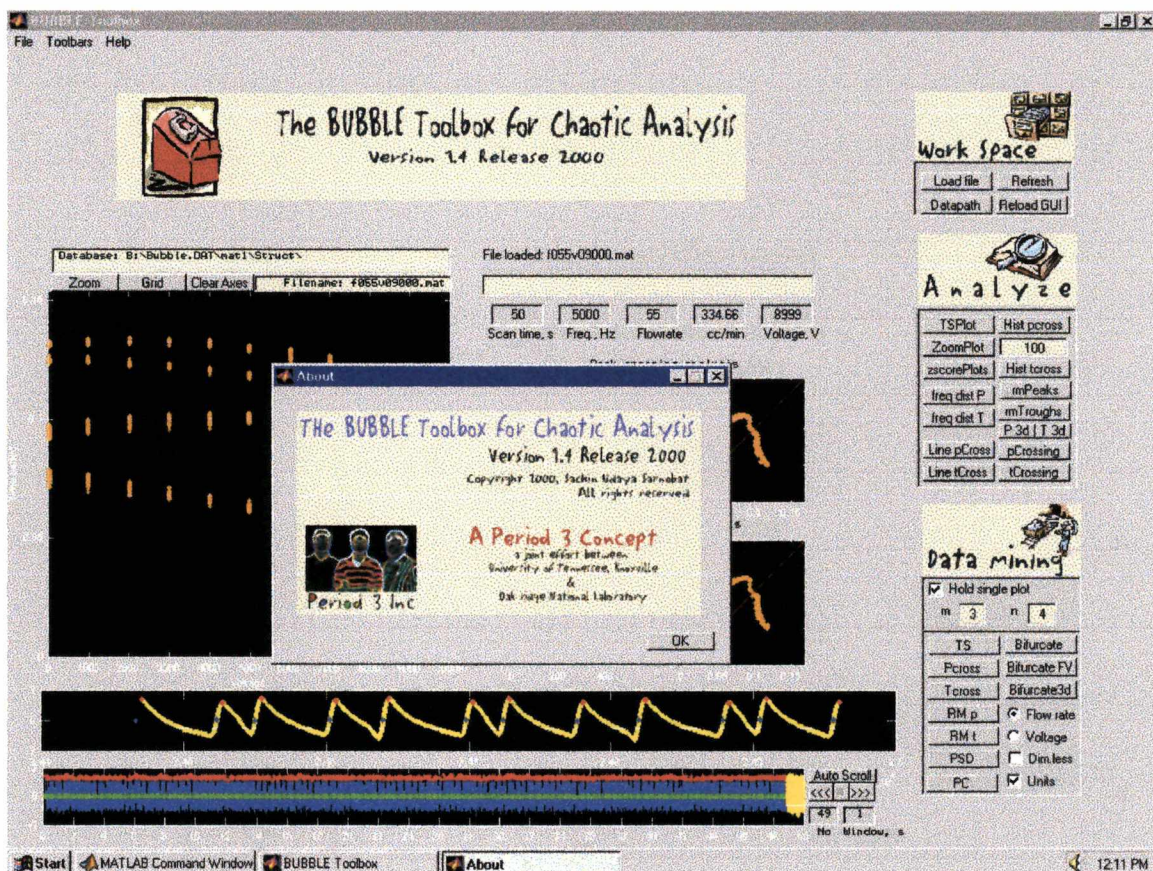


Appendix A 10 Progressive time return map for constant flow-rate and increase in applied electrostatic potential from 0 kV to 10kV



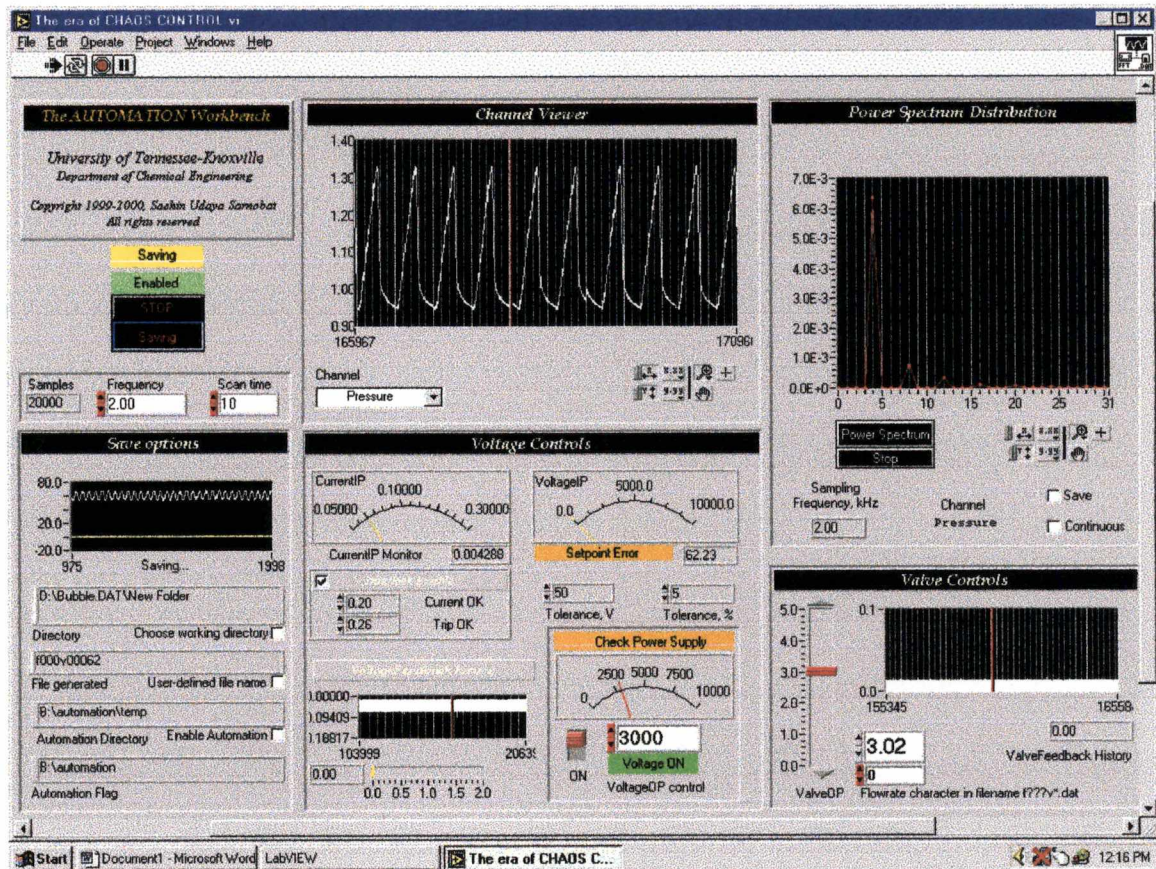
Appendix A 11 Progressive time return map for constant flow-rate and increase in applied electrostatic potential from 0 kV to 10kV



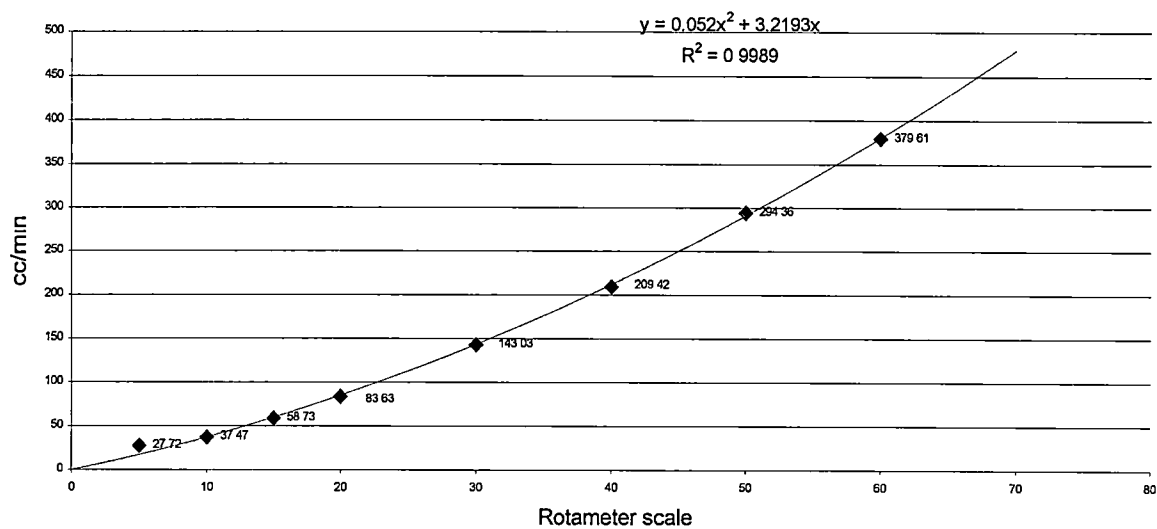


Appendix B.1 Screen shot of the BUBBLE Toolbox for Chaotic Analysis (Sarnobat, 2000).





Appendix C.1 Screen shot of the BUBBLE Automation Workbench (Sarnobat, 2000)



Appendix D 1 Rotameter calibration at 10 psig

**Nomenclature**

$B_e$	modified Bond number
$B_o$	Bond number
$c$	control vector
$D$	diameter
$e$	eigenvector
$E$	electric field
$f$	left eigenvector
$Fr$	Froude number
$g$	gravitational acceleration
$J$	Jacobian
$k$	Embedding dimension
$M$	mapping matrix
$N$	Dimension number
$N_w$	Tsuge flow-rate number
$p$	system parameter
$s$	shift vector
$t$	time
$u$	superficial velocity
$x$	system state
$We$	Weber number
$\rho$	density
$\lambda$	eigenvalue
$\varepsilon$	permittivity
$\sigma$	surface tension

***Vita***

Sachin Udaya Sarnobat was born in Bombay, India on February 14, 1977. He lived his childhood in Bandra East studying at the Cardinal Gracious School and New English High School. He then moved on to studying Science with a minor in Computer Science, at D.G. Ruparel College of Arts, Commerce & Science, Matunga, after which he pursued a Chemical Engineering major as the first batch of Dwarkadas J. Sanghvi College of Engineering, Vile Parle under the University of Bombay. Following his graduation, Sachin entered the Masters' program in Chemical Engineering at the University of Tennessee, Knoxville. During his studies at Tennessee, he was able to actively pursue sailing and photography apart from doing research at the Oak Ridge National Laboratory. The degree was awarded in August 2000.